Role of FBXW5-loss in Centrosome Abnormalities and Cell Physiology

Dissertation
der Mathematisch-Naturwissenschaftlichen Fakultät
der Eberhard Karls Universität Tübingen
zur Erlangung des Grades eines
Doktors der Naturwissenschaften
(Dr. rer. nat.)

vorgelegt von
Tim Scholta
aus Spremberg

Tübingen
2021

Gedruckt mit Genehmigung der Mathematisch-Naturwissenschaftlichen Fakultät der Eberhard Karls Universität Tübingen.

Tag der mündlichen Qualifikation: 12.07.2021

Dekan:	Prof. Dr. Thilo Stehle
1. Berichterstatter:	Prof. Dr. Nisar Malek
2. Berichterstatter:	Prof. Dr. Alfred Nordheim

Content

1 Abbreviations

AMPHO	Amphotropic
Amp^R	Ampicillin resistance
APC/C	Anaphase promoting complex/cyclosome
BAC	Bacterial artificial chromosome
BNL CL.2	BALB/c liver cell line
BSA	Bovine serum albumin
C57BL/6	C57 black 6
CPAP	centrosomal P4.1-associated protein
Cdk	Cyclin dependent kinase
cDNA	Complementary DNA
CIN	Chromosomal instability
CiP	Calf intestinal phosphatase
CM^R	Chloramphenicol resistance
CRISPR	Clustered Regularly Interspaced Short Palindromic Repeats
DAPI	4',6-diamidino-2-phenylindole
DLC1	Deleted in Cancer 1
DMEM	Dulbecco's modified eagle medium
DNA	Deoxyribonucleic acid
dNTP	Deoxynucleotide triphosphate
DSB	Double strand break
dsDNA	Double stranded DNA
DTT	Dithiothreitol
E. coli	*Escherichia coli*
ECL	Enhanced chemiluminescence
EDTA	Ethylenediaminetetraacetic acid
ES cells	Embryonic stem cells
EtOH	Ethanol
FAH	Fumarylacetoacetate hydrolase
FBS	Fetal bovine serum
FBXW5	F-box and WD repeat domain containing protein 5
GFP	Green fluorescent protein
h	Hour
HBS	Hepes buffered solution
HDTVi	Hydrodynamical tail vein injection
HEK	Human embryonic kidney
HR	Homologous recombination
HU	Hydroxyurea
HUVEC	Human Umbilical Vein Endothelial Cells
KLF	Kruppel-like factor
Kan^R	Kanamycin resistance
LB	Luria-Bertani
Min	Minutes
MOI	Multiplicity of infection
MT	Microtubule
MT-FBXW5	Myc tagged FBXW5
MTOC	Microtubule organizing center
NaOH	Sodium hydroxide
NEB	New England Biolabs
Neo^R	Neomycin resistance
NHEJ	Non-homologous end joining
NIH/3T3	Murine fibroblasts

PAGE	Polyacrylamide gel electrophoresis
PBS	Phosphate buffered saline
PCM	Pericentriolar material
PCR	Polymerase chain reaction
PFA	Paraformaldehyde
PLK	Polo-like kinase
PLK4	Polo-like Kinase 4
$Puro^R$	Puromycin resistance
PVDF	Polyvinylidene difluoride
qRT-PCR	Quantitative real-time PCR
RFU	Relative fluorescence units
RIPA	Radioimmunoprecipitation assay
RNA	Ribonucleic acid
RNAi	RNA interference
RPA2	Replication protein A2
SAK	Serine/threonine-protein kinase PLK4
SAC	Spindle assembly checkpoint
SAS6	Spindle assembly abnormal protein 6 homolog
SCF	Skp, Cullin, F-box containing complex
SD	Standard deviation
SDS	Sodium dodecyl sulfate
sgRNA	Single guide RNA
shRNA	Short hairpin RNA
ssDNA	Single stranded DNA
TAE	Tris-acetate-EDTA
TBS	Tris buffered saline
TE	Tris-EDTA
TSC1	Tuberous sclerosis 1 (Hamartin)
TSC2	Tuberous sclerosis 2 (Tuberin)
UV	Ultraviolet

2 Abstract

Centrosome duplication is a tightly regulated process during cell division and should, like DNA replication, occur only once per cell cycle. The equal distribution of centrosomes to the cell poles, with simultaneous migration of chromosomes, ensures genomic stability during mitosis. In most tumors, the centrosome cycle is disrupted, although it remains unclear whether centrosome abnormalities are the cause or consequence of the tumor formation process. In previous work Puklowski et al. demonstrated that the ubiquitin E3 ligase SCF^{FBXW5} plays a central role in the initiation of the centrosome cycle. Upon reduction of cellular SAS6 (spindle assembly abnormal protein 6 homolog) by RNAi-induced destabilization of FBXW5, centrosome amplifications and the formation of multinucleated cells were observed [1].

In the present work, such destabilization of FBXW5, so far performed only in human cancer cells, was applied to untransformed murine fibroblasts and liver cells. It was shown that *in vitro* the loss of FBXW5 - in addition to the increased occurrence of supernumerary centrosomes - also leads to reduced cell division and cell migration. Further studies in synchronized FBXW5-suppressed cells revealed that the growth and migration disturbances are accompanied by the increased appearance of multipolar spindles. Presumably, this phenotype leads to a delay in the transition from mitosis to G1 phase and thus to a later onset of the next cell cycle. Although genomic instability and tumor development have been postulated to also occur with the formation of multipolar spindles [2], no transformation was observed *in vitro* in FBXW5-deficient cells.

Downregulation of FBXW5 was also attempted *in vivo*. Hydrodynamic tail vein injection of transposon-based shRNAs, or CRISPR/Cas9 RNAs, was aimed to specifically reduce FBXW5 in mouse liver. However, no tumor formation or other pathophysiological consequences were observed - neither in wild-type nor in p53-, p21-, and p19arf-deficient mice. Presumably, the depletion of FBXW5 alone is not a sufficient trigger of tumorigenesis. Yet, the loss of FBXW5 could not be demonstrated beyond doubt *in vivo*. To uncover potential regulatory mechanisms that might suppress transformation of FBXW5-deficient cells, a genome-wide CRISPR/Cas9 library screen was performed. Here, different regulators, such as replication protein A2 (RPA2) or cell stress-associated genes like ang5 or map4k2 were identified.

3 Zusammenfassung

Die Zentrosomenduplikation ist ein streng regulierter Prozess während der Zellteilung und sollte, ähnlich wie die DNA Replikation, nur einmal pro Zellzyklus stattfinden. Durch die gleichmäßige Aufteilung der Zentrosome, mit gleichzeitiger Wanderung der Chromosomen, zu den Zellpolen wird die genomische Stabilität während der Mitose sichergestellt. Bei den meisten Tumoren ist der Zentrosomenzyklus gestört, wobei nach wie vor unklar ist, ob die Zentrosomen-Anomalien Ursache oder Folge eines Tumorbildungsprozesses sind. In früheren Arbeiten konnten Puklowski et al. [1] zeigen, dass die Ubiquitin-E3-Ligase SCF^{FBXW5} eine zentrale Rolle bei der Initiierung des Zentrosomenzyklus spielt. Nach einer Absenkung des zellulären SAS6 (spindle assembly abnormal protein 6 homolog) durch RNAi-induzierte Destabilisierung von FBXW5 wurden Zentrosomenamplifikationen und die Bildung von mehrkernigen Zellen beobachtet.

In der vorliegenden Arbeit wurde diese, bislang nur in humanen Krebszellen durchgeführte Destabilisierung von FBXW5, auf nicht transformierte murine Fibroblasten und Leberzellen übertragen. Hierbei zeigte sich, dass *in vitro* der Verlust von FBXW5 - neben dem vermehrten Auftreten überzähliger Zentrosomen - auch zu langsamere Zellteilung und Zellmigration führt. Weiterführende Untersuchungen in synchronisierten FBXW5-supprimierten Zellen ergaben, dass die Wachstums- und Migrationsstörungen mit dem vermehrten Auftreten multipolarer Spindeln einhergehen. Vermutlich führt dieser Phänotyp zu einer Verzögerung des Übergangs von der Mitose zur G1-Phase und damit zu einem späteren Beginn des nächsten Zellzyklus. Obwohl bei Bildung multipolarer Spindeln auch genomische Instabilität und Tumorentwicklung postuliert wurden [2], konnte *in vitro* in FBXW5-defizienten Zellen keine Transformation beobachtet werden.

Die Absenkung von FBXW5 wurde auch *in vivo* versucht. Durch hydrodynamische Schwanzveneninjektion transposonbasierter shRNAs, oder CRISPR/Cas9 RNAs, sollte FBXW5 gezielt in der Mausleber reduziert werden. Dabei wurden keine Tumorbildungen oder andere pathophysiologische Folgen festgestellt - weder im Wildtyp noch in p53-, p21- und $p19^{arf}$-defizienten Mäusen. Vermutlich ist die alleinige Absenkung von FBXW5 kein hinreichender Auslöser der Tumorgenese. Allerdings konnte der Verlust von FBXW5 *in vivo* nicht zweifelsfrei nachgewiesen werden. Um mögliche regulatorische Mechanismen aufzudecken, die eine Transformation FBXW5-defizienter Zellen unterdrücken könnten, wurde ein genomweiter CRISPR/Cas9-Bibliotheksscreen durchgeführt. Hierbei konnten verschiedene Regulatoren, wie z.B. das Replikationsprotein A2 (RPA2) oder Zellstress-assoziierte Gene wie *ang5* oder *map4k2* identifiziert werden.

4 Introduction

4.1 The importance of centrosomes in maintaining genomic stability

Centrosomes are the major microtubule organizing center (MTOC) of eukaryotic cells, determining cell shape, polarity, motility, spindle formation, chromosome segregation and cell division [3, 4]. Like DNA, the centrosome is duplicated exactly once during each cell cycle. This ensures the equal segregation of the genetic material to the daughter cells and thereby ensuring genomic stability. "A typical mammalian centrosome is composed of two centrioles surrounded by a meshwork of a proteins embedded in matrix called the pericentriolar material (PCM)" [5]. The centriole itself represents one of the best recognizable structures of all cell organelles. Nine triplet microtubules arrange in a cylinder-like structure with a diameter of approximately 250 nm and a length of 500 nm, while the triplet microtubules represent the cylindrical barrel of the centriole and the basal bodies [6] (Figure 1).

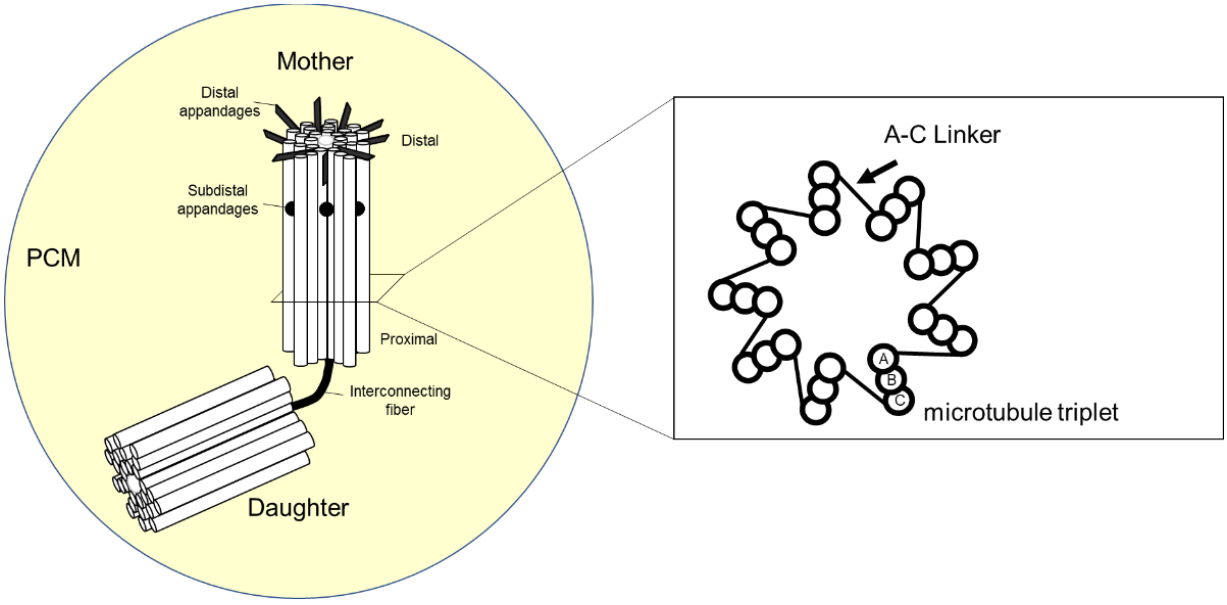

Figure 1 Structure of the centrosome. The centrosome consists of two orthogonally arranged microtubule structures, called centrioles. One centriole is composed of 9 microtubule triplets, with each triplet consisting of the A-, B-, and C-tubules and a unique twist angle of 40° between two adjacent triplets. The mother centriole, in contrast to the daughter centriole, harbors subdistal and distal appendages, which contribute to centriole stability [7]. Finally, the centrosome is surrounded by an electrodense cloud called pericentriolar material (PCM), which is composed of proteins like pericentrin, ninein and γ-tubulin.

Since the postulation of Theodor Boveri, it is hypothesized that centrosome amplification beyond duplication is responsible for genomic instability, potentially resulting in tumor formation [2, 8]. There is also clinical evidence which indicates, that centrosome amplification is accompanied with “a greater risk for initiation of malignant transformation, tumor progression, chemoresistance and ultimately, poor patient prognosis” [9]. Similarly, aberration in centrosome number correlates with multiple diseases like ciliopathies, brain diseases and cancer [2, 8, 10]. So far it is unknown whether amplified centrosomes are the origin of such tremendous changes in the cell physiology. However, overamplification of centrosomes induces the development of multipolar mitotic spindles, leading to a mitotic catastrophe, mitotic slippage, or apoptosis [11]. On the other hand, cells with too many centrosomes can regain bipolar spindles by a mechanism called centrosome clustering, which describes the ability to reconfigure the multipolar spindle into a bipolar spindle [11, 12].

Despite this, abnormalities of centrosomes in number and structure are well documented and, as reviewed by German A. Pihan [11], there are at least three different mechanisms described from which supernumerary centrosomes result:

1. template-mediated over-replication of pre-existing centrosomes *(over-replication* pathway): Here, cancer cells that become arrested in S- or G_2-phase by hydroxyurea (HU) or aphidicolin undergo multiple rounds of templated centriole duplications. Upon Cdk2 activation, centrosome precursors are assembled in the nucleus and exported to the cytoplasm. These precursors are subsequently elongated and maturated, leading to functional centrosomes that enter mitosis [11, 13].

2: *de novo* formation during interphase (*de novo* pathway): Here, a new centriole is synthesized in absence of a pre-existing mother centriole during S-phase. However, the precise molecular mechanism is unknown [11, 14, 15].

3: Accumulation of replicated centrosomes due to failed cell division after replication of centrosomes (accumulation pathway). Usually this accumulation pathway is associated with depletions (e.g. p53, cdk2) or amplifications (PLK-4, SAS6, Cyclin F) of regulatory proteins [11, 16-18].

4.2 Centrosome amplification – Cause or consequences of tumor formation?

Regardless of the mechanism underlying their induction, amplified centrosomes will affect the cell fate during mitosis. Maloriented kinetochores as a result of microtubules that originate from multiple poles will induce multipolar chromosome attachment, which in turn causes chromosomal instability (CIN) [19]. In CIN, one distinguishes between numerical (nCIN) and structural (sCIN) abnormalities, although both subtypes usually co-exist [20]. While nCIN describes the spectrum from gain and loss of chromosomes or chromosomal fragments, sCIN includes translocations, inversions, end-fusions and other complex rearrangements. Chromothripsis, the term for such random chromosomal alterations, is a result of premature mitotic entry, a common feature in carcinomas and neural tumors and mostly operative in micronuclei [11, 21-23]. Micronuclei in cancer are quite frequent as a result of a merotelic kinetochore attachment, where one kinetochore is attached to the microtubules of both spindle poles. The reason for such micronuclei is a transient state of multipolar mitotic spindles, as a result of supernumerary centrosomes implicating centrosome dysfunction as a cause of sCIN [11, 24, 25]. Changes within the DNA, as well as changes in chromosomal number can already be observed in preneoplastic lesions and small benign tumors. Especially in hepatocellular carcinoma a high degree of de-differentiation processes, as well as a high amount of aneuploidy can be observed [26]. Importantly, analyses of over 20.000 solid tumors revealed that aneuploidy is one of the main hallmarks of the progression of the disease [27].

To address the question if amplified centrosomes are the cause or the consequence of the malignant transformation process, multiple investigations have been performed over the last decades. The first proven evidence that aberrations in centrosome number initiate tumorigenesis was provided by a study from Basto et al. [28]. An *in vivo* Drosophila line harbored extra centrosomes in 60% of somatic cells, which were induced by the overexpression of SAK, the Drosophila homolog of PLK4 [28]. It could be shown that this SAK overexpressing cells could also form multipolar spindles, yet, through spindle assembly checkpoint (SAC) mediated clustering, the spindles became bipolar over time, resulting in a stable diploid state [28]. Importantly, when larval brain cells with extra centrosomes where transplanted into the abdomen of wild-type hosts, metastatic tumor formation was induced in this model [28]. From this experiment it was

concluded that centrosome amplification is the primary cause of the tumor formation. Similar observations were made in a study from Sabino et al. [29], which showed that SAK overexpressing wing tissue could also form tumors. However, both studies were unable to show tumor formation in SAK overexpressing donor flies itself. Furthermore, both studies state that there was no striking increase in genetic instability. On the contrary, flies with extra centrosomes maintained a stable diploid genome over many generations [28, 29]. Nevertheless, these studies confirm that SAK/PLK4 is one the major components in maintaining centrosome homeostasis. In human breast cancer, structural and numerical alterations in centrosomes have been first described systematically. Furthermore, it is known that PLK4 upregulation is found in 86.7% of breast cancer patients, which strengthens the Boveri hypothesis [30].

First *in vivo* mouse studies have shown that centrosomes amplification causes microcephaly [31], when PLK4 was tissue specifically overexpressed in the developing central nervous system. Specifically, neural stem cells that were unable to cluster supernumerary centrosomes were eliminated from the cycling population [31, 32]. In general, considering developmental stages in mammals, it seems that amplified centrosomes rather induce tissue degeneration, than tumor formation. A similar result was shown by Vitre et al. (2015) [33]. Here, PLK4- overexpression mediated centrosome amplification in mice did not induce spontaneous tumorigenesis [33]. Quite the contrary, chronic PLK4 overexpression beginning early in embryogenesis turned out to be lethal. Furthermore, p53 seemed to limit the continued cycling of cells which harbor supernumerary centrosomes, although PLK4-overexpression did still not affect tumorigenesis in p53 null mice [33].

Interestingly, a recent study from Levine et al. (2017) is contradictory to the before mentioned observations. Levine and colleagues state that PLK4 mediated centrosome amplification promotes spontaneous tumorigenesis in mammals, showing the development of lymphomas, squamous cell carcinoma and sarcomas after 36 weeks upon Dox inducible PLK4 overexpression [34]. In contrast to the previous studies, the overexpression of PLK4 was quite modest and did not exceed a 1.5-fold change compared to the control, and the animals had been observed over a much longer time period. Consistent with these results, loss of Kruppel-like factor (KLF)14 also triggers centrosome amplification and tumorigenesis [35]. Here, KLF14 functions as a transcriptional repressor of PLK4, suggesting the critical role of PLK4 regulation during

centrosome duplication. Furthermore, Fan et al. (2015) have identified a negative correlation between KLF14 and PLK4 in human cancers, supporting a negative regulation of PLK4 through KLF14 [35].

4.3 Centrosome and Centrosome cycle

Despite this controversy regarding the pathophysiology of centrosomes, their important role to maintain genomic stability at every cell division is proven. To ensure the unidirectional progress throughout every cell division cycle, multiple processes must be coordinated.

Hereby, the centrosome cycle is divided into 4 stages [36]: 1. disengagement/licensing 2. initiation 3. maturation/elongation 4. disjunction/bipolar spindle formation (Figure *2*)

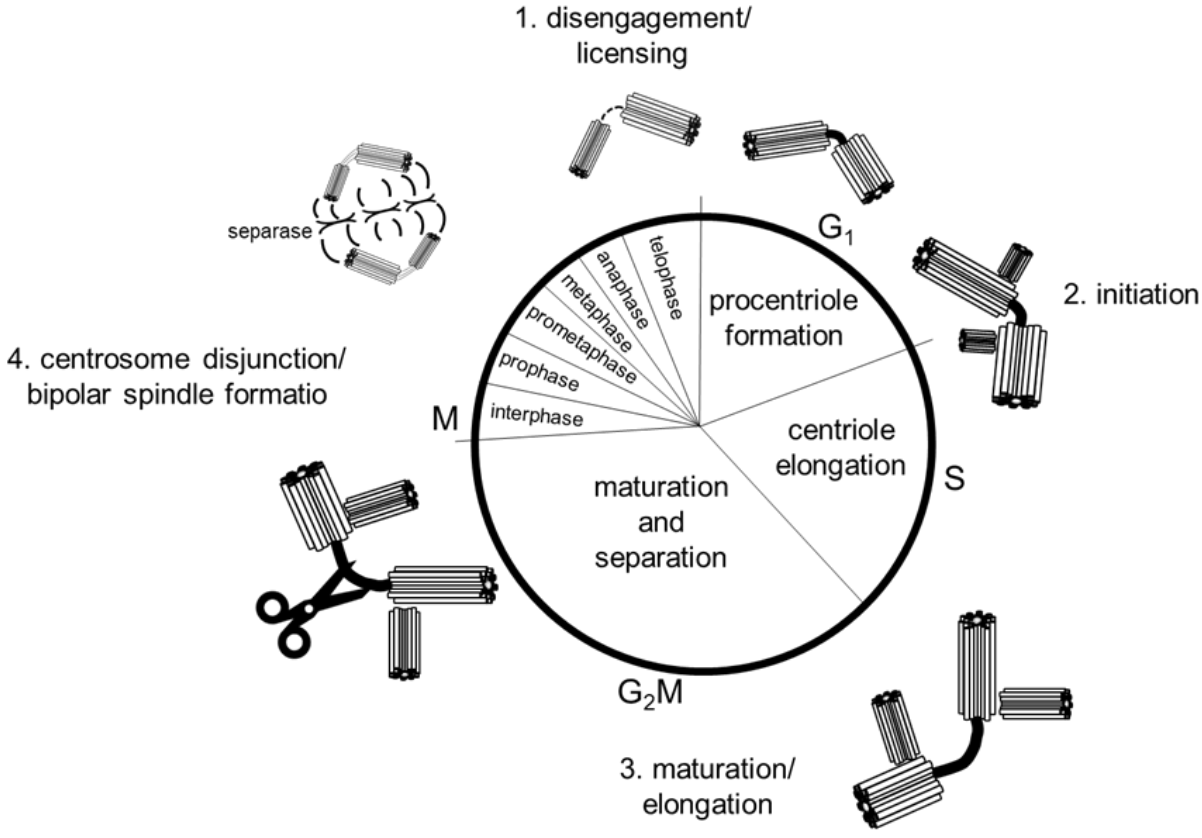

Figure 2 Centrosome cycle. Throughout the cell cycle, the centrosome is duplicated exactly one time. At the transition from G1 to S-Phase the duplication is initiated at the orthogonal proximal site of the mother centriole [7]. The newly synthesized procentriole elongates and matures throughout S- and G_2 Phase. In the beginning of mitosis and prior to anaphase, the connection of the duplicated centrosomes becomes disassembled. In late mitosis, the duplicated centrosome is separated, together with the duplicated chromosome, thereby licensing the newly synthesized centrosome for the next round of duplication (adapted from Fujita et al.2016 [7]).

4.3.1 Disengagement/licensing of the centrosome

The prelude to a new round of centrosome duplication starts in fact at the end of mitosis, where mother and daughter centrioles are physically separated and disorientated [7]. This disengagement is viewed as a crucial step licensing the centrosome for the next duplication round and prevents reduplication [7]. The disengagement of the duplicated centrosome is facilitated at anaphase, requires the anaphase-promoting complex and the protease separase, and is independent of exit from mitosis [7, 37]. Separase is activated by targeting its inhibitor, securin, through the E3 ligase Anaphase-Promoting-Complex/Cyclosome (APC/C)–Cdc20, which induces the proteasomal degradation of securin [38-40]. However, proteins like the microtubule- and kinetochore-associated protein Astrin or the AKT kinase-interacting protein 1 (Aki1) also localize to the centrosomes and regulate the stability of centriole cohesion, for example by inhibiting separase [41-43]. This interplay between cohesion stability and centrosome disengagement plays an important role to prevent premature cleavage and is crucial for the precise transition from metaphase to anaphase.

4.3.2 Initiation of centrosome duplication and maturation/elongation

The duplication of the centrosome starts at the transition from G1 to S-Phase, when the procentriole forms orthogonal to the proximal site of the mother centriole (Figure 3) [44]. At the same time the duplication of the DNA must be coordinated with the entry of the cell into the centrosome cycle [4]. These challenges of the cell machinery are primarily under the control of multiple ubiquitin ligases. For instance, quiescent cells ubiquitinate various regulatory proteins like S-Phase kinase associated protein 2 (Skp2) through the Anaphase-Promoting Complex/Cyclosome (APC/C), thus triggering the accumulation of p27 and therefore inhibition of the cell cycle progression in G_1 [10, 45]. At the same time, the E3 ubiquitin ligase APC/C^{Cdh1} targets central centrosomal proteins like CPAP, SAS6 for ubiquitination and proteasomal degradation to prevent premature centrosome duplication in early G_1 phase [46, 47]. However, at the transition from G_1-Phase to S-Phase CDK2/Cyclin A mediated phosphorylation of CDH1 inactivates the APC^{CDH1} complex. After activation of multiple phosphorylation dependent reactions, the CDK2/Cyclin E complex initiates the transition from G_1 into S-Phase [6, 48]. In parallel, the procentriole formation at the proximal end of each mother centriole takes place. The key protein responsible for the centrosome duplication initiation is the kinase polo-like kinase 4 (PLK4), which regulates the

precise reproduction of centrosomes in cooperation with Cdk2, CP110 and SAS6 [49-51]. In the beginning of procentriole formation PLK4 is recruited to the proximal site of the mother centriole together with the centrosomal protein (Cep) 192 and Cep 152 [52]. Here PLK4 recruits and phosphorylates STIL, as well as SAS6. This STIL-SAS6 interaction is a crucial step in the cartwheel formation and also recruits CPAP which later triggers the assembly of the microtubules [49, 53, 54].

After formation of the procentriole, the elongation of the daughter centriole starts with the entry into S-Phase and reaches out until G2 phase. Here, polo-like kinase 2 (PLK2) limits the procentriole formation and elongation by phosphorylating CPAP at the S589 and S595 residues [55]. The interaction of STIL with CPAP together with SAS6 stabilizes the cartwheel and recruits the microtubule triplets during the elongation process [7, 46, 56, 57]. During this elongation process in the S- and G2-phase Cep295 recruits POC5 and POC1B to the distal half centriole in G2, where the acetylation and glutamylation of the triplet MT is facilitated [58, 59]. The slow assembly of the centriolar MT controls the correct length of the centrioles, and throughout this process CPAP acts as the major regulatory protein within the centriole elongation [56, 57, 60].

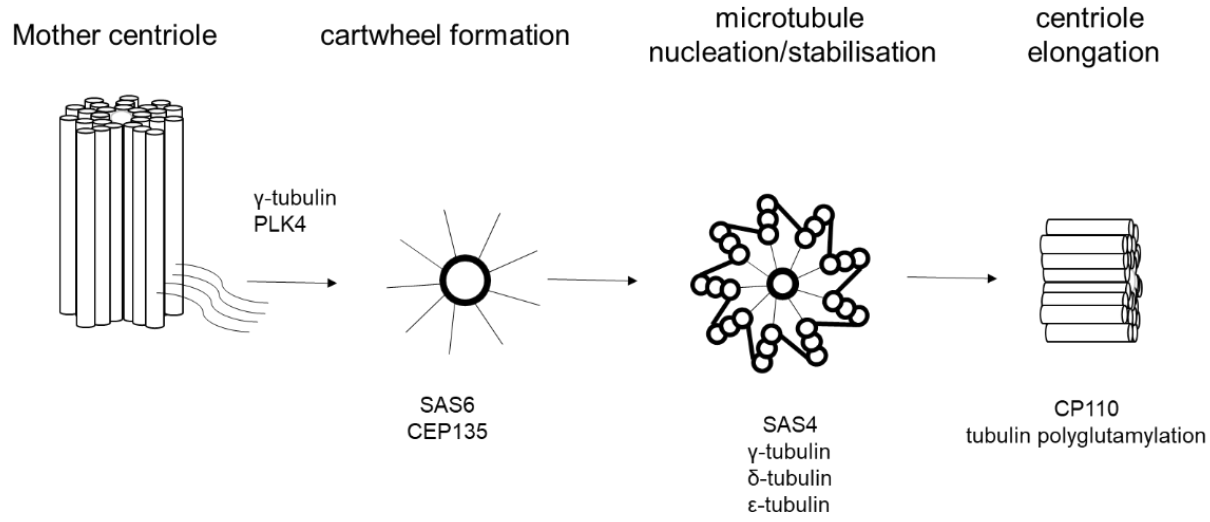

Figure 3 Cartwheel formation at G_1/S transition. At the transition of G_1 to S-phase, the polo like kinase 4 recruits SAS6 and CEP135 to the orthogonal proximal site of the mother centriole. The proteins are responsible to form the centrosomal cartwheel structure, which is the template for the formation of the 9-fold microtubule triplets. Together with SAS4, γ-tubulin, ε-tubulin and δ-tubulin this microtubule nucleation/stabilization takes place. After establishment of the new procentriole, posttranslational tubulin polyglutamylation, as well as the recruitment of CP110 ensures the centriole elongation (adapted from Wang [61]).

4.3.3 Centrosome disjunction and bipolar spindle formation

Following DNA and centrosome replication, the bipolar spindle formation takes place with the subsequent chromosome separation for correct chromosome segregation. By the end of centriole elongation, the parenteral centrioles are still connected to each other by the linker proteins C-Nap1 and rootletin [62]. This connection was established during the centrosome disengagement process in the previous cycle (see 4.3.1). At the mitotic interphase this connection will be disassembled, a process known as centrosome disjunction [63]. In a model from Mardin et al. (2011) [63], Mst2 assembles the NIMA (never in mitosis A) related kinase Nek2A and PP1y. Thereby, PP1y counteracts the kinase activity of Nek2A. The Nek2A/PP1 y complex ensures the premature centrosome separation prior to mitosis.

Following PLK1 mediated phosphorylation of Mst2, Nek2A becomes phosphorylated, which in turn phosphorylates the linker proteins C-Nap1 and rootletin. This leads to the disconnection of the centrosomes and bipolar spindle formation [62-64]. In parallel, PLK1 also activates the Nek9/Nek6/Eg5 cascade, which is crucial for the phosphorylation of the kinesin5/Eg5 and the spindle bipolarity [65-67].

4.4 The centrosome cycle initiation is controlled by the ubiquitin E3-ligase SCF^{FBXW5}

As mentioned, controlling the level of SAS6 at the transition from G_1 to S-phase is of high importance in regulating the initiation of the centrosome cycle. The interplay between activation and inhibition of SAS6 is a tightly controlled process regulated by the ubiquitin-proteasome system. SAS6 becomes specifically and covalently linked with multiple ubiquitin molecules, a small globular protein consisting of only 76 amino acids, ultimately licensing it for proteasomal degradation [68]. Ubiquitin-labelling of proteins (ubiquitination) is catalyzed by a cascade of three enzymes, which are named by their order of reaction: ubiquitin-activating enzyme E1 (or UBA), ubiquitin-conjugating enzyme E2 (or UBC), and ubiquitin ligase E3 (or UBR for ubiquitin recognition factor) [69-71].

In the initial step of this cascade, ubiquitin becomes activated in an ATP-dependent reaction by the ubiquitin-activating enzyme (E1, or UBA). For activation, a thioester bond is established between a thiol group (-SH) of an E1 cysteine and the C-terminal carboxyl group (-COOH) of glycine 76 of the ubiquitin molecule [72]. In a second step,

the activated ubiquitin becomes transferred by a transacylation reaction to the thiol group of a cysteine of the ubiquitin-conjugating enzyme E2, or UBC [73]. Finally, an E3 ubiquitin ligase catalyzes the transfer of the ubiquitin molecule to its substrate protein, resulting in an isopeptide bond between the carboxyl group of glycine 76 of ubiquitin and the ε-amino group of an internal lysine of the substrate protein [74].

Once the first ubiquitin molecule has been linked to its target protein, a polyubiquitin chain is formed in which the carboxy terminus of the next ubiquitin is linked to a lysine of the previous ubiquitin [75]. While the E2 enzymes influence the nature of the ubiquitin linkage [76], the E3 ubiquitin ligases provide substrate specificity by binding specific recognition motifs of the substrate proteins.

Prior to procentriole formation, the level of SAS6 is regulated via PLK4 and the E3-ubiquitin ligase SCF^{FBXW5} [1]. FBXW5 (F-Box and WD Repeat Domain Containing 5) is a member of the substrate recognition component of both SCF (SKP1-CUL1-F-box protein) and DCX (DDB1-CUL4-X-box) E3 ubiquitin-protein ligase complexes[1]. It consists of 566 amino acids and has a molecular mass of 64 kDa. In addition to the N-terminal F-box it carries three WD-repeats and a D-box – the D-box or destruction box promotes ubiquitination and degradation of a protein in a cell-cycle dependent manner [77].

One major interest of the regulatory function of FBXW5 is described by the study from Puklowski et al. (2011). It identifies the ubiquitin ligase SCF^{FBXW5} as a major target of PLK4 [1]. Once PLK4 is recruited to the mother centriole, FBXW5 is phosphorylated at S151 resulting in the dissociation of SAS6 from the SCF^{FBXW5} complex and the stabilization of STIL/SAS6 at the proximal end of the centriole [1, 78]. Loss of FBXW5, or expression of the phospho-mutant $FBXW5^{S151A}$, has led to an increase in the overall centrosome number in HeLa and U2OS cells.

4.5 Aim of the study

As outlined above, centrosome duplication is tightly regulated and must occur only once per cell division. As mitosis progresses, equal segregation of correctly duplicated centrosomes and chromosomes to the cell poles is required to maintain genomic stability. Interestingly, the centrosome duplication cycle is corrupted in most types of

[1] https://www.genecards.org/cgi-bin/carddisp.pl?gene=FBXW5

tumors, and it is still unclear whether centrosome abnormalities are cause or consequence of the tumor formation process.

Previous work from this laboratory has shown that the SCF E3-ubiquitin ligase FBXW5 acts as a major regulator of centrosome duplication. SCF^{FBXW5} ubiquitylate the spindle assembly abnormal protein 6 homolog (SAS6), an essential protein in the initiation of the centrosome duplication, thereby converting it into a proteasomal target. Depletion of the SCF^{FBXW5}-dependent degradation system leads to the development of supernumerary centrosomes and additional mitotic spindles [1]. However, these studies were performed in human cell lines already displaying malignant transformation phenotypes, i.e. HeLa and U2OS. While HeLa cells have a p53 null status [79], U2OS cells are known to overexpress MDM2, a negative regulator of p53 [80]. p53 deficiency is known to perturb normal centrosome homeostasis [17].

To evaluate a potential link between FBXW5 depletion, centrosome amplification and tumor formation it is therefore necessary to analyze cells under more physiological and healthier, i.e. uncompromised p53 expression conditions. To this end, this study applied two basic strategies to reduce the expression of FBXW5: (i) RNA interference (RNAi), specifically the microRNA embedded shRNA (miR shRNA) methodology and (ii) CRIPSR/Cas9 for a targeted gene editing of *Fbxw5*. Once FBXW5 is sufficiently suppressed, cells were analyzed regarding the number of centrosomes, as well as the impact of centrosome amplification towards the cell physiology, namely cell proliferation, cellular migration and cell transformation.

Furthermore, an *in vivo* mosaic mouse model is applied to answer the question whether a dysregulated centrosome cycle is sufficient to promote carcinogenesis in the mouse liver. Using the hydrodynamic tail vein injection (HDTVi) technique, the most potent shRNA as well as sgRNA shall be applied to attempt FBXW5 suppression in the murine hepatocytes *in vivo*.

5 Material and Methods

5.1 Biologicals

5.1.1 Bacterial strains

Stbl3: chemically competent *E. coli* for cloning of unstable DNA or plasmids harboring long tandem repeats (LTR)
DH5α-E: electrocompetent *E. coli*
DH5α: chemically competent *E. coli*
SW102: DH10α-derived strain containing a defective λ prophage, as well as *exo*, *bet*, and *gam* recombination proteins that are controlled by the temperature-sensitive repressor *cI*857.
SW106: Like SW102. Also, contains a tightly controlled arabinose-inducible *cre* gene.

5.1.2 Cell lines used

HEK 293T: human embryonal kidney cells; constitutively express the simian virus 40 (SV40) large T antigen[2]
Phoenix AMPHO: derived from HEK 293T, continuously expressing amphotropic envelope protein
NIH/3T3: mouse embryonal fibroblasts
BNL CL.2: mouse embryonal liver cells

5.2 Medium and substances

5.2.1 Antibiotics

Ampicillin	100	mg/ml
Kanamycin	25	mg/ml
Puromycin	10	mg/ml
G418 (Geneticin)	50	mg/ml

5.2.2 Cell culture medium and substances

All solutions and buffers used in cell culture were filter sterilized or autoclaved

[2] https://www.lgcstandards-atcc.org/products/all/CRL-11268.aspx?geo_country=de#generalinformation

DMEM („Dulbecco's Modified Essential Medium")-culture medium:

1x DMEM was purchased by Gibco. It consists of 4.5 g/l glucose, 4 mM L-glutamine.

Fetal bovine serum (FBS)

Fetal bovine serum (FBS) was purchased from Biochrom. 500 ml of FBS was heat inactivated at 65°C and aliquoted in 50 ml under sterile condition. The aliquoted FBS-stocks were stored at -20°C

PBS cell culture grade (Phosphate Buffer Solution)

Was purchased from Gibco and stored at 4°C

10x Trypsin/EDTA solution

Was purchased from Biozym. To prepare 1x Trypsin/EDTA solution, the 10x stock was diluted with Ca^{2+}/Mg^{2+} free PBS.

Full medium	DMEM
	10 % FBS
	100 U/ml Penicillin
	0.1 g/ml Streptomycin
Trypsin/EDTA	0.5 % Trypsin
	0.02 % EDTA

5.2.3 Microbiological medium and substances

All solutions and buffers used were sterile or autoclaved

LB-medium (according G. Bertani):	10 g/l Bacto-Tryptone
	5 g/l Yeast extract
	10 g/l NaCl
	pH 7.5 with NaOH
SOC-medium:	20 g/l Tryptone
	5 g/l Yeast extract
	0.6 g/l NaCl
	0.2 g/l KCl
	2.0 g/l $MgCl_2$ x 6 H_2O
	2.5 g/l $MgSO_4$ x 7 H_2O
	pH 7.0
	add 20 ml 1 M glucose (filter sterilized)
LB-agar:	LB-Medium
	15 g/L Agar
	autoclaved
	Storage at 4°C

LB- agar/amp:	100 µg/ml Ampicillin Storage at 4°C
LB-agar/kana:	30 µg/ml Kanamycin Storage at 4°C

5.2.4 Buffer and solutions for virus amplification

2 x HBS-buffer:	50 mM HEPES, pH 7.04 10 mM KCl 12 mM Dextrose 280 mM NaCl 1.5 mM Na_2HPO_4
2x $CaCl_2$:	2 M $CaCl_2$
Chloroquine:	100 mM

5.2.5 Buffer and solutions for DNA-extraction, -purification and genotyping

Proteinase K buffer:	10 mM Tris pH 8.0 5 mM EDTA pH 8.0 200 mM NaCl 0.2 % SDS
Isopropanol	p.A.
EtOH	70%
NaOAc-solution:	3 M NaOAc pH 5.2 using acetic acid
TE (Tris- EDTA-buffer):	10 mM Tris 1 mM EDTA pH 7.5

<u>Buffer for Plasmid isolation:</u>

P1-buffer:	50 mM Tris/HCl 10 mM EDTA 100 µg/ml Ribonuclease A pH 8.0
P2-buffer:	200 mM NaOH 1 % SDS
P3-buffer:	3 M Potassium Acetate pH 5.5

Buffers for agarose gel electrophoresis:

50xTAE (Tris-acetate-EDTA):	2	M Tris-Base
	250	mM NaOAc
	50	mM EDTA
0.5x TAE:	1	Vol. 50x TAE
	99	Vol. ddH_2O
10x Loading dye:	50	% Glycerol
	0.25	% bromophenol blue
	0.25	% xylene cyanole FF
		in 1x TAE buffer

5.2.6 Buffer and solutions for immunohistochemistry

3,7 % Paraformaldehyde:	14.8	g Paraformaldehyde
	200	ml PBS
DAPI-stock solution:	1	mg/ml in PBS
DAPI-working solution:		1:10000 dilution of DAPI-Stock in PBS
Propidium iodide-staining solution:	10	µg/ml Propidium iodide
	0.25	mg/ml RNase A in PBS
10xPBS:	80	g NaCl
	2	g KCl
	11.5	g Na_2HPO_4*$7H_20$
	2.4	g KH_2P0_4
		add to 1l with ddH_2O

5.2.7 Buffer and solutions for biochemical analysis

RIPA-buffer:	50	mM Tris-HCl, pH 8,0
	80	mM NaCl
	50	mM NaF
	20	mM $Na_4P_20_7$
	1	mM EDTA
	1	mM EGTA
	1	% (w/v) NP-40
	1	% (w/v) DOC
	0.1	% (w/v) SDS
4x-SDS-sample buffer:	2	% (w/v) SDS
	5	% (v/v) -Mercaptoethanol
	10	% (v/v) Glycerol
	62	mM Tris
	0.001	% (w/v) Bromophenol blue
		in H_2O, pH 6.8

10x SDS-running buffer:	250	mM Tris-HCl, pH 8.3 - 8.6
	1.92	M Glycine
	1	% (w/v) SDS
10x Washing buffer (TBS-T):	100	mM Tris; pH 7.6
	1.5	M NaCl
	0.5	% (v/v) Tween20
Blocking-solution:	5	% w/v non-fat dry milk powder in 1xTBST
Transfer buffer	25	mM Tris
	190	mM glycine
ECL solution 1	25	mM Luminol
	0.4	mM p- coumaric acid
	100	mM Tris- HCl, pH 8.5
ECL solution 2	100	mM Tris- HCl
	0.02	% H_2O_2

5.2.8 Oligonucleotides

All oligonucleotides (primer) used for the study are listed in (Table 1). Sequences of the hairpin oligonucleotides used are listed in (Table 7). Oligonucleotides were purchased from Sigma-Aldrich.

Table 1 List of cloning primers

ID	Sequence	Annealing temperature
5′miR-30-XhoI	tacaatactcgagaaggtatattgctgttgacagtgagcg	52°C
3′miR-30-EcoRI	acttagaagaattccgaggcagtaggca	
5’miR-E-Xho-short	agaaggctcgagaaggtatattgc	56°C
3’miR-E-EcoPlasmid	gctcgaattctagccccttgaagtccgagg	
5’miR-E-Xho	tgaactcgagaaggtatattgctgttgacagtgagcg	
3’miR-E-EcoOligo	tctcgaattctagccccttgaagtccgaggcagtaggc	
Myc-tag AgeI fw	ggccaccggtaaagctatggagcaaaa	45°C

ID	Sequence	Annealing temperature
Myc-tag AgeI rev	ggccaccggtagtcctcttcagaaatgag	45°C
lox-Neo-lox fw	gagactgcggcagaaccacaacagcacatcagtcctttcccctctgcct ccagcccagagccctctcccttctcgagttcctgcagcccaattccgatcat	63°C
lox-Neo-lox rev	caggtacgccaactctttgagaacacaggggtccctggccgcttcttgttc caaggtgaggcaggggcatcatcccctcgagggacctaa	
frt-Neo-frt fw	ggtgggctccagggcttgggtatgggcttcagcaggtgggtgtgggctca gaagttcctattctctagaaagtataggaacttcaggtctgaagaggagttt	60°C
frt-Neo-frt rev	ccagatatagccatgccgatcttcagccccactgtgggatagcatctgga ataacttcgtatagcatacattatacgaagttatattatgtacctgactg	
Spe UP fw	ataactagtaagcttgtcatctggggaa	60°C
Age UP rev	ataaccggtcgatgcccacctagaacag	
AgeI DOWN fw	agcgaccggtggtcctccaagagactgaagag	60°C
XbaI DOWN rev	acgctctagaaaagttctgacctgggttctgg	

Table 2 *Fbxw5* screening primer

ID	Sequence	Annealing temperature
F1	agccctgtacctggtcactttg	60°C
B1	acagtgcttaagcccacacc	
F2	ggcagaaccacaacagcacatc	
B2	agtctgggtgcctcctcttatg	
F3	tgcctacacacccaatgacgag	
Neo B1	ccagaaagcgaaggagcaaagc	
Neo F1	tgaccgcttcctcgtgctttac	
B3	agaggcagacatcaccatgacg	
B4	tggccctgtcaaagtcccaaat	
Fbxw5 E4 fw	caaccaggatgactcactgc	58°C
Fbxw5 E6 rev	cattgcactctggaggcttg	

Table 3 Standard sequencing primer

ID	Sequence	Annealing temperature
mirR seq	tgtttgaatgaggcttcagtac	60°C
U6 sponge F	ggactatcatatgcttaccgtaacttga	60°C

Table 4 qPCR primer

ID	Sequence	Annealing temperature
qPCR Fbxw5 fw	cacgtactcaccgcatcagatc	60°C
qPCR Fbxw5 rev	ggtccagggcatcaaagaag	
18S rRNA for	cggctaccacatccaaggaa	60°C
18S rRNA rev	gctggaattaccgcggct	
18S rRNA sonde	[joe]tgctggcaccagacttgccctc[tam]	

Table 5 Primers for NGS by CeGAT

ID	Sequence	Annealing temperature
sg2 seq	ctgataacaggtgggcctgg	60°C
BC sg2 rev	gtctcgtgggctcggagatgtgtataagagacagtgctgaagcccatacccaag	58°C
BC sg2 fw	tcgtcggcagcgtcagatgtgtataagagacagccttctttgatgccctggac	
MiSeq Library fw	tcgtcggcagcgtcagatgtgtataagagacagcttgaaagtatttcgatttcttgg	50°C
MiSeq Library rev	gtctcgtgggctcggagatgtgtataagagacagactcggtgccacttttttcaa	

Table 6 Mouse genotyping primers

ID	Sequence	Annealing temperature
p19 Arf-1	agtacagcagcgggagcatgg	65°C
p19 Arf-2	tttgaggaggaccgtgaagccg	
p19 Arf-3	accacactgctcgacattggg	
p21-exon-144	gaactttgacttcgtcacgg	56°C
p21-genU	acaacacctcctggtcagagg	
p21 PGK-neo3	gaagaacgagatcagcag	
p53 loxP A	cacaaaaacaggttaaaccca	58°C
p53 loxP B	agcacataggaggcagagac	
Cre fw	ggaaatggtttcccgcagacc	60°C
Cre rev	acggaaatccatcgctcgacc	
FAH A	ctaggtcaatggctgtttgg	56°C
FAH B	ggacataccaatttggcaac	
FAH C	taaaatgaggaaattgcatcg	

Table 7 Templates for shRNA cloning

ID	Sequence
shFbxw5.553	tgctgttgacagtgagcgccacccagttttcccagttcaatagtgaagccacagatgtattgaactgggaaaactgggtgttgcctactgcctcgga
shFbxw5.1730	tgctgttgacagtgagcgaagcgacgatgccactatcaaatagtgaagccacagatgtatttgatagtggcatcgtcgctgtgcctactgcctcgga
shRPA2.359	tgctgttgacagtgagcgcaacattgtttacaagatagatagtgaagccacagatgtatatcttgtaaacaatgttggttgcctactgcctcgga
shRPA2.876	tgctgttgacagtgagcggacgatcactttaagtctacatagtgaagccacagatgtatagacttaaagtgatcgtcgttgcctactgcctcgga
shRen.713	tgctgttgacagtgagcgcaggaattataatgcttatctatagtgaagccacagatgtatagataagcattataaattcctatgcctactgcctcgga

Table 8 Oligonucleotides for sgRNA cloning

ID	Sequence
sgFbxw5.2 sense	*cacc*ggtcggctaccactgagcca
sgFbxw5.2 anti-sense	*aaac*tggctcagtggtagccgac*c*
sgFbxw5.3 sense	*caccg*attctaccgctactaccag
sgFbxw5.3 anti-sense	*aaac*ctggtagtagcggtagaat*c*
sgFbxw5.4 sense	*caccg*gaggtccgggctatcaaag
sgFbxw5.4 anti-sense	*aaac*ctttgatagcccggacctc*c*
sgFbxw5.18098 sense	*caccg*gatgacagctatctcgcctg
sgFbxw5.18098 antisense	*aaac*caggcgagatagctgtcatc*c*
sgFbxw5.18105 sense	*caccg*gcgtgtgtttgatagcgtct
sgFbxw5.18105 antisense	*aaac*agacgctatcaaacacacgc*c*

5.3 Methods

5.3.1 Cultivation of bacteria

E. coli were plated on 15% LB agar plates containing the appropriate antibiotics and incubated at 37°C. From these plates, single colonies were picked for further cultivation. The cultivation of transformed bacteria was performed as continuously rotating liquid culture at 37°C. The sterile LB medium was supplemented with the appropriate antibiotic (kanamycin, ampicillin) for selection.

5.3.2 *E. coli*-Transformation through heat shock

25 µl of chemo competent DH5α *E. coli* (Invitrogen) were mixed with 100 ng of plasmid DNA or ligation mixture respectively, and incubated on ice for 15 min. Subsequently the cells were incubated at 42°C for 20 sec followed by incubation on ice for another 5-10 min. For recovery, the cells were taken up in 500 µl SOC-medium and incubated for 30 min at 37°C with continuous shaking. Finally, the cells were plated on LB-agar containing the appropriate antibiotic (ampicillin; final concentration 100 µg/ml; kanamycin; final concentration 50 µg/ml) and incubated overnight at 37°C. Next day single colonies were picked and transferred to 5 ml LB medium to prepare an overnight culture. After verification of the isolated plasmids (Miniprep; see 5.3.17.1) a glycerol stock of the bacteria culture was prepared (15% Glycerol, 85% culture broth) and stored at -80°C. From the remaining culture 1/100 was used to inoculate a large culture of 200 ml for maxiprep preparation.

5.3.3 Electroporation of *E. coli*

50 µl of ElectroMAX™ DH5α-E™ Competent Cells (Invitrogen) were mixed with 100 ng plasmid DNA, or 100 ng ligation mixture respectively and incubated on ice for 5min. For electroporation, the bacteria were transferred to a 0.2 cm Gene Pulser®/Micropulser™ electroporation cuvette and put to the Gene Pulser electroporation device. The setting for electroporation was 25 µF, 200 Ω und 1,75 kV. For recovery, the cells were taken up in 1 ml prewarmed SOC medium and incubated at 37°C for 1 h at continuous shaking. Finally, the cells were plated on LB-agar containing the appropriate antibiotic at different dilutions (10^4-10^6) and incubated overnight at 37°C.

For library electroporation, the step of electroporation was repeated two more times.

After recovery one representative dilution of 1:10^4 was prepared. The remaining recovered bacterial cells were distributed on LB-agar plates and incubated overnight. Next day cells were collected and subjected to maxiprep for isolation of the plasmid DNA library.

5.3.4 Cultivation and passaging of eukaryotic cells

All cells were cultured using 1x DMEM containing 10%FBS and penicillin/streptomycin to avoid contamination. On a regular basis, cells were splitted. For this purpose, the cells were washed once with Ca^{2+} free PBS and incubated in 1x Trypsin/EDTA to detach cells from the bottom of the flasks at 37°C for 3-5 min. Subsequently, trypsin was inactivated by adding four times the volume of culture medium, which encompasses 10% FBS, that contains protease inhibitors like α_1-antitrypsin and α_2-macroglobulin and stop the trypsinization process. After centrifugation (5 min at 800 xg) the supernatant was removed, and the cell pellet suspended in culture medium. From this solution one third was used for onward cultivation. For cell number determination, the Neubauer counting chamber was used. This chamber is square-shaped and divided in four equal sub-squares. For the determination of the approximate cell number, the average value of all four squares - corresponding to 0.1 mm^3 - equals the cell number in 1 ml of the medium. The appropriate cell number was determined using the following formula:

$$\frac{\textbf{Cell number}}{\textbf{number of squares}} * \textbf{dilution factor} * \mathbf{10^4} = \textbf{cell number/ml}$$

5.3.5 Determination of doubling time of cells

Cells were seeded at a defined cell number. Every 24 h, cells were counted according to (5.3.4). For the calculation of the growth rate the following formula was applied:

$$gr = ln\left(\frac{N(t)}{N(0)}\right)/t$$

gr: growth rate
N(t): number of cells at time
t N(0): number of cells at time *0*
t: time in *h*

Based on the growth rate the doubling time was calculated using the formula:

$$doubling\ time = \frac{\ln(2)}{growth\ rate}$$

5.3.6 Migration assay

Cells were seeded in a 60mm-tissue plate and grown to confluency. Later, cells were washed 3 times with PBS. Afterwards a scratch was done using a 10µl white tip for each sample and the cells were supplemented with starvation media containing 2% FCS. Pictures were taken immediately after the scratch, and after 24 h (Zeiss Axiocam ERc 5s, Jena). Cells were incubated for an additional 24h after h which the photographs were taken for the wounded area. The migrating cells were calculated according to the following formula:

$$\textbf{Migration Index} = \frac{\textbf{Width of the wound}_{\textbf{0h}} - \textbf{Width of the wound}_{\textbf{24h}}}{\textbf{Width of the wound}_{\textbf{0h}}} \times \textbf{100}$$

5.3.7 Cryopreservation of cells

Cryopreservation in liquid nitrogen was used for long-term storage of eukaryotic cells. For this purpose, the cells were detached using 1x Trypsin/EDTA and centrifuged (5min; 800 xg, 4°C). The cells were counted and $1x10^6$ cells were resuspended in 1 ml freezing medium (90% FBS and 10% DMSO). The cells were given in a polypropylene cryotube and slowly frozen to -80°C (1°C/min). After 48 h the vials were transferred to liquid nitrogen for long-term storage. For control one representative vial was thawed and incubated at 37°C until the cell suspension was liquefied. This suspension was added to 10 ml prewarmed culture medium and centrifuged (5min, 800 xg) to remove the remaining DMSO. The cell pellet was resuspended in 10 ml culture medium and transferred to the appropriate culture dish.

5.3.8 Transfection of BNL CL.2 cells

Transfection is a technique to insert exogenous nucleic acids into eukaryotic host cells. The efficiency of transfection was determined by the overexpression of a reporter gene like GFP (green fluorescent protein). Using fluorescence microscopy, the overall cell number of GFP-positive cells could be analyzed.

Transfection von BNL CL.2-Zellen using Effectene® Transfection Reagent

Effectene is a non-liposomal lipid Transfection Reagent spontaneously forming micelle structures. It is capable of forming complexes with highly condensed DNA, thus representing an effective way to transfer foreign DNA into eukaryotic cells. For transfection, cells were seeded to 40-60% density followed by the instructions given according to the manufactures protocol.

5.3.9 Virus work

The lenti- or retroviruses used are assigned to be security level 2 (S2) since they are replication deficient. To produce replication deficient retroviruses the PHOENIX-AMPHO packaging cell line was used. To produce replication deficient lentiviruses HEK293T was used.

5.3.9.1 Retrovirus production

Retrovirus production was done according to Serrano et al. [81]. PHOENIX AMPHO cells were transfected with 20 µg retroviral plasmid DNA according to Chen & Okayama [82], carrying the gene of interest together with gag (encoding the structural proteins of the virus), pol (encoding reverse transcriptase) and env (encoding the envelope protein). The day before transfection PHOENIX AMPHO cells were seeded to have 60% confluency next day. Before preparing the transfection mixture, cells were washed once with PBS and incubated with fresh culture medium containing 25 µM chloroquine. For transfection 20 µg of plasmid DNA was mixed with 62.5 µl 2 M $CaCl_2$ and filled up to 500 µl with ddH_2O. After addition of 500 µl 2x Hepes buffer under bubbling the solution was incubated for 15 min at room temperature. Subsequently the transfection mixture was added dropwise to the cells, which were incubated 12 h at 37°C. Next the medium was changed and the supernatant harvested every 12 h for 2 days. The retrovirus containing supernatant samples were sterile filtered and used for the transduction of the target cells. The retrovirus suspension was stored at 4°C for short term (1 week) or at -20°C for long term storage (up to 3 months).

5.3.9.2 Lentivirus production

For lentivirus production, HEK293T cells were transfected with 20 µg of lentiCRISPR V2 plasmid DNA according to Chen & Okayama [82], VSV-G, and pCMV-dR8.2 encoding for the gene of interest (e.g. CRISPR/Cas9 elements) together with gag, pol and env. Transfection was done according to 5.3.8. 12-16 h after transfection, the medium was changed. The lentivirus containing supernatant was harvested every 12 h for 2 days, sterile filtered and used for the transduction of target cells. The retrovirus suspension was stored at 4°C for short term (1 week) or at -20°C for long term (up to 3 months).

5.3.10 Transduction of cells

Target cells were transduced at a confluency of 30% with a MOI of 0.3 to achieve 30% transduction efficiency. To increase the transduction efficiency, polybrene was added to a final concentration of 10 µg/ml. The infected target cells were incubated at 37°C and 5% CO_2 for 48 hours. To achieve stable transduction, cells were treated with 3 µg/ml puromycin for 24-48 hours.

5.3.11 Crystal violet staining

To visualize the cell colonies, cells were washed twice with PBS and fixed for 30 min at room temperature with 4% formaldehyde. Afterwards, cells were washed 2x with PBS and incubated with crystal violet staining solution (0.02% crystal violet) for 1 h. Staining solution was discarded, and the fixed and stained cell colonies were washed twice with water and air dried.

5.3.12 Cell synchronization

5.3.12.1 Cell cycle synchronization of cells in S phase

Cell cycle arrest in S-phase was achieved by treating the cells with high concentrations of thymidine, which interrupts the deoxynucleotide metabolism pathway resulting in an inhibition of DNA replication.
Thymidine was added to asynchronous growing cells at a concentration of 2 mM. After 16 h of treatment with thymidine cells are assumed to be arrested at the G1/S transition. Next, cells were washed twice with prewarmed culture medium and harvested and analyzed for cell cycle release in short time intervals.

5.3.12.2 Cell cycle synchronization of cells in G2/M phase

Cell cycle arrest in G2/M phase was achieved by treating the cells with the microtubule-depolymerizing chemical nocodazole (Sigma). Nocodazole was given to asynchronous growing cells at a concentration of 400 ng/ml. After 16 h of treatment, the metaphase arrested cells had adopted a round shape and could be shaken off. The remaining cells were assumed to be in G2 phase. These cells were washed once with prewarmed PBS and twice with prewarmed nocodazole-free culture medium. For analysis, cells were harvested in short time intervals for cell cycle release.

5.3.12.3 Flow cytometry cell cycle analysis

To determine the cell cycle status of a cell population, fluorescence-activated cell sorting (FACS) was employed. To this end samples were permeabilized and treated with the fluorescence dye propidium iodide, which's fluorescence intensity correlates with the amount of DNA. Since the amount of DNA of cells in G2 phase is doubled compared to cells in G1 or G0 phase it is possible to clearly distinguish the individual cell populations in a histogram.

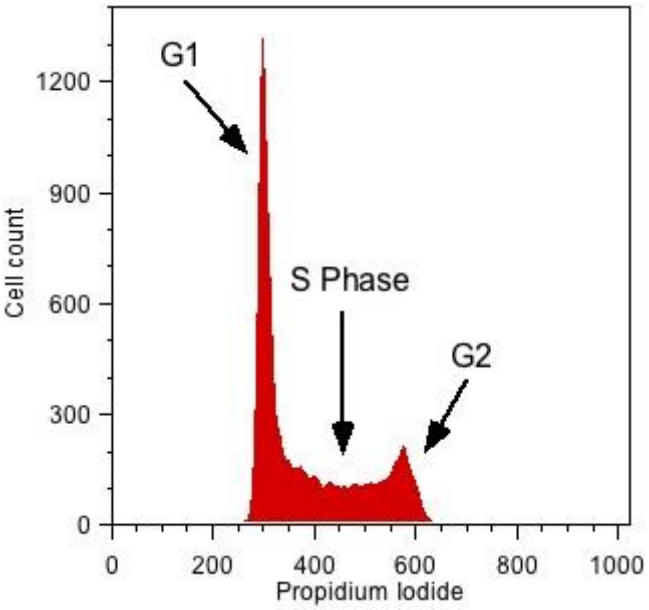

Figure 4: Typical DNA histogram with propidium iodide stained cells: (source: https://bitesizebio.com/20298/cell-proliferation-round-1-using-thymidine-analogs-with-flow-cytometry/)

In addition, light scattering and diffraction can be used to measure the size and granularity of the cells. To analyze the different cell cycle phases, cells were harvested from the culture dish by trypsinization for 5 min. Subsequently trypsin was inactivated by adding 4x volume of culture medium - which contains 10%FBS - and transferred to a 15 ml Falcon tube. The cell pellet was washed twice with PBS to remove remaining trypsin and fixed in ice-cold 70% ethanol for at least 12 h at -20°C. For staining, cells were pelleted (800 rpm, 5 min, 4°C) and resuspended in 1 ml propidium iodide staining solution and incubated for 30 min at room temperature in the dark. Flow cytometry analysis was performed using the BD LSRII fortessa cell analyzer and evaluated with the FlowJo™ software (Version 10; Becton, Dickinson and Company; 2019.).

5.3.13 Molecular biological methods

5.3.13.1 Endonuclease restriction of nucleic acids

To cut DNA into defined size at specified foci special restriction endonuclease enzymes were used. Such endonucleases can recognize specific sequences within the DNA and hydrolyze the phosphodiester bond between the nucleotides. To modify the plasmid DNA, type II restriction endonucleases (e.g. XhoI, EcoRI) were used. Such enzymes “cut” the DNA specifically within a defined sequence, allowing the characterization of plasmid DNA (restriction analysis), or to create fragments suitable for cloning. For all enzymes used, the manufacturer’s buffers and protocols were applied. A typical reaction mixture is:

10xNEBuffer	5	µl
Enzyme 1	1-2	µl
Enzyme 2	1-2	µl
10xBSA	4	µl
Plasmid-DNA (10 µg)	x	µl
ddH2O	add to 50	µl

5.3.13.2 Dephosphorylation of 5‘-ends

The enzymatic cleavage of plasmid DNA results in a 5’-triphosphonucleotide and 3’-hydroxylgroup residue. The resulting gap can be used to insert a DNA fragment having the same cohesive ends and “glued” together using the enzyme ligase. To avoid re-ligation of the vector DNA, it is recommended to convert the 5’-triphosphate to a 5’ monophosphate residue. The calf intestinal phosphatase (CiP; NEB) is an enzyme that non-specifically catalyzes the dephosphorylation of 5´ and 3´ ends of linearized DNA. After the enzymatic digestion of plasmid DNA, 0.5-1.0 U of CiP was given to the reaction and incubated for another 1.5 h at 37°C. Since CiP is a Zn^{2+}- and Mg^{2+}-dependent enzyme, the metal chelator EDTA is added to the reaction for inactivation.

Restriction approach	20	µl
10xCIP-buffer	4	µl
CIP	1	µl
ddH2O	add to 40 µl	

5.3.13.3 Blunt ending of overhangs

As mentioned before the incorporation of a DNA fragment into enzymatically cleaved plasmid DNA requires compatible cohesive ends. However, different type II restriction endonucleases recognize different sequence patterns which may result in 3'-overhangs, 5'- overhangs, or blunt ends, respectively. To combine non-compatible ends, it is useful to convert non-matching 3´- or 5´-overhangs to blunt ends using T4 DNA polymerase. The T4 DNA polymerase is an enzyme which catalyzes the synthesis of DNA in the 5´→ 3´ direction, but also has a 3´→ 5´ exonuclease activity. This offers the possibility to blunt end 3' or 5' overhangs. For the reaction, 50 µl linearized plasmid DNA should be dissolved in 1x reaction buffer (NEB) supplemented with 100 µM dNTPs and 1 U T4 DNA polymerase. The mixture is incubated for 15 min at 12°C. For inactivation, 10 mM EDTA (final concentration) was given to the reaction and incubated at 75°C for 20 min.

5.3.13.4 Precipitation of nucleic acids

To precipitate DNA from a solution, 0.1 V 3 M NaOAc and 2.5 V 100% EtOH was added to the solution. DNA is precipitated by the addition of 0.1 V 3M NaOAc and 2.5 V 100% EtOH and incubation for 30 min at -80°C. Under these conditions the nucleic acids become insoluble because of their polar phosphate group and can be precipitated at -80°C for 30 min. After centrifugation at 17000g for 30min the precipitated DNA pellet was washed with 2.5 V 70%EtOH to remove remaining traces of NaOAc, followed by an additional centrifugation (17000g; 15 min; 4°C). The supernatant was discarded and the DNA pellet air dried for 5-10 min. Finally, the DNA was dissolved in 20-50 µl ddH_2O, or TE-buffer respectively.

5.3.13.5 DNA-size separation (electrophoresis)

Agarose gel electrophoresis is used to separate DNA fragments by length/size through a three-dimensional matrix of agarose molecules across an electric field. It serves for the estimation of DNA fragment size after endonuclease II digestion of plasmids, control of PCR amplified fragments, or for separation and isolation of DNA fragments for cloning. The DNA fragment solutions were mixed with 10x DNA-loading dye and separated on a 0.8-2.0% agarose gel (containing 10 µg/ml EtBr), depending on the fragment size. For electrophoresis, the gel is covered with 0.5x TAE-buffer. The settings for DNA separation were 120 V for 0.5-1.5 h. DNA fragments were visualized on a UV-illumination table.

5.3.13.6 Ligation of DNA-fragments

To covalently join two DNA fragments, ligases were used. These enzymes form a phosphodiester bond between the free 3'OH group of one nucleotide with the tertial 5'-phosphate group of another nucleotide. This enzymatic reaction is ATP-dependent and was performed in a molecular ratio of 1:5 (Vector: Insert). The amount of insert and vector DNA was calculated using the following formula:

$$\mathbf{5} * \mathbf{X_{ngVector}} * \frac{\mathbf{Insert_{basepairs}}}{\mathbf{Vector_{basepairs}}} = \mathbf{x_{ng\ Insert}}$$

The ligation was performed at 16°C for 1h or at room temperature overnight, followed by inactivation at 65°C for 10 min. 1-5 µl of this ligation mixture was used for transformation of chemically competent *E. coli* DH5α. Alternatively, the DNA was extracted with phenol and precipitated with EtOH. The precipitated DNA was dissolved in 5-10 µl ddH_2O, and 1-5 µl were used for electrotransformation in ElectroMAX™ DH5α-E™ competent cells. The ligation reaction is:

Vector	100	ng
Insert	x	ng
10x Ligation buffer	2	µl
Ligase	0.5	U
ddH_2O	add to 20	µl

5.3.14 Plasmids used for the design of a conditional *Fbxw5* targeting vector

All plasmids were purchased from the NCI AT FREDERICK laboratory.

BAC$^{e3.6}$: Bacterial artificial chromosome (GenBank Accession No. U80929) clone RP23-47P18 containing mouse DNA sequence on chromosome 2 (including *Fbxw5*) chloramphenicol antibiotic resistance [83].

pL451: pL451 was constructed by Liu et al. [84] and contains a *FRT–PGK–EM7–NeobpA–FRT–loxP* selection cassette, which is suitable for gene targeting in ES cells. The PGK driven *Neo* works efficiently for selection in eukaryotes and the EM7 driven *Neo* for *E.coli*. *FRT* displays a DNA recognition site for a Flp recombinase. DNA located between two *FRT* sites can be excised by transient expression of a genetically enhanced Flp recombinase as described previously [85].

pL452: pL452 consist a *loxP–PGK–EM7–NeobpA–loxP* cassette. Whereas the PGK permits efficient *Neo* expression in mammalian cells, the EM7 allows *Neo* to be expressed in bacterial cells resulting in a kanamycin resistance. Cre recombinase recognizes both *loxP* sites, resulting in a removal of the PGK-EM7-NeobpA cassette leaving a single *loxP* site behind [84].

pL253DT: A pBluescript-derived plasmid for retrieval of DNA from a BAC. This plasmid contains a diphtheria toxin fragment A cassette for negative selection in ES cells and an ampicillin selection cassette for selection in *E.coli* [84].

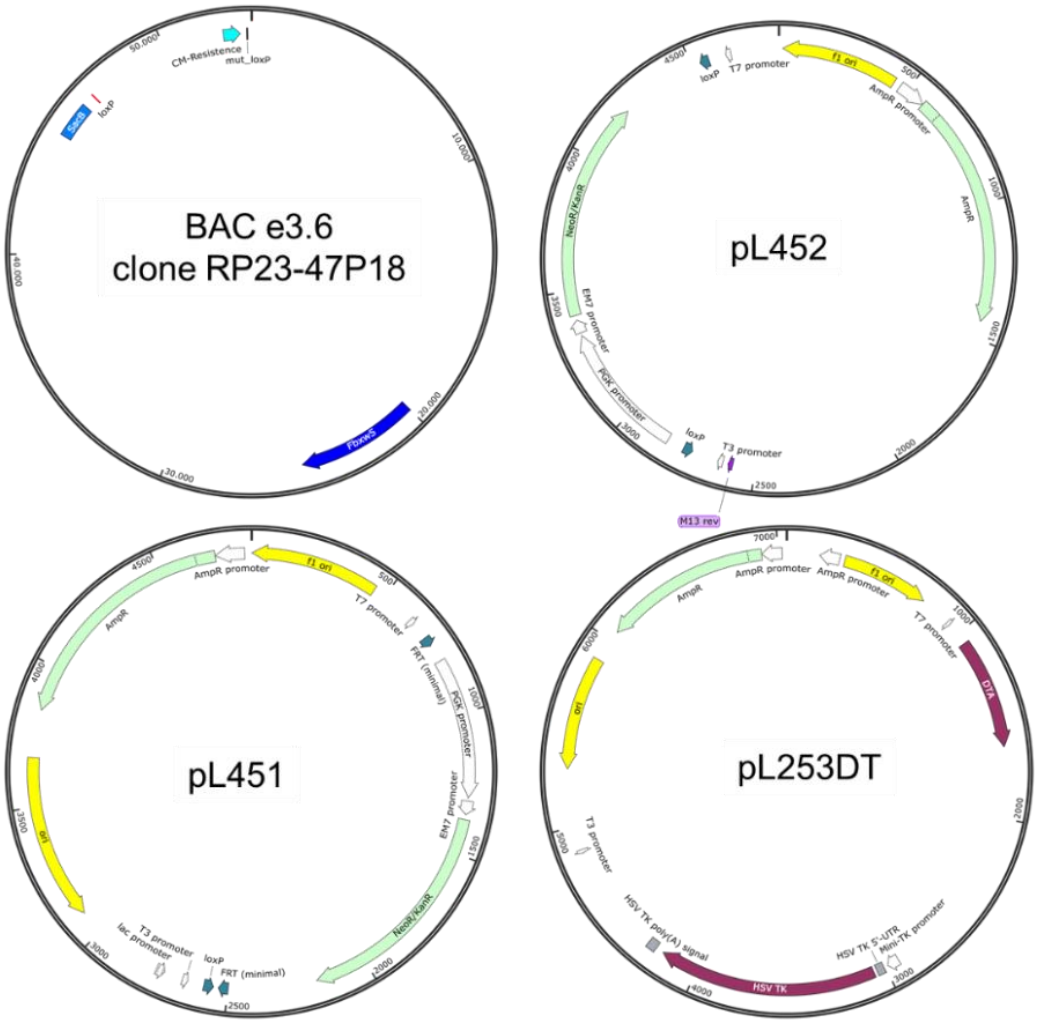

Figure 5 Overview of plasmids used for the design of a conditional *Fbxw5* targeting vector. Upper left: Bacmid DNA containing mouse *Fbxw5*. Upper right: Plasmid pL452 containing loxP–PGK–EM7–NeobpA–loxP cassette. Lower left: pL451 containing FRT–PGK–EM7–NeobpA–FRT–loxP. Lower right. DNA retrieval vector pL253DT containing diphtheria toxin fragment A for negative selection in ES cells.

5.3.15 Generation of CRISPR/Cas9 vectors, and microRNA-based shRNAs, to suppress FBXW5 expression *in vitro* and *in vivo*

The microRNA (miR) embedded shRNA against *Fbxw5* was designed according to Fellmann et al. (2013) [86], using an online siRNA prediction tool (DSIR; http://biodev.extra.cea.fr/DSIR/DSIR.html). The two most promising sequences were used to design the miR-shRNA oligonucleotides (5′-TGCTGTTGACAGTGAGCG-$(N)_{22\text{-Sense}}$-TAGTGAAGCCACAGATGTA-$(N)_{22\text{-guide}}$-TGCCTACTGCCTCGGA-3′), and are named based on their Watson/Crick binding position within the gene transcript, namely, shRNA.553 and shRNA.1730.

5.3.15.1 Cloning of miR-30 based shRNA vectors

For the *de novo* generation of the miR-30 shRNA, the two designed 97mer oligonucleotides were PCR-amplified with 0.4 µM of the primers 5’ miR30-XhoI and 3’ miR30-EcoRI, 2mM dNTPs and 2.5 units Accuzyme™ DNA Polymerase (Bioline) for 28 cycles, using the 97mer oligonucleotides shFbxw5.553 and shFbxw5.1730 as templates, respectively. Following amplification, the pMSCV based MLP-miR30 vector (Figure 6 A), as well as the 100nt PCR fragments were digested with EcoRI and XhoI to generate compatible overhangs. EcoRI/XhoI digested MLP-miR30 vector backbone and amplification products were ligated and transformed into chemically competent DH5α.

The resulting retroviral vectors MLP-miR30-shFbxw5.553 and MLP-miR30-shFbxw5.1730, encode for the structural virus protein “gag” as well as the respective microRNA embedded shRNA. The expression of these genes is driven from a specially designed 5’ long terminal repeat (LTR) from the murine stem cell PCMV virus, allowing enhanced transcriptional activation. For selection of successfully transduced cells, a puromycin resistance- as well as a GFP reporter gene is expressed under the control of a phosphoglycerate kinase (PGK) promoter, divided by an internal ribosomal entry site (IRES), to allow simultaneous expression.

The pMSCV based MLP-miR30-shRen.713 vector was kindly provided by Prof. Dr. Lars Zender. This shRNA targets a Renilla Luciferase and served as an internal control. The backbone of the plasmid MLP-miR30-shRen.713 plasmid was used for the generation of the *Fbxw5* targeting plasmids.

For *in vivo* analysis of shRNA mediated knockdown in adult hepatocytes, a transposon mediated delivery system for miR-30-shRNA was applied. Here the miR30-embedded

shRNA is flanked by inverted repeats (IR/DR), which are recognized by the transposase Sleeping Beauty 13. The mirR30-embedded shRNA becomes a transposable element, which is excised from the plasmid DNA and randomly integrated into TA-rich region within the host genome, resulting in a stable and physiological model to study pathophysiological processes in liver. To this end, the miR-30 shFbxw5.1730 cassette was subcloned from the MLP-plasmid into the transposable vector pCaggs-miR-30, or pCaggs-FAH-IRES-GFP-miR30 (FAHIG). The vector pCaggs-miR-30 (Figure 6 B) encodes for a GFP reporter gene, which is coupled to a miR-30 shRNA. The vector FAHIG (Figure 6 C) encodes for a miR-30-shRNA coupled GFP, which is additionally preceded by an IRES and a recombinant fumarylacetoacetate hydrolase to allow for simultaneous expression.

The expression is driven by a Caggs promoter, a synthetic construct consisting of cytomegalovirus (CMV) enhancer and the chicken beta-actin promoter to allow for strong expression. The Caggs promoter, as well as the GFP-coupled miR-30 shRNA is flanked by inverted repeat sequences (designated as IR/DR). These IR/DR sequences are recognized by a transposase, to allow the random transfer of the transgene into a mammalian hosts genome.

For subcloning, the miR-30 cassette was isolated from the MLP-miR-30 plasmid (Figure 6 A) using the endonucleases AgeI and MluI and then cloned into an empty recipient vectors pCaggs-5'-miR-30 (only harboring the 5' miR30 sequence) using the restriction sites AgeI and AscI, resulting in pCaggs-miR30-shFbxw5.1730.

For subcloning of the miR-30-shFbxw5.1730 cassette from the pCaggs-miR-30 into the FAHIG-vector, the restriction enzymes AgeI and NheI were used, applying standard cloning techniques.

The vectors pCaggs-5'-miR-30 and FAHIG were kindly provided by Prof. Dr. Lars Zender.

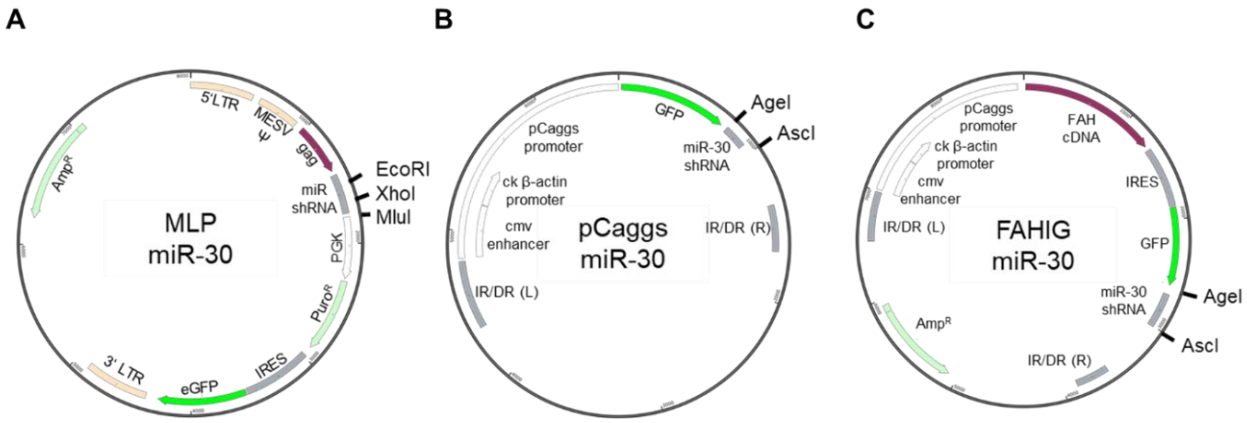

Figure 6 Overview of miR-30 vectors. (A) pMSCV based vector, encoding for retroviral structure protein (gag), miR-30 embedded shRNA, and GFP reporter gene. (B) pCaggs transposable vector encoding for GFP reporter gene and miR-30 shRNA. (C) Transposable vector encoding for FAH cDNA and miR-30 shRNA conjugated GFP, divided by an IRES to allow for simultaneous expression.

5.3.15.2 Cloning of miR-E based shRNA vectors

For *de novo* generation of miR-E shRNA, the designed 97 mer oligonucleotide was PCR amplified using 20 pM oligonucleotide template shFbxw5.1730 (Table 7), 0.4 µM 5' miRE-Xho, 0.4 µM 3' miR-E-EcoROligo 2mM dNTPs and 2.5 units Accuzyme™ DNA Polymerase (Bioline) for 30 cycles. Alternatively, for the generation of miR-E shRNA from pre-existing miR-30 shRNA, 50 ng of miR-30 shRNA plasmid DNA, 0.4 µM 5'-miRE-Xho-short, 0.4 µM 3' miRE-EcoRPlasmid were used.

Following amplification, the pMSCV based LPE-miRE (Figure 7 A), or pQCXIX based RT3-GEPIR (Figure 7 B) retroviral expression vector, as well as the 125nt PCR fragment were digested with EcoRI and XhoI to generate compatible overhangs. EcoRI/XhoI modified recipient vectors (LPE, RT3-GEPIR) backbones and the respective amplification products were ligated and transformed into chemically competent DH5α.

The resulting retroviral vectors LPE-miRE-shFbxw5.553 and LPE-miRE-shFbxw5.1730, encode for the structural virus protein "gag" as well as the two-microRNA embedded shRNAs, respectively. The expression of these genes is driven from a specially designed 5' long terminal repeat (LTR) form the murine stem cell PCMV virus, allowing enhanced transcriptional activation. For selection of successfully transduced cells, a puromycin resistance- as well as a GFP reporter gene is expressed under the control of a phosphoglycerate kinase (PGK) promoter, divided by an internal ribosomal entry site (IRES), to allow simultaneous expression.

The resulting RT3-GEPIR-shFbxw5.1730E vector also encodes for the structural virus protein “gag”, GFP, miR-E embedded shRNA, a puromycin resistance gene, and a reverse tetracycline transactivator (rtTA). The 5’LTR promoter drives the expression of the gag. The expression of the GFP reporter gene as well as the miR-E shRNA is under control of a tetracycline responsive element (TRE) promoter, allowing gene expression only in presence of a tetracycline transactivator, e.g. doxycycline. The puromycin resistance as well as the rtTA encoding gene is expressed under the control of a PGK promoter, divided by an internal ribosomal entry site (IRES), to allow simultaneous expression. In presence of doxycycline, the rtTA can bind to the TRE to drive the expression of GFP and the miR-E shRNA.

Both vectors, LPE miR-E and RT3-GEPIR kindly provided by Prof. Dr. Lars Zender.

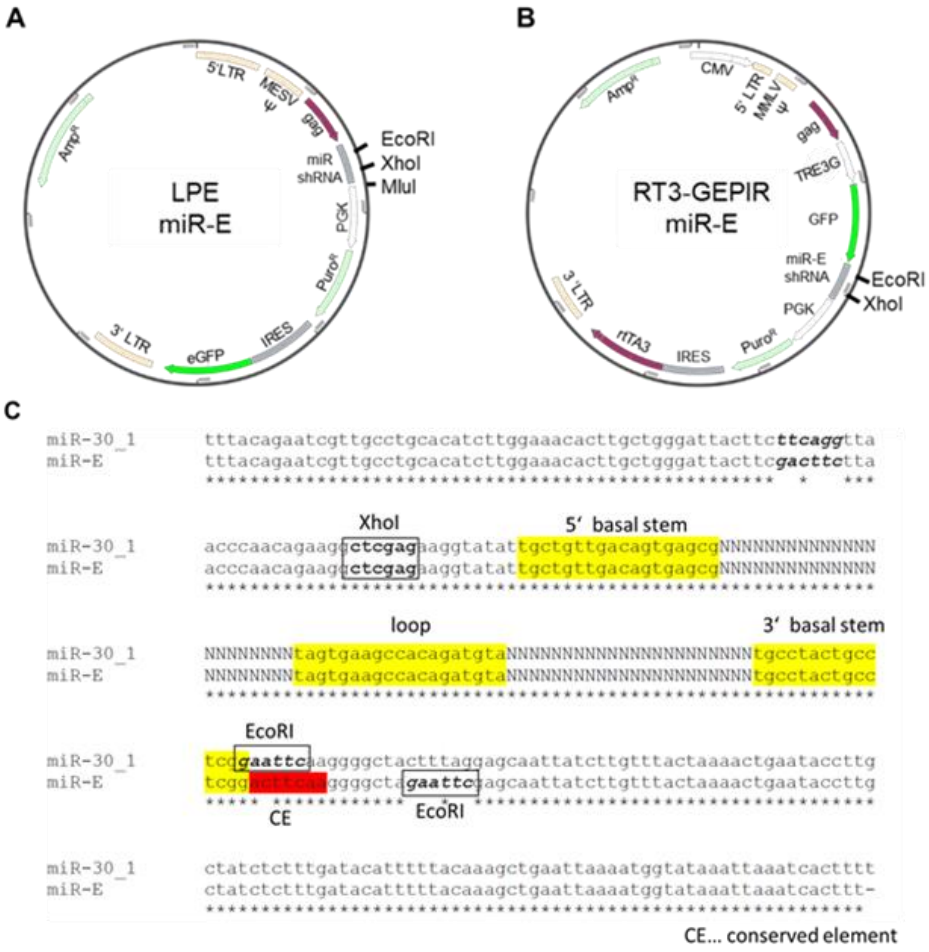

Figure 7 Overview of miR-E vectors. (A) pMSCV based retroviral vector constitutively expressing miR-E embedded shRNA (B) pQCXIX based retroviral vector map expressing a Tet inducible miR-E embedded shRNA. (C) Alignment of miR-30 and miR-E embedded shRNA (highlighted in yellow). miR-E contains a modified 3’ end harboring a conserved element (highlighted in red) that allows for more efficient processing of the shRNA (according to Fellmann et al. 2013 [86]

5.3.15.3 Cloning of CRISPR/Cas9 vectors

In addition to the shRNA mediated knockdown approach, the CRISPR/Cas9 mediated gene editing was used as a second tool to deplete FBXW5 expression.

This technique requires the design of a single guide RNA (sgRNA), which carries the variable 20 nt CRISPR RNA (crRNA) containing the targeting sequence for *Fbxw5*, and the stable 100 nt trans-activating crRNA (tracrRNA), which resembles the Cas9 nuclease recruiting sequence.

The crRNA directed against *Fbxw5* was designed using an online sgRNA prediction tool (http://www.broadinstitute.org/rnai/public/analysis-tools/sgrna-design). Based on the predicted high on-target activity and minimized off-target effects three crRNA sequences were chosen. The three oligonucleotides, designated sgFbxw5.2, sgFbxw5.3 and sgFbxw5.4 (sense and antisense, respectively), carry additional nucleotides that are complementary to overhangs generated by BbsI digestion at their 5' end. Alternatively, the crRNAs were obtained from the pGecko whole genome library and labelled with their corresponding identification numbers [87] (Table 2). All sequences are shown in Table 2.

For cloning, the crRNA-sense- (5'–caccgNNNNNNNNNNNNNNNNNNN- 3') and crRNA-antisense (5'-aaacNNNNNNNNNNNNNNNNNNNc-3') oligonucleotides were phosphorylated, annealed and ligated into the BbsI digested CRISPR/Cas9 expression vector pX458 (Figure 8 A; Addgene), which is suitable for transient sgRNA and Cas9 expression *in vitro*, and *in vivo*.

The resulting vectors pX458-sgFbxw5.2, pX458-sgFbxw5.3 and pX458-sgFbxw5.4 encode for sgFbxw5.2, sgFbxw5.3 and sgFbxw5.4, respectively, which are composed of the 20nt crisprRNA (crRNA) followed by a 100 nt trans-activating crRNA (tracrRNA), driven by a humanized U6 promotor. sgRNA sequences which were obtained from the pGecko library are designated as pX458-sgFbxw5.18105 and pX458-sgFbxw5.18098. Additionally, a 3xFlag-tagged Cas9 endonuclease as well as an GFP reporter gene is expressed under the control of a chicken β-actin promoter.

Alternatively, the phosphorylated and annealed 20 nt oligonucleotides were ligated into a BsmBI digested lentiCRISPRv2 vector (Figure 8 B; Addgene), which is suitable for the production and delivery of CRISPR/Cas9 lentiviruses.

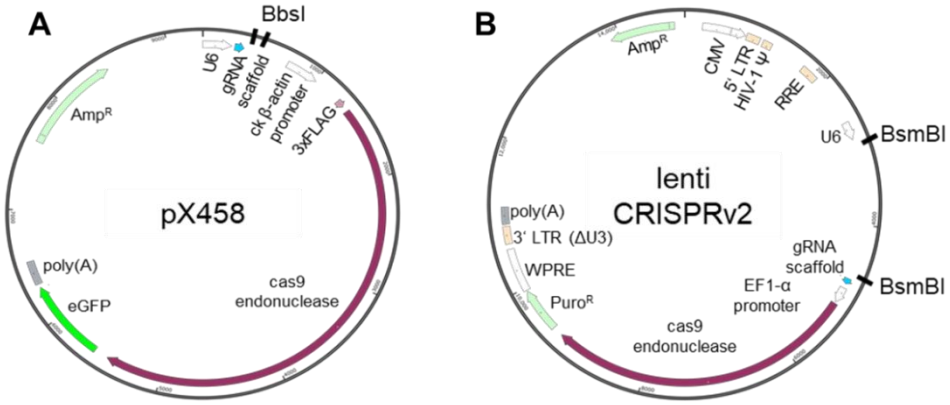

Figure 8 Overview of CRISPR/Cas9 vectors. (A) Eukaryotic expression vector encoding single guide RNA, Cas9 endonuclease for CRISPR/Cas9 gene editing. Additionally, a GFP reporter gene is expressed as well for monitoring transfected cells, or for flow cytometry. (B) Lentiviral producing vector, enabling the delivery of Cas9 and sgRNA for targeted gene knockout.

5.3.15.4 Cloning of Myc-tagged FBXW5 (MT-FBXW5)

6xMyc-tag encoding DNA fragment was PCR amplified from pCS2+MT (Addgene) using 0.4µM of the primers Myc-tag AgeI fw and Myc-tag AgeI rev, 2mM dNTPs and 2.5 units Accuzyme™ DNA Polymerase (Bioline) for 28 cycles. Following amplification, the pCMV-sport6-FBXW5 (Dharmacon; ID: 4211592) vector, as well as the 250nt PCR fragments were digested with AgeI to generate compatible overhangs. AgeI digested pCMV-sport6-FBXW5 vector backbone and the 6xMyc-tag amplification product were in-frame ligated and transformed into chemically competent DH5α. The correct in frame orientation of the 6xMyc tagged was verified by DNA sequencing.

The resulting vector pCMV-sport6-MT-FBXW5 encodes for the CMV promotor driven expression of Myc-tagged FBXW5 (MT-FBXW5).

5.3.15.5 Sequencing

DNA Sequencing was performed by Microsynth Seqlab (Göttingen) with the appropriate sequencing primers (see Table 1).

5.3.16 The GeCKO CRISPR knockout library

The mouse GeCKOv2 CRISPR knockout pooled library was a gift from Feng Zhang (Addgene cat # 1000000052) and is delivered on the lentiCRISPRv2 backbone plasmid, which expresses both Cas9 and an sgRNA.

CRISPR knockout pooled library (GeCKO v2), obtained from Addgene (cat # 1000000052), is delivered on the lentiCRISPRv2 backbone plasmid, which expresses both Cas9 and an sgRNA. The library contains 130,209 unique sgRNAs, which is divided in two sub-libraries (A and B). Each sub-library contains 3 sgRNAs per gene

when used separately. Additionally, both A and B libraries contain 1000 control sgRNAs designed not to target in the genome [87].

5.3.16.1 GeCKOv2 CRISPR library amplification

To ensure equal representation of each sgRNA, it is important to amplify the library using the protocol according to the manufacturer's protocol by electroporation.

The GeCKO library was diluted to 50 ng/µl in water. 100ng GeCKO library was then given to 25µl of electrocompetent cells (Invitrogen # 11319019) with an efficiency of >100 cfu (colony forming units)/µg. Electroporation was done in using Gene Pulser®/MicroPulser™ Electroporation Cuvettes (Biorad #1652089) at 1.75 kV, 200Ω and 25 µF. Electroporated *E. coli* were recovered in 975µl SOC medium, transferred in additional 1ml of recovery medium and rotated at 250 rpm for 1 hour at 37°C. The procedure was repeated for a total of 4 electroporation for each GeCKO library pool.

The total pooled 8 ml electroporated *E.coli* were spread on 20, prewarmed LB-Agar plates containing 100µg/ml ampicillin. All plates were grown for 14 hours at 32°C, to avoid recombination between the lentiviral long terminal repeats (LTRs).

To determine the transformation efficiency, a 40,000-fold dilution of the full transformation was plated on a separate LB-agar plate containing 100µg/ml ampicillin.

To harvest the colonies, 500 µL of LB was given onto each 10 cm^2 petri dish and the colonies were scraped off with a cell scraper. The scraped colonies were transferred into a tube. This procedure was repeated a second time to collect as many colonies as possible. GeCKO library plasmid isolation was done with a maxi prep as described in chapter 5.3.17.2

5.3.16.2 Identification of individual sgRNA of GeCKOv2 CRISPR library

Lentiviral delivery of sgRNAs directed against all genes, together with Cas9, was used to perturb thousands of genomic elements in parallel and was done as described in 5.3.9.2 . Two days after transduction, BNL CL.2 cells were selected using 3µg/µl puromycin. After 48 hours the puromycin was removed and washed out and the cells were recovered for one week, changing the medium every 2^{nd} day. To identify the single sgRNAs from the pooled library the genomic DNA of the transduced and selected cells were isolated as described in 5.3.17.3 . To amplify the sgRNA cassette from the genomic DNA, 2.5 units Accuzyme DNA polymerase (Bioline #BIO-21052), 20µM MiSeq Library fw primer, 20µM MiSeq Library rev primer and 0.25µg DNA was

used. Cycling parameters were 94°C for 5 min; 38 cycles of 94°C for 45 s, 50°C for 30 s, and 72°C for 30 s; 72°C for 5 min.

Illumina deep sequencing analysis identifying the genes as well as the amounts of total reads to the corresponding sgRNA-sequences an was done by CEGAT GmbH. To calculate the total percentage of reads, the amount of reads per sgRNA was added by one, to calculate the total percentage of reads. To calculate the x-fold change in enrichment or deprivation of the single sgRNAs wildtype control cells were compared to *Fbxw5* knockout cells.

5.3.17 Isolation of Nucleic acids

5.3.17.1 Miniprep

Mini-preparation was performed to purify low amounts of plasmid DNA (~20 µg). For plasmid DNA isolation, 5 ml LB-Medium (containing the appropriate antibiotic) was inoculated with the desired transgenic bacteria glycerol stock, or a single colony from LB-agar plates. After cultivation overnight at 37°C and 180 rpm, 1.5 ml of the culture was taken for the mini-preparation of the desired plasmid. The bacteria were harvested by centrifugation at 17000g for 10 min. Subsequently the cell pellet was resuspended in 200 µl buffer P1. Next cells were lysed with buffer P2 containing SDS and NaOH. To neutralize the alkaline solution, buffer P3 was added to the samples, followed by incubation for 15 min on ice. To remove the remaining cell debris, the samples were centrifuged for 15 min at 17000g and 4°C. The supernatant containing the plasmid DNA was transferred to a new reaction tube and resuspended in 0.7 V isopropanol. Plasmid DNA was collected by centrifugation (17000g, 30min, 4°C) and washed with 500 µl 70% (v/v) EtOH. After centrifugation (17000g, 10min, 4°C), the supernatant was removed and the DNA pellet air dried for 5-10min. The plasmid preparation was dissolved in 20 µl ddH_2O and stored at -20°C.

5.3.17.2 Maxiprep

To isolate larger amounts of plasmid DNA, bacteria were inoculated into 200 ml LB-medium supplemented with the appropriate antibiotic (ampicillin or kanamycin) and incubated at 37°C overnight. The maxi-prep was performed using the NucleoBond® Xtra Midi / Maxi kit (MACHEREY-NAGEL) according to the manufacturer's protocol. The purity and concentration of the isolated plasmids were photometrically determined. Additionally, the plasmid DNA was analyzed by enzymatic restriction and agarose gel electrophoresis.

5.3.17.3 DNA-Extraction from mammalian cells and tissue

Cultured cells, or the tissues of mouse ear biopsies, respectively, were incubated at 56°C in 1x Proteinase-K buffer containing 50 µg/ml Proteinase K overnight. After inactivation at 95°C for 10 min, the remaining residues were centrifuged (13000 rpm, 5min). The DNA in the supernatant was precipitated by adding 1 volume of isopropanol followed by 5 min centrifugation at 13000 rpm. To remove remaining isopropanol from the gDNA precipitate, the pellet was washed once with 70% EtOH, followed by 5 min centrifugation at 13000 rpm. The supernatant was removed, the gDNA pellet air dried and resuspended in 50 µl ddH_2O. The isolated DNA was stored at 4°C for short term and at -20°C for long term.

5.3.17.4 RNA Extraction from tissues

50-100mg of liver tissue biopsy was transferred to a Precellys Keramik- tube (Peqlab, 1.4 mm) containing 1ml TRIsure (Bioline), which composed guanidinium thiocyanate and phenol to digest the lysates. After mechanical dissociation the sample was incubated at room temperature for five minutes. Then 200 µl of chloroform was added to the lysate and incubated for additional three minutes at room temperature. Subsequently, the lysate was centrifuged at 4 ° C and 12,000xg for 15 minutes. The supernatant was transferred to a new reaction tube and RNA precipitation was achieved by mixing it with 0.5 ml cold isopropyl alcohol. After an incubation time of 10min, the sample was centrifuged at 12,000xg for 10 minutes at 4°C. The precipitate was washed once with 1ml 75% ethanol. After a final centrifugation step (7,500 x g; 5 min at 4 °C), the supernatant was removed, the RNA pellet air dried and dissolved in DEPC-treated water. The RNA was used either directly for cDNA synthesis or stored at -20°C for short term, or at -80°C for long term storage.

5.3.17.5 RNA-Extraction from cells

For extraction and purification of total RNA the “NucleoSpin® RNA II” isolation kit (Macherey&Nagel, Düren) was used. The procedure was performed according to the manufacturer’s protocol.

Firstly, cells or tissue were lysed with mRNA lysis buffer and applied to a DNA-binding column to remove genomic DNA. The eluate was mixed with the same volume of 70% ethanol for mRNA precipitation and given to an RNA-binding column. After washing of the column with RNA-wash buffer I and II the RNA was eluted from the column with 30 µl RNase-free water. For total determination of RNA concentration, its absorption

at 260 nm and 280 nm was measured using the NanodropND-1000™ instrument (Peqlab). The calculation of the amount of RNA from the OD at 260 nm is based on Beer's law, using an extinction coefficient of 0.025 (µg/ml)cm^{-1} for single stranded RNA, resulting in an OD260 of 1 at a concentration of 40 µg/ml and a pathlength of 1 cm. Subsequently the RNA was used either directly for cDNA synthesis or stored at -20°C for short term, or at -80°C for long term storage.

5.3.18 cDNA synthesis

To synthesize complementary double-stranded DNA (dsDNA) from single-stranded total RNA, the RevertAid First Strand cDNA Synthesis Kit (ThermoFisher Scientific) was used. After hybridization of a random hexamer primer to the RNA, reverse transcriptase is able to synthesize the complementary cDNA. RNA templates are effectively protected from degradation by addition of an RNase inhibitor. The reverse transcription reaction was performed according to the manufacturer's instructions.

5.3.19 Polymerase-Chain-Reaction (PCR)

PCR is a valid method for amplification of specific DNA segments. The basic principle is the specific binding ability of two different primers (oligonucleotides) in opposite directions flanking the region of interest. These primers hybridize to single stranded DNA (ssDNA) and act as a starting sequence for the DNA polymerase. The polymerase transforms the ssDNA to double stranded DNA (dsDNA) by using added deoxyribonucleotide-tri-phosphates (dNTPs). The procedure typically is done in multiple steps of 1. denaturation of dsDNA, 2. hybridization of primers to ssDNA (annealing) and 3. synthesis of dsDNA by the polymerase (elongation).

Table 9 Standard PCR mixture

10xPCR-Buffer	5µl
dNTPs (10mM)	1µl
Forward Primer (10 µM)	1µl
Reverse Primer (10 µM)	1µl
DNA-Polymerase	1µl
ddH_2O	Add to 50µl

Table 10 Standard PCR Program

94°C	5 min	
94°C	30 sec	
X°C	1 min	25-35 cycles
72°C	1:30 sec	
72°C	5 min	
10°C	storage	

5.3.20 qPCR

The synthesized cDNA was used to conduct a quantitative real-time PCR (qRT-PCR), using the 7500 real-time PCR system cycler (Applied Biosystems). The underlying principle of a qRT-PCR is comparable to conventional PCR. In contrast to conventional PCR, real-time PCR allows quantification of rare transcripts and small changes in gene expression. This is done by using the fluorescence dye SYBR-green which incorporates into newly synthesized dsDNA. The fluorescence of the DNA-dye-complex can be quantified and serves as a measure for the newly synthesized dsDNA. The quantification of the amplified DNA is done during the exponential phase, using the "fit point Method". During the exponential amplification phase the reaction is not affected by the limitation of a reaction component, as it might happen in the plateau phase [55, 57].Analyses were performed according to W. Pfaffl, by setting a "crossing point" (CP)-which is the same for all amplificants- and by using the following equation [55].

$$\mathbf{ratio} = \frac{\mathbf{E_{target}}^{\Delta \mathbf{CP_{target}(sample-control)}}}{\mathbf{E_{ref}}^{\Delta \mathbf{CP_{ref}(sample-control)}}}$$

During this study, it was presumed that the amplification efficiency of the target and reference gene (18S rRNA) had optimal and identical conditions during the exponential phase, meaning that E=2. The primers for real-time PCR and the annealing temperature are summarized in (Table 1) and the reaction mixture for the real-time PCR in (Table 11).

Table 11 Formulation of qRT-PCR

Mastermix: 18S rRNA	**Mastermix: Fbxw5**
10µl 2x Taqman Mastermix	10µl 2x SYBR-Green Mastermix
2µl 500nM 18S rRNA sense primer	3µl 2000nM Fbxw5 sense primer
2µl 500nM 18S rRNA antisense primer	3µl 2000nM Fbxw5 antisense primer
1µl 4000nM 18S rRNA TAMRA sonde	2µl H_2O
3µl H_2O	
2µl cDNA [50 ng]	2µl cDNA [50 ng]

5.3.21 Protein Isolation

5.3.21.1 Preparation of protein lysate from cell culture

The cells were washed twice with PBS, mechanically detached from the culture dish and transferred to a 15 ml Falcon tube. After centrifugation (5 min, 135 xg) the cell pellet was resuspended in RIPA-buffer and incubated on ice for 30 min. The remaining intact cells were disrupted by sonification (15 sec, amplitude 40) and the cell debris

was separated from the protein containing supernatant by centrifugation (12000 xg, 4°C, 30 min). The amount of protein was determined with the DC Protein Assay (Biorad) according to the manufacturer's protocol.

5.3.21.2 Preparation of protein lysate from mouse liver

The liver tissue biopsy was transferred to a Precellys Keramik-tube (1.4 mm) and mechanically dissociated in 1 ml RIPA buffer with the Precellys® Homogenisator (Peqlab). Tissues were homogenized using Minilys homogenizer (Peqlab) directly in the buffer. Afterwards the samples were incubated on ice for 30 min and centrifuged (30 min, 13000rpm, 4°C). The supernatant was transferred into a new Eppendorf tube and stored at -20°C. For the determination of the protein concentration the samples were diluted 1:100, followed by the DC Protein Assay from Biorad.

5.3.21.3 Determination of protein concentration

For the determination of the protein concentration, the DC protein assay (Biorad) was used which is based on the Lowry protein assay [88]. The protein solutions are mixed with an alkaline solution of the divalent copper salt, Cu^{2+} (cupric ions). Under alkaline conditions the cupric ion chelates with peptide bonds and reduces the cupric ion to the monovalent ion Cu^{+} (cuprous ion). The cuprous ion and radical groups of tyrosine, tryptophan, and cysteine react with the yellow Folin reagent to produce an unstable product that becomes reduced to molybdenum/tungsten blue with a characteristic color. The amount of color produced is proportional to the amount of peptide bonds as well as to the amount of protein/peptide [88]. The color change from yellow to blue can be measured by photometry (absorption 750 nm, 650 nm or 540 nm). Values are calibrated via a BSA dilution series. Protein quantification was performed according to the manufacturer's protocol from Biorad. The color change was measured by a photometer at 690 nm.

5.3.22 Discontinuous SDS-polyacrylamide gel electrophoresis (SDS-PAGE)

The discontinuous SDS gel electrophoresis according to Laemmli [89] separates proteins depending on their molecular weight. The anionic detergent SDS denaturizes the three-dimensional structure of proteins which is supported by the addition of reducing agents like β-mercaptoethanol or dithiothreitol (DTT) to break disulfide bonds. In addition, the natural charge of the proteins will be rendered insignificant by the negative charge of SDS resulting in negatively charged protein complexes, having a

constant mass-charge ratio. Using an electric field across a porous polyacrylamide gel the negatively charged proteins migrate towards the anode and are separated according to their molecular mass.

5.3.22.1 Preparation of polyacrylamide and electrophoresis

The gels were prepared in two tightened glass plates and placed into the appropriate electrophoresis chamber. The prepared mini-gels consist of a 4% stacking gel and a 10-12% separation gel depending on the molecular weight of the protein. The preparation of the different gels is listed in Table 12.

Table 12 SDS-Gel recipe

	Stacking gel	**Separation gel 10%**	**Separation gel12%**
ddH_2O / ml	3.92	4.1	3.4
Acrylamide / ml	1.13	3.3	4.0
1.5 M Tris, pH 8.8 / ml	-	2.5	2.5
0.5 M Tris, pH 6.8 / ml	1.75	-	-
10% SDS / µl	70	100	100
10% APS / µl	70	105	105
TEMED / µl	7	15	15

For SDS-PAGE, the protein mixture to be analyzed was reconstituted with 4x sample buffer (Roth) and heated to 95°C for 5 min, immediately before loading onto the polyacrylamide gel. For enrichment of the proteins in the stacking gel a voltage of 80 V was applied. For the separation of the proteins in the separation gel the voltage was increased to 140 V.

5.3.23 Western blot

Western blot analysis allows immunologic detection of proteins using specific antibodies. For this purpose, proteins separated by SDS-PAGE are transferred to a membrane using a constant electric field. Due to the negative charge of the proteins, the proteins migrate to the anode and get fixed onto a nitrocellulose or PVDF membrane. For detection of a protein of interest, specific antibodies are used. Primary antibodies recognize protein epitopes - a specific sequence of amino acids - which can be continuous or discontinuous. Continuous epitopes, also called linear epitopes, are based on the primary structure of the protein, whereas discontinuous epitopes are based on the three-dimensional structure and therefore the folding of the protein.

5.3.23.1 Transfer of proteins onto nylon membranes

Separated proteins were transferred from the SDS-gel to the PDVF membrane by wet blot technique (60 min, 450 mA). Before assembling the blot, the Immobilon® (Millipore, Germany) PVDF membrane was incubated in methanol for 1 min. After blotting, the membrane was incubated in 1x transfer buffer for 2 min. To prevent unspecific binding, the membrane was then blocked with 5% (w/v) milk powder/TBS-T for 1 h at ambient temperature and subsequently incubated with the primary antibody overnight at 4°C. Unbound antibodies were removed by washing the membrane with TNT. Following three washing steps, the membrane was incubated with the secondary HRP-conjugated antibody for 1 h at ambient temperature. Additional washing steps with TNT were done immediately before the chemiluminescence reaction was performed. For this purpose, the membrane was incubated for 5 min with ECL solution (GE Healthcare, Buckinghamshire). The total exposure time was 3 -10 min before the Amersham Hyperfilm (GE Healthcare) was developed.

Table 13 List of Antibodies used in Western Blot

antibody ID	cat. no.	company	dilution	reactivity
α-Actin	8691001	MP Biomedicals	1:70000	mouse
FBXW5 (N2C2)	GTX120049	GeneTex	1:1000	rabbit
GFP (FL)	sc-8334	SantaCruz	1:5000	rabbit
Mouse IgG-HRP coupled	NA931-IML	GE Healthcare	1:10000	sheep
Myc-9E10	sc-40	SantaCruz	1:10000	mouse
Rabbit IgG-HRP coupled	NA934-IML	GE Healthcare	1:10000	donkey
RPA32/RPA2	ab76420	Abcam	1:5000	rabbit
SAS6 (91.390.21)	sc-81431	SantaCruz	1:1000	mouse

5.3.24 Histology methods

5.3.24.1 Fixation and paraffin embedment of liver samples

Liver tissues were fixed with 4% PFA in PBS overnight at room temperature and subsequently embedded into liquid paraffin. After cooling down to 4°C, the embedded samples were sectioned and 4 µm slices were fixed onto a glass slide and stored at ambient temperature.

5.3.24.2 Immunofluorescence staining of cells

For immunofluorescence staining, cells were washed two times with PBS. Subsequently, the cells were fixed using ice-cold methanol for 15 min at 4°C. Methanol was removed and the cells were air-dried for 10-15 min. To avoid unspecific binding, the cells were blocked with 5% BSA for one hour at ambient temperature. The incubation with the primary antibody was done overnight at 4°C. After removing the primary antibody, the cells were washed three times with PBST and incubated with a secondary, cyanine-conjugated antibody directed against the primary antibody (primary and secondary antibodies are summarized in Table 6). For staining of the nuclei, the cells were incubated with 0.5 µg/ml DAPI in PBS. DAPI intercalates into the DNA at AT-rich regions and yields blue fluorescent nuclei. The stained cells were spread with Prolong® and covered with thin cover slips for fluorescence microscopy. Quality of the fluorescence labelling was examined using a Leica fluorescence microscope, with constant exposure times during digital imaging for the different markers.

Table 14 List of antibodies used in IF and IHC

antibody ID	cat. no	company	dilution	reactivity
y-tubulin	GTX113286	GeneTex	1:1000	rabbit
y-tubulin	ab11316	Abcam	1:1000	mouse
pericentrin	ab4448	Abcam	1:1000	rabbit
FAH	ab81087	Abcam	1:1000	rabbit

5.3.24.3 Centrosome counting

Centrosomal staining (y-tubulin; pericentrin) was analyzed using the Leica DMI 6000 Microscope and the Metamorph software for microscope acquisition. For the determination of the average centrosome number, a minimum of 100 cells were counted on at least 5 different regions of interest (ROI). The centrosome number was determined as the number of centrosomes per cell.

5.3.24.4 Native fluorescence

Liver tissues were fixed with 4% PFA in PBS for 4 hours at 4°C. Afterwards, the PFA solution was replaced by 30% sucrose and incubated at 4°C overnight. The sampled were embedded into Tissue Tek® Compound and stored at -80°C. For analysis 4 µm slices were fixed onto a glass slide.

5.3.24.5 HE staining

The paraffin embedded tissue was sectioned into 5µm slices, followed by a deparaffinization step in Xylene. After rehydration in 3 different and decreasing concentrations of ethanol, the slides were washed with distilled water. The nucleus was stained with hematoxylin solution (Merck) for 5-10 sec. For the development of the hematoxylin staining, the slides were washed with running tap water for 10 min. After that, the samples were washed 2 times with distilled water. Cytoplasm staining was done with acidified eosin solution (Sigma-Aldrich) for 2 min. Sections were washed, dehydrated using increasing ethanol concentrations and mounted with a xylene-based mounting medium.
The histopathological analysis of murine livers was done by the board-certified pathologist Prof. Dr. Ludwig Wilkens.

5.3.25 Mouse work

5.3.25.1 Genotyping of knockout mice

During this project, different mice strains were used (FAH, p53AlbCre, p21, p19). To determine the correct genetic background of the mice, ear biopsies were taken to mark the mice within one cage and to get tissues samples for the genotyping procedure. For $p19^{arf}$ genotyping three different primers (arf-1, arf-2, arf-3) were used to recognize either the wildtype allele (415 bp) or the mutant allele (250 bp). PCR conditions were: 0.16 mM dNTPs, 4 % DMSO, 0.4 µM of Arf-1, 0.96 µM of Arf-2 and 0.32 µM of Arf-3 primers. For p21 genotyping three different primers (p21-exon-144, p21-GenU, p21-PGK neo-3) were used to recognize either the wildtype allele (685 bp) or the mutant allele (150 bp). For FAH genotyping, three different primers (A, B, C) were used to recognize either the wildtype allele (a+b; 180 bp) or the mutant allele (c+b; 240 bp).
For $p53^{loxP/loxP}$ genotyping, four different primers (A, B, C, D) were used to recognize either the wildtype allele (A+B=288bp; C+D= 431bp) or the mutant allele (A+B=370bp; C+D= 584bp). Additionally, FAH knockout mice were treated with the drug NTBC (2-[2-nitro-4-trifluoromethylbezoylcyclohexane-1,3-dione) at 19.2 mg/l drinking water to prevent liver failure according to Wuestefeld et al. [90].
For Cre genotyping, two different primers (Cre1, Cre2) were used to recognize a 500 bp band, representing the Cre transgene.

5.3.25.2 Hydrodynamic tail vein injection

Using hydrodynamic tail vein injection, it is possible to deliver transposable elements into the mouse liver, making it a powerful tool for genetic modification. To this end, a solution containing naked plasmid DNA is injected into the tail vein of a 4-6 weeks old mouse within 5-7 seconds. The volume of the solution covers 1/10 of the mouse body weight, leading to an increase of pressure in the *Vena cava,* which in turn results in a backflow of the solution into the *Ateria hepatica*. Here the DNA containing solution leaks out of the intrahepatic capillaries and is taken up by the surrounding tissue. Since intrahepatic capillaries are highly porous, the uptake and the expression of the foreign DNA primarily happens within the liver. It is however still possible that other organs are affected as well, like the spleen or the kidneys. The animal experiments performed within this project have been approved by the Regierungspräsidium Tübingen (grant number M17/14).

5.3.25.3 Dissection of murine livers

Experimental mice were sacrificed at a defined time point after HDTV. The murine livers were carefully excised, photographed and sampled regarding the subsequent analysis.

5.3.25.4 GFP imaging of murine livers

Ex vivo GFP imaging of murine livers was performed using the Hamamatsu Imaging system.

6 Results

6.1 Validation of miR-shRNAs for FBXW5 suppression *in vitro*

To achieve FBXW5 suppression under physiological conditions, it was taken advantage of the well-established microRNA embedded shRNA (miR30-shRNA) technique. In particular, use of miR30-shRNA allows for constitutive or inducible, potentially tissue-specific expression under control of endogenous polymerase II and does not significantly interfere with the host cell expression machinery [86, 91, 92]. Two different miR-30 embedded 22mer shRNAs were designed, namely shRNA.553 and shRNA.1730, where 553 and 1730 refer to the annealing position within the target gene. These two sequences resemble the best choice with respect to high specificity and low off-target effects, as optimized by an algorithm provided by the online prediction tool "DSIR[3]". Plasmids MLP-miR30-533 and MLP-miR30-1730 were engineered to encode these shRNAs.

To investigate the potency of FBXW5 suppression for both shRNA variants, plasmid pCMV-sport6-MT-FBXW5 expressing a Myc-tag FBXW5 (MT-FBXW5) was introduced into HEK293T cells, together with a 10-fold molecular excess of the appropriate MLP-shFbxw5 plasmid. Plasmid MLP-shRen.713, encoding shRNA against the Renilla luciferase (shRen.713), served as control. Suppression efficiency was analyzed by qPCR and western blot. As shown in Figure 9 A, miR-30 embedded shFbxw5.1730 silenced MT-FBXW5 expression relative to the control (shRen.713) to about 50% regarding the transcript, and almost completely with respect to the protein level. miR-30 shFbxw5.553 reduced expression to about 50%, both on the transcript level and the amount of protein. To further improve the efficiency of the shRNAs, particularly for shFbxw5.553, both existing miR-30 shRNAs were converted into optimized miR-E shRNAs according to Fellmann et al. (2013). To this end, a conserved ACNUCAA-motif was generated in each miR-shRNA at the 3' end of the basal stem as well as a critical element at the 5' end of the guide strand (Figure 1 C). These elements strongly improve processing of shRNA in general and thereby increase the efficiency of shRNA-mediated suppression [86]. Plasmids LPE-miR-E-shFbxw5.533 and LPE-miR-E-shFbxw5.1730 encode the improved miR-E shRNAs. As before, HEK293T cells were co-transfected with pCMV-sport6-MT-FBXW5 and the respective LPE-miR-E plasmid

[3] http://biodev.extra.cea.fr/DSIR/DSIR.html

and analyzed for suppression efficiency by qPCR and western blot. As shown in Figure 9 B, the improved shRNAs Fbxw5.553E and Fbxw5.1730E cause almost complete removal of the transcript but show a marked difference in the residual amount protein. Thus, shRNA Fbxw5.1730E with the highest efficiency was used for all further suppression studies and is referred to as “shFbxw5”.

6.2 Validation of guide RNAs for CRISPR/Cas9 mediated-targeting of *Fbxw5 in vitro*

The CRISPR/Cas9 technology allows the modification of chromosomal targets, e.g. the disruption of a target gene, with high fidelity and was applied to create a disruption within the *Fbxw5* gene. The CRISPR/Cas9 expression plasmid used (pX458) encodes an adjustable single guide RNA (sgRNA), as well as the endonuclease Cas9 mediating a double strand break (DSB) at the position of a specifically bound sgRNA. With the help of an online prediction tool[4], three different sgRNA variants were constructed to align within the *Fbxw5* open reading frame (orf) at the positions *1422* (sgFbxw5.2), *281* (sgFbxw5.3) and *911* (sgFbxw5.4).

To test for CRISPR/Cas9-mediated effects on FBXW5 expression, HEK293T cells were co-transfected with plasmid pCMV-sport6-MT-FBXW5 and, at a molecular ratio of 1:10, the respective pX458 plasmid expressing sgFbxw5.2, sgFbxw5.3 or sgFbxw5.4. Binding of sgRNA to *MT-Fbxw5* DNA is expected to trigger a DSB, introduced by the co-expressed Cas9 endonuclease at the sgRNA binding site, ultimately destroying the pCMV-sport6-MT-FBXW5 plasmid DNA. For all three constructs, CRISPR/Cas9 abolished MT-FBXW5 transcription almost completely as shown by qPCR (Figure 9 B). As revealed by western blot analysis (Figure 9 B)., however, only sgFbxw5.2 and sgFbxw5.4 prevented FBXW5 protein expression to a large extent suitable for depletion studies. sgFbxw5.2 was chosen for further studies and is referred to as “sgFbxw5”.

[4] http://www.broadinstitute.org/rnai/public/analysis-tools/sgrna-design

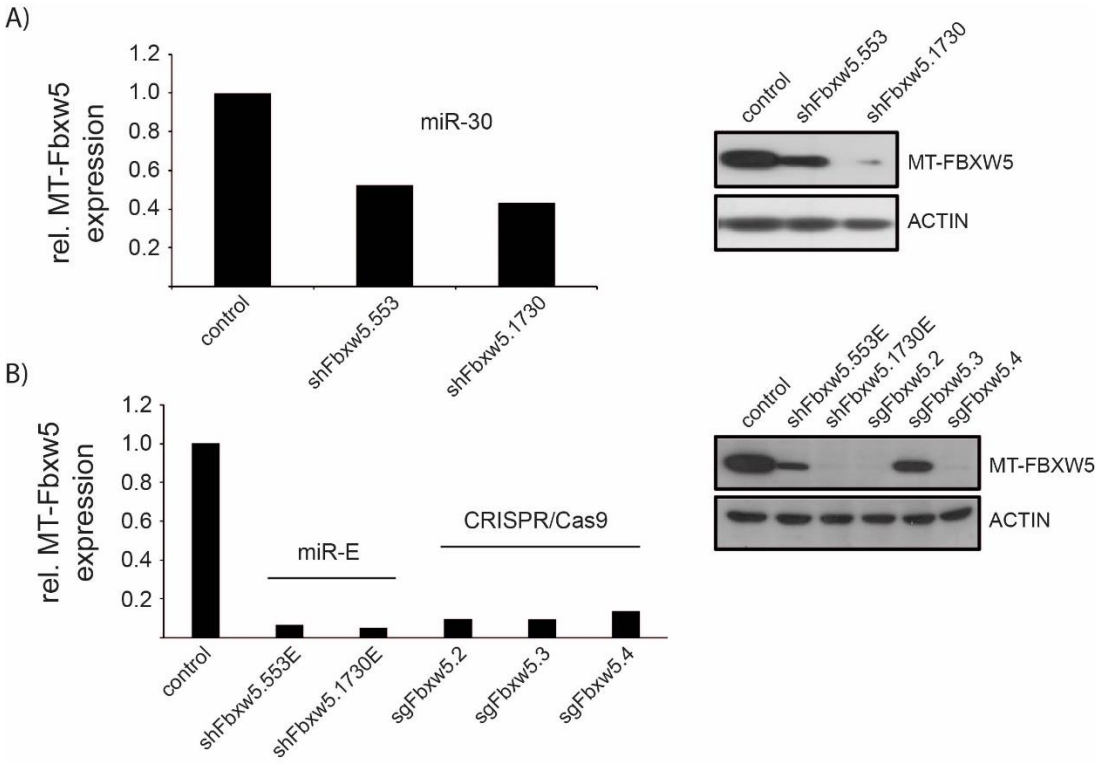

Figure 9 Verification of shRNA mediated suppression and CRISPR/Cas9 mediated depletion of exogenous MT-FBXW5 in HEK293. (A) Left panel: miR-30 mediated suppression of exogenous MT-FBXW5 as determined by qPCR. Right panel: miR-30 mediated suppression of exogenous MT-FBXW5 as determined by western blot, using anti-Myc-tag antibody. (B) Left panel: miR-E mediated suppression, and CRISPR/Cas9 mediated depletion of exogenous MT-FBXW5 as determined by qPCR. Right panel: miR-E mediated suppression, and CRISPR/Cas9 mediated depletion of exogenous MT-FBXW5 as determined by western blot, using anti-Myc-tag antibody.

6.3 Depletion of FBXW5 leads to abnormalities in centrosome number

The new tools for efficient *Fbxw5* downregulation (shFbxw5) or depletion (sgFbxw5) were used to re-evaluate the connection between FBXW5 deficiency, centrosome number and a putative tumor formation process in two different cell lines: mouse embryo fibroblasts (NIH/3T3) and murine liver cells (BNL CL.2).

NIH/3T3 fibroblasts represent a genetically stable and healthy genotype with intact p53 expression and a normal centrosome phenotype, i.e. two centrosomes per cell. To study consequences of FBXW5 suppression, these fibroblasts were transduced with a retrovirus harboring RT3-GEPIR-shFbxw5.1730E, which represents a doxycycline-inducible system to manipulate shFbxw5 expression. qPCR demonstrated a robust reduction of *Fbxw5* transcript, 72h after induction of the shRNA with doxycycline (Figure 10 A). Moreover, western blot analyses detected a significant decrease in FBXW5 abundance, confirming the robust efficiency of the miR-E based shRNA

technique (Figure 10 B). To visualize and quantify the number of centrosomes in these FBXW5-defiecient NIH/3T3 cells, γ-tubulin was used as a centrosomal marker. As shown in Figure 10 C, the suppression of FBXW5 produced an increase in the number of cells having more than two centrosomes. Whereas control cells carrying shRen.713, or non-induced shFbxw5 cells show a 5-15% population with more than two centrosomes, this number increases significantly to almost 40% once FBXW5 has been suppressed by shFbxw5 (Figure 10 C, D).

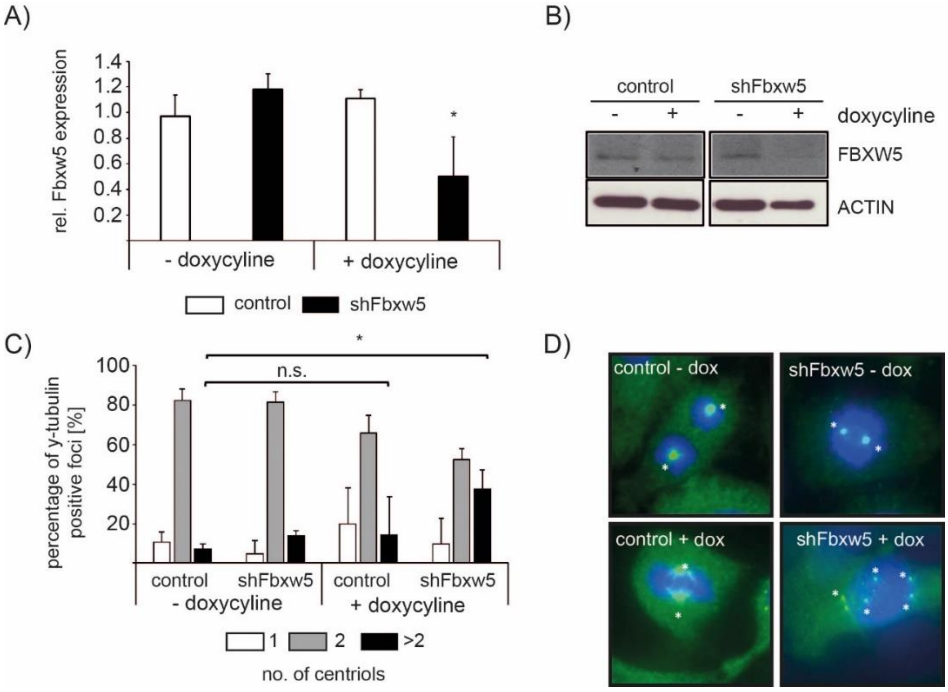

Figure 10 Suppression of FBXW5 leads to amplified centrosome number in NIH/3T3 cells (A) Verification of inducible FBXW5 suppression in NIH3T3 cells upon doxycycline treatment by qPCR. (B) Verification of inducible FBXW5 suppression in NIH/3T3 cells by immunoblotting using the indicated antibodies. (C) Quantification of centrosomal number upon doxycycline induced FBXW5 suppression in NIH/3T3 cells. (D) Representative picture of centrosome stained NIH/3T3 using y-tubulin as centrosomal marker (green) and DAPI for visualization of the nuclei, while the white stars indicate the centrosome position. Significance was calculated by a two-tailed *t*-test resulting in the following p-values: * P <0.05, *** P <0.001. Control cells resemble NIH/3T3 cells carrying the control plasmid (shRen.713).

Similar effects were observed in BNL CL2 cells, a murine liver cell line also presenting a non-tumorigenic phenotype with a stable number of centrosomes. Here, vector LPE-miRE-shFbxw5.1730 was used to produce a retrovirus, which upon transduction into BNL CL.2 cells lead to constitutive expression of shFbxw5 and subsequent suppression of FBXW5 (Figure 11). The reduction in the protein level of FBXW5 was verified by western blot analysis, however it was less pronounced as before in the NIH/3T3 cell line. Nevertheless, the number of cells with more than two centrosomes increased noticeably to about 20%, as compared to control cells (Figure 11 C, D).

Correspondingly, only a moderate increase in the cartwheel protein SAS6, an early stage component in centriole formation downregulated by FBXW5 [1], is observed (Figure 11 A). For a more rigorous test of reduction, CRISPR/Cas9 mediated gene editing of *Fbxw5* was carried out. BNL CL.2 cells were stably transduced with lentiviral vector lentiCRISPRv2 expressing sgFbxw5 together with Cas9 endonuclease. Western blot analysis verified the depletion of FBXW5 and revealed a more pronounced increase in the level of SAS6 (Figure 11 A). Another result of a CRISPR/Cas9-assisted DSB with subsequent non-homologous end joining (NHEJ), transduced cells should display InDel (**In**sertion/**Del**etion) mutations within *Fbxw5* gene. In fact, deep sequencing analysis verified the occurrence of multiple deletions, resulting in a loss of function mutation and the disruption of *Fbxw5,* which is accompanied with a SAS6 stabilization (Figure 11 A, B). As a consequence, an increase in the cell population with more than two centrosomes to almost 30% was observed in the CRISPR/Cas9 FBXW5 depleted cells (Figure 11 C, D).

Taken together, the data shown above extend the observations of Puklowski et al. [1] to cells with unperturbed p53 expression, thus corroborating a link between downregulation of *Fbxw5* and the appearance of supernumerary centrosomes.

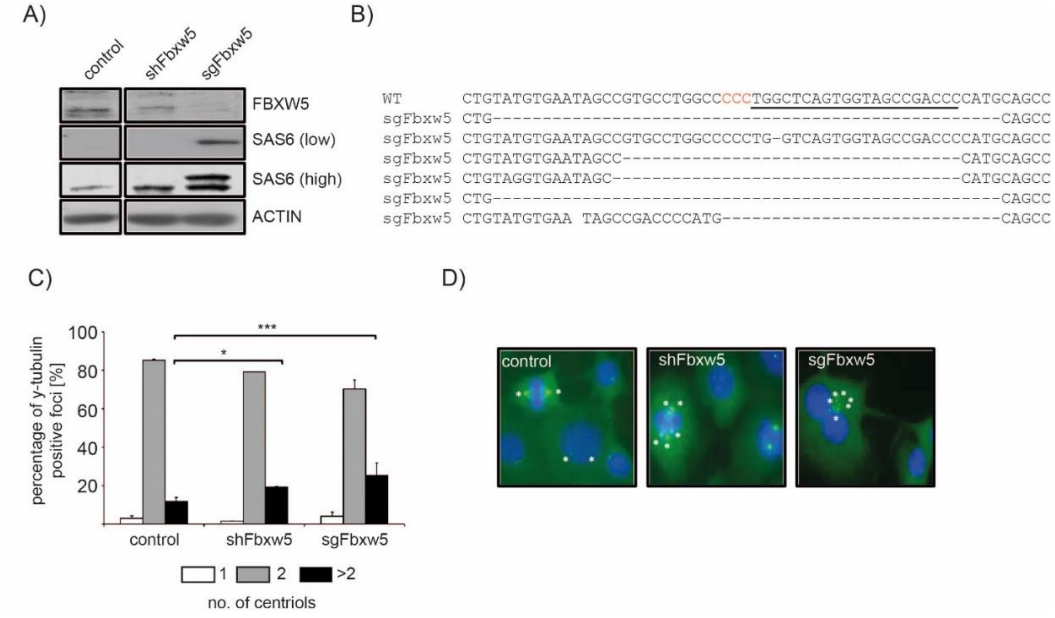

Figure 11 Depletion of FBXW5 leads to centrosome amplification BNL CL.2 cells. (A) Verification of FBXW5 suppression in BNL CL.2 cells and determination of HsSAS-6 protein levels after depletion of endogenous FBXW5 by immunoblotting using the indicated antibodies. (B) Illumina deep sequencing of CRISPR/Cas9 mediated and NHEJ repaired DSB within the *Fbxw5* gene. (C) Quantification of centrosomal number upon FBXW5 suppression (shFbxw5) and depletion (sgFbxw5). (D) Centrosome stained BNL CL.2 cells, using γ-tubulin as centrosomal marker (green) and DAPI for visualization of the nuclei, while the white stars indicate the centrosome position. Significance was calculated by a two-tailed *t*-test resulting in the following p-values: * P <0.05, *** P <0.001. Control cells resemble BNL CL.2 cells carrying the control plasmid (shRen.713).

6.4 Consequences of FBXW5 depletion for the regulation of G_2M transition

Next, it was of major interest to examine cell cycle progression in FBXW5 suppressed cells, since the occurrence of supernumerary centrosomes might have multiple consequences during mitosis, like multipolar cell divisions (cell death), centrosome clustering (bipolar division), mitotic exit (cell arrest) or cell transformation (tumorigenesis).

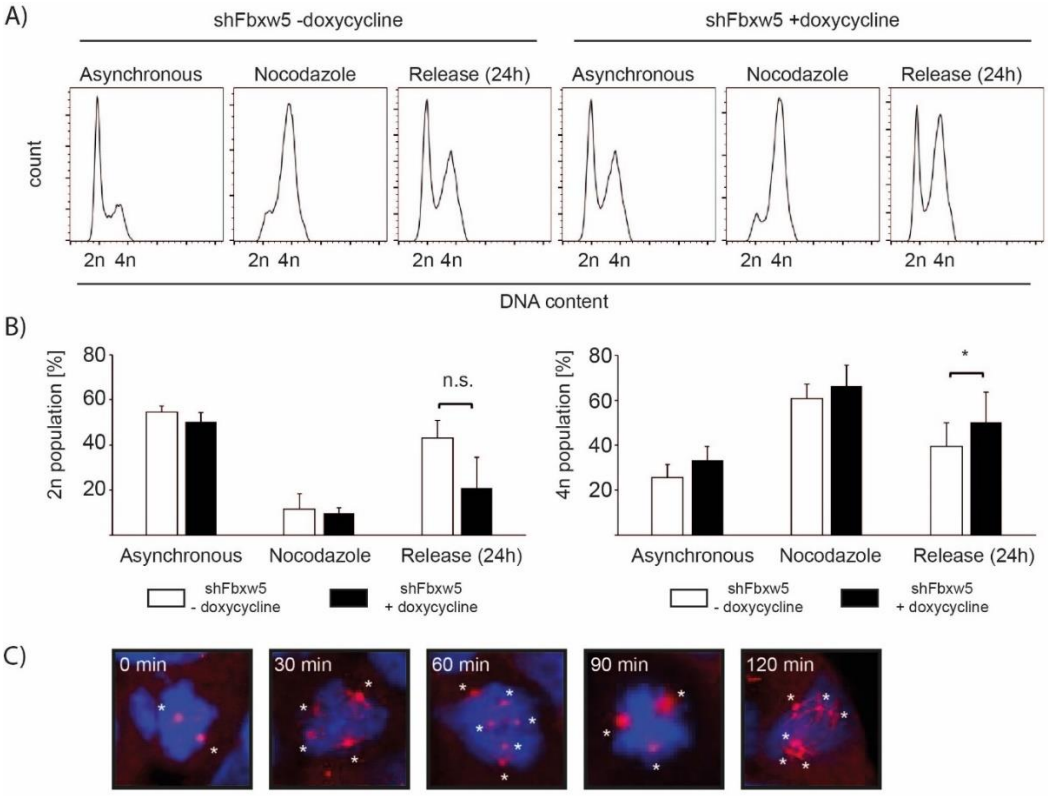

Figure 12 Suppression of FBXW5 leads to mitotic delay in NIH/3T3 cells. DNA content of synchronized NIH/3T3 cells was determined using propidiumiodid staining and FACS analysis**.** A) Representative picture of synchronized NIH/3T3 cells. (B) Quantification of 2n (G_1; left panel) and 4n (G_2M, right panel) population in nocodazole synchronized NIH/3T3 cells. Significance was calculated by a two-tailed *t*-test resulting in the following p-value: * P <0.05 (C) Fluorescence microscopy of doxycycline induced and Fbxw5 suppressed and synchronized NIH/3T3 using y-tubulin (red) to visualize centrosomes and DAPI (blue) to identify nuclei, while the white stars indicate the centrosome position.

To study cell cycle progression during mitosis, cells need to be synchronized to allow precise measurements. To this end, FBXW5-suppressed NIH/3T3 fibroblasts were arrested in the prometaphase of mitosis using the spindle toxin nocodazole [93], and released from this block after 16 h. Flow cytometry analysis performed 24h after nocodazole withdrawal found a considerable larger G_2M population for FBXW5-suppressed cells compared to non-induced cells with unperturbed expression of

FBXW5 (Figure 12 A, B). Furthermore, when spindle formation during mitosis was visualized using antibodies against γ-tubulin, FBXW5-deficient cells exhibited two different spindle arrangements within the first hour after nocodazole withdrawal: bipolar and multipolar. At later time points, a rearrangement of the spindles into a predominant bipolar pattern was observed, indicating a reorganization of the centrosomes during cell division (Figure 12 C).

The impact of loss of FBXW5 on cell cycle progression was also analyzed in BNL CL.2 cells. In contrast to the previous experiment, cells were arrested during S phase using a single thymidine treatment, which interferes with deoxynucleotide utilization and drastically slows down DNA replication [94, 95]. After withdrawal of thymidine, cells start to progress through the cell cycle synchronously. Using flow cytometric analysis, it could be shown that BNL CL.2 cells released from the thymidine block remain synchronized within the first 4 h through the cell cycle, indicating that S- and early G_2-phase are not affected by the FBXW5 status (Figure 13 A, B). 8 hours after the release, however, the cell line with CRISPR/Cas9-mediated FBXW5 depletion shows a G_2M fraction representing 50-60% of the whole cell population, a significant increase compared to 25-30% G_2M cells in the control. Remarkably, no significant differences can be detected between control cells and cells expressing shFbxw5. Both cell lines show a G_2M population of roughly 25-30% 8 hours after the release from the thymidine block (Figure 13 A, B). Nevertheless, as compared to control cells with mostly bipolar spindle structures, multipolar spindles are more frequent in FBXW5-suppressed (shFbxw5) cells and in FBXW5-depleted (sgFbxw5) cells (Figure 13 C). These findings suggest that multipolar spindle formation in response to centrosome amplification leads to the observed delay in cell cycle progression, presumably at the G_2M checkpoint. In line with this, CRISPR/Cas9-mediated FBXW5 depletion - causing a greater fraction of cells to develop supernumerary centrosomes (Figure 2 D) - also causes a more pronounced G_2M delay. It is also possible that the cell population with amplified centrosomes must reach a critical threshold of around 30% in order to detect the resulting cell cycle delay after a single thymidine treatment.

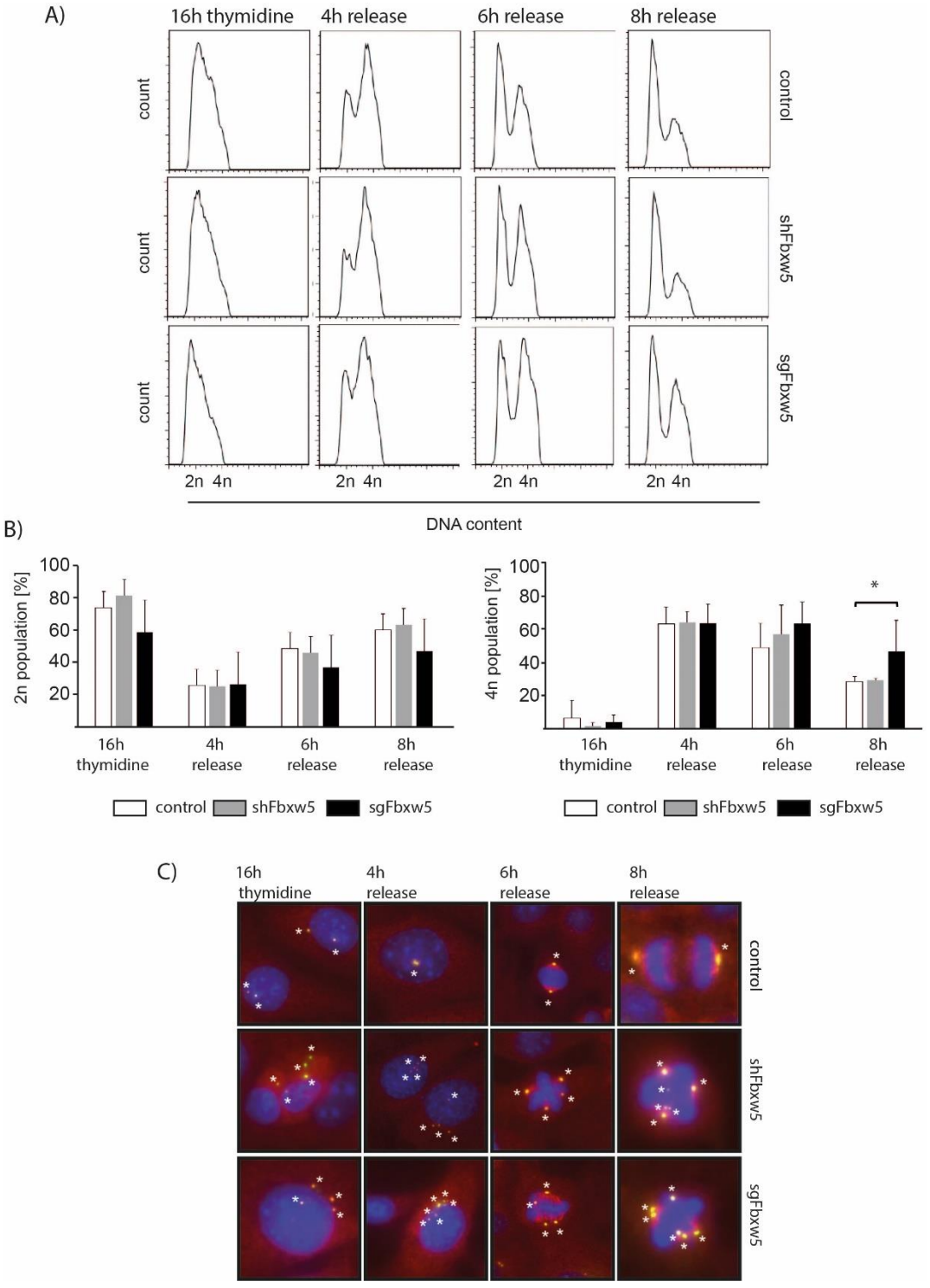

Figure 13 Depletion of FBXW5 leads to delay in G_2M transition. DNA content of synchronized BNL Cl.2 cells was determined using propidiumiodid staining and FACS analysis**.** (A) Representative picture of synchronized BNL CL.2 cells using single thymidine block. (B) Quantification of 2n (G_1; left panel) and 4n (G_2M, right panel) population in thymidine synchronized BNL CL.2 cells. (C) Fluorescence microscopy of FBXW5 suppressed and synchronized BNL CL.2 cells using y-tubulin (red) and pericentrin (green) to visualize centrosomes and DAPI (blue) to identify nuclei, while the white stars indicate the centrosome position. Cells with amplified centrosomes are illustrated, but without detailed quantification, due to the small sample size. Upper panel: control cells (counted cells: n=38). Middle panel: FBXW5 suppressed cells using miR-E based shRNA (counted cells, n=30). Lower panel: FBXW5 depleted cells using CRISPR/Cas9 mediated gene depletion (counted cells: n=60). Control cells resemble BNL CL.2 cells carrying the control plasmid shRen.713.

6.5 Consequences of reduced FBXW5 expression for cell growth, migration and *in vitro* transformation

Based on the previous observation that a reduction in FBXW5 delays G_2M transition, a more detailed analysis of cell proliferation and migration was performed in BNL CL.2 cells. The doubling time of BNL CL.2 with or without downregulation of FBXW5 was determined by counting cells every 24 h for up to 5 days. Whereas control cells and cells suppressed via shFbxw5 did not manifest any significant differences, cells with CRISPR/Cas9-mediated depletion showed a strong increase in the doubling time. Specifically, control cells (carrying shRen.713) and shFbxw5 cells exhibit an approximate doubling time of 25 hours, while sgFbxw5 cells show a doubling time of 38 hours (Figure 14 A, B). In addition, an Alamar Blue assay, which measures NADH-dependent conversion of resazurin to resorufin, revealed reduced metabolic activity developing over time for the cultures with FBXW5-depleted cells, consistent with a lower number of cells relative to control cultures (Figure 14 C).

It has been previously shown, that cells with supernumerary centrosomes often form extra cilia, which could give an advantage in cell movement [96]. To gather more insight into this potential physiological consequence of FBXW5 deprivation, motility of BNL CL.2 cells was analyzed. The *in vitro* scratch assay is a simple method to determine cell migration *in vitro*. It involves creating a “scratch” in a cell monolayer which closes up again over time due to the healing by cell migration. To determine the migration index which is a measure of the migration rate of the cells, images of the scratch are captured at the beginning and at regular intervals during the wound closure [97]. As shown in Figure 14 D and E, migration is impaired in cells with sgFbxw5-mediated *Fbxw5* disruption, since the wound closed only to 20% within 24 hours, whereas the control cells achieved a wound closure of 55-60% in the same period of time (Figure 14 D, E). In contrast, the migration indices of FBXW5-suppressed shFbxw5 cells and BNL CL.2 cells carrying the control plasmid did not show significant differences.

In addition to their defects in proliferation and migration, cells with supernumerary centrosomes are also believed to undergo malignant transformation processes, e.g. through occurrence of gain- or loss of function mutations, originating from chromosomal translocations [26, 27]. To analyze such patho-physiological alterations, BNL CL.2 cells with downregulated FBXW5 were tested for oncogenic transformation

by performing a semi-solid soft agar assay. The ability of cells to grow in semisolid agar into three-dimensional structures is an indicator that they are able to grow anchorage-independent, which in turn correlates with tumorigenicity [98]. As shown in Figure 14 F, BNL CL.2 cells with a FBXW5 deficiency, resulting from either shFbxw5 or sgFbxw5 expression, did not form colonies in the semi-solid agar, even after a cultivation period of two months. In contrast, c-Myc/Nras^{G12V} overexpressing hepatocytes, which served as a positive control, clearly did form colonies. This indicates that the loss of FBXW5 alone is insufficient to promote cellular transformation of BNL CL.2 cells *in vitro* (Figure 14 F).

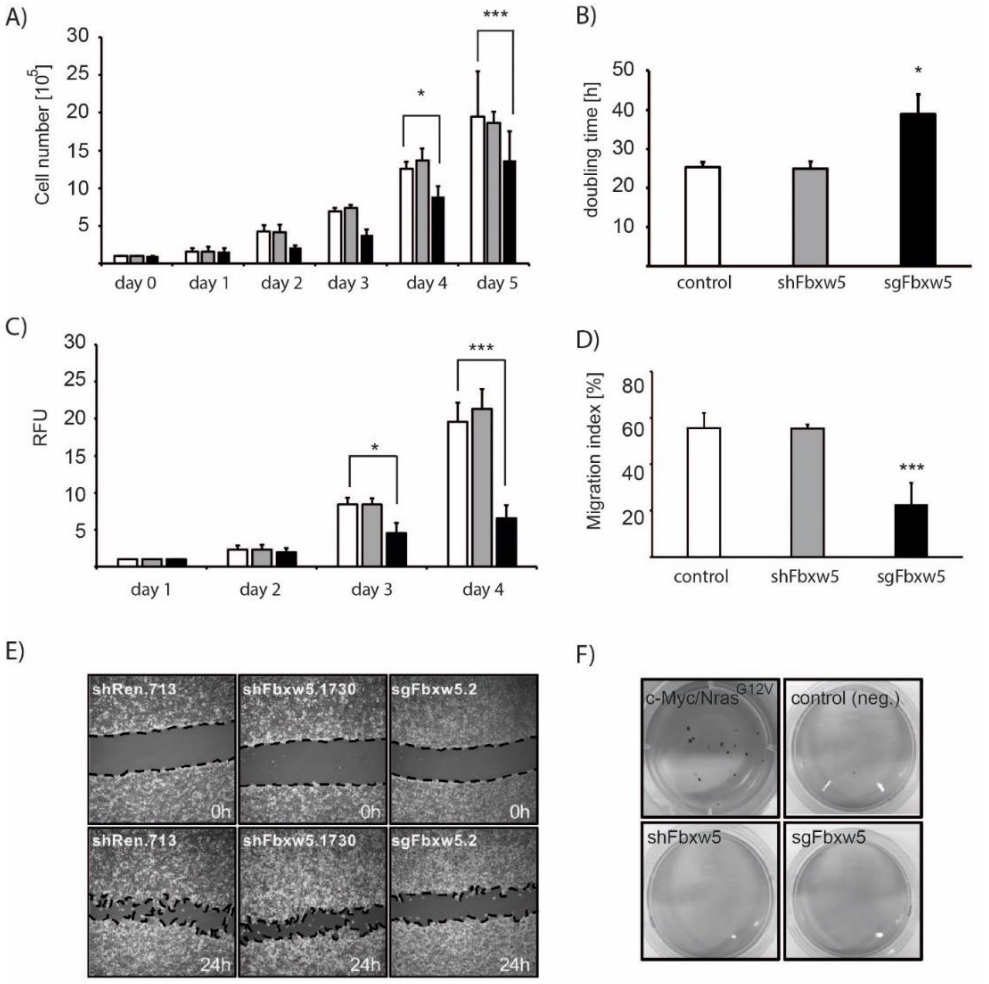

Figure 14 Effect of reduced FBXW5 expression on cell growth, migration and *in vitro* transformation. (A) Determination of BNL CL.2 cell number using trypan blue staining (error bars represent SD from at least three experiments (n=3). The significance was calculated by a two-tailed *t*-test and scored as follows: * P <0.05, :*** P <0.001). (B) Effect of shRNA or CRIPSR/Cas9 mediated *Fbxw5* silencing on cell doubling time. (C) Cell viability assay as determined with Alamar Blue assay (n=3). (D) Depletion of FBXW5 leads to impaired migration as determined by a scratch assay (n=3). Representative picture is illustrated in (E). (F) Depletion of FBXW5 by shRNA or CRISPR/Cas9 does not affect *in vitro* transformation as determined by a semisolid soft agar assay. Cells that undergo an oncogenic shift will form single colonies in semisolid agar. Positive control: c-Myc-NRAS^{G12V} overexpressing hepatocytes.

6.6 Creation of stable FBXW5 deficient cells for a genome wide screen using a CRISPR/Cas9 library

In the previous sections it has been shown that RNAi expression as well as CRISPR/Cas9 mediated gene editing are capable of silencing *Fbxw5*, and that this downregulation of FBXW5 gives rise to supernumerary centrosomes. Interestingly, the appearance of supernumerary centrosomes in cells unperturbed for FBXW5 [96], as well as depletion of FBXW5 without apparent effect on centrosome number [99-101], have both been linked to tumorigenesis in previous studies. Yet, the findings presented here indicate that loss of FBXW5 alone, even if associated with supernumerary centrosomes as consistently observed in this study, is not sufficient to induce tumor formation. On the contrary, depletion of FBXW5 significantly reduced proliferation and migration. One possible explanation for this apparent discrepancy might reside in the different genetic backgrounds of the various cell lines used, wherein additional genetic alterations might be present or absent, in accordance with the multistep model of cancer development [102, 103]. Especially in the light of the delay in the G_2M transition (Figure 13), which needs to be overcome for enhanced proliferation, it is hypothesized that the depletion of another tumor suppressor or the activation of an additional oncogene is required for tumor development. Thus, a genome wide screen was designed to uncover such potential targets that would rescue FBXW5$^{-/-}$ induced cell cycle delay and potentially induce tumorigenesis,

The mouse GeCKO CRISPR/Cas9 library (Addgene) consists of 130209 unique sgRNAs targeting over 21000 different genes, thus covering around 70% of the entire genome including a fraction of putative tumor suppressors or oncogenes. [87] Using this library enables an unbiased almost genome-wide functional screen to identify loss-of-function mutants which overcome the deficit in proliferation associated with the lack of FBXW5, as well as genes possibly involved in the homeostasis of the centrosome number. For the purpose of this screen, a new cell line carrying an internal deletion within FBXW5 was generated. Specifically, exon 5 was deleted using CRISPR/Cas9 gene editing. To this end, BNL CL.2 cells were transiently co-transfected with two plasmids which expresses a GFP-reporter gene alongside to the CRISPR/Cas9 element, with the first plasmid recognizing exon 4 (using pX458-sgFbxw5.18105) and the second plasmid exon 6 (using pX458sgFbxw5.18098) within *Fbxw5* (Figure 15 A).

Following transient transfection, cells were harvested for fluorescence-activated cell sorting (FACS) analysis. Hereby, cells expressing GFP upon successful transfection were detected and sorted into a 96-well plate as single cells (Figure 15 B). Cells were expanded and analyzed for deletion of exon 5. CRISPR/Cas9 mediated exon 5 deletion was verified by PCR; semiquantitative RT-PCR (Figure 15 C, D) and DNA sequencing (data not shown). To analyze the cells for the mutant phenotype, i.e. for the occurrence of supernumerary centrosomes, cells were stained for the centrosomal markers γ-tubulin and pericentrin (Figure 15 E, F). Centrosomes were quantified using immunofluorescence microscopy. As shown in Figure 15 E, the FBXW5$^{\Delta Exon5}$ mutant clearly shows an increase in cells having more than 2 centrosomes by 30% (Figure 15 E), which is comparable to the effects observed previously in cell lines depleted in FBXW5 (Figure 11). Therefore, cells were considered to be suitable for the GeCKO genome wide library screen.

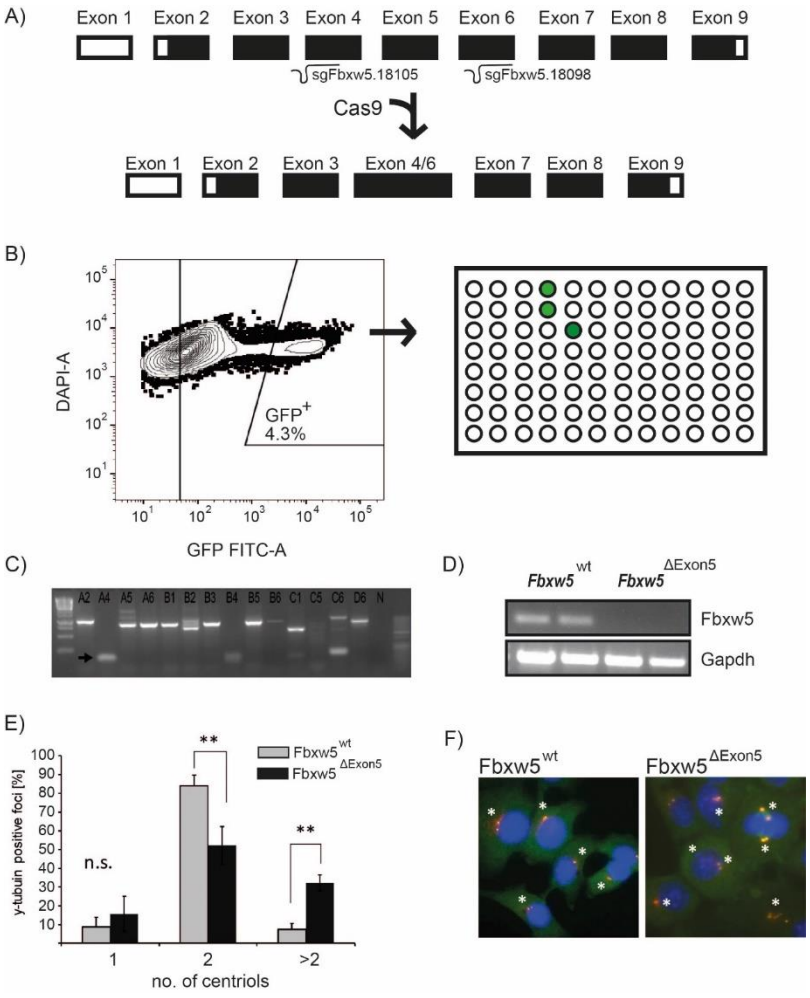

Figure 15 Cell sorting and screening for *Fbxw5* deletion. (A) Schematic illustration of the *Fbxw5* gene editing. sgRNAs targeting exon 4 and exon 6, resulting in a deletion of exon 5 within *Fbxw5*. (B) Illustration of flow cytometric analysis and single cell sorting. Cells were transfected with pX458-sgFbxw5.18105 (targeting exon 4) and pX458-sgFbxw5.18098 (targeting exon 5). (C) Exon 5 deletion was validated by PCR. Clone A4 was identified as an FBXW5$^{\Delta Exon5}$ mutant. (D) Fbxw5 depletion in clone A4 verified by semiquantitative PCR. (E) Quantification of centrioles per cell. Error bars represent ±s.d. from at least three experiments (n=3). The significance was calculated by a two-tailed *t*-test and scored as follows: **P<0.005. (F) Fluorescence microscopy *Fbxw5*^{wt} and *Fbxw5*$^{\Delta Exon5}$ cells using γ-tubulin (green) and pericentrin (red) to visualize centrosomes and DAPI (blue) to identify nuclei, while the white stars indicate the centrosome position (Magnification 600x).

6.7 CRISPR/Cas9 genome wide library identifies Replication Protein A2 (RPA2) to partially rescue FBXW5 knockout phenotype in BNL CL.2 cells

The GeCKO genome wide library is provided as two half-libraries (A and B), each containing 3 sgRNAs per gene. When used together, the library consists of 6 sgRNAs per gene. However, due to the huge size of the whole library it was decided to utilize only the sgRNAs represented in pool B (~ 62800 sequences). This library is delivered on a lentiviral backbone together with Cas9. For screening, BNL CL.2 wildtype cells and the *Fbxw5*$^{\Delta Exon5}$ deletion mutant cell line (clone A4; Figure 15) were transduced with the lentiviral particles at a low multiplicity of infection (MOI) and cultured with puromycin for 48h. Subsequently, cells were grown for 7 days without puromycin, followed by another 24 h period of selective growth in the presence of puromycin to eliminate cells that escaped the selection.

To monitor and quantify the abundance of each sgRNA, potentially amplified or depleted within the BNL CL.2 wildtype or *Fbxw5*$^{\Delta Exon5}$ mutant population, genomic DNA from both populations was isolated to amplify the sgRNA cassette via PCR as outlined in Figure 16 A). Subsequent Illumina deep sequencing analysis of both cell populations determined for each sgRNA sequence in the library the percentage among the total reads and identified the corresponding gene (Figure 16 B). The percentage values were used to calculate the x-fold change in enrichment or diminution of each single sgRNAs by comparing BNL CL.2 *Fbxw5*$^{\Delta Exon5}$ mutant to BNL CL.2 wildtype cells. Here, the frequency of the majority of sgRNAs did not significantly increase or decrease compared to the wildtype cells. However, several individual sgRNA sequences were found to be enriched as illustrated in Figure 16 C. Since each gene is represented by 3 different sgRNAs within the library sequence pool used, the relevance of a potential hit was evaluated based on the consistency of appearance of the entire sgRNAs triple for that target among all amplified sgRNAs. As a cutoff criterion for further evaluation, 2 out of 3 sgRNAs must reveal a ≥ 5-fold positive change. Out of overall 62,800 different sgRNAs, 6 triplets were identified to be enriched in the *Fbxw5*$^{\Delta Exon5}$ mutant cell line (Figure 16 D). As these data suggest, *Fbxw5*$^{\Delta Exon5}$ cells might gain a survival advantage from a reduction, or complete removal, of functions associated with anyone of these 6 candidate genes found.

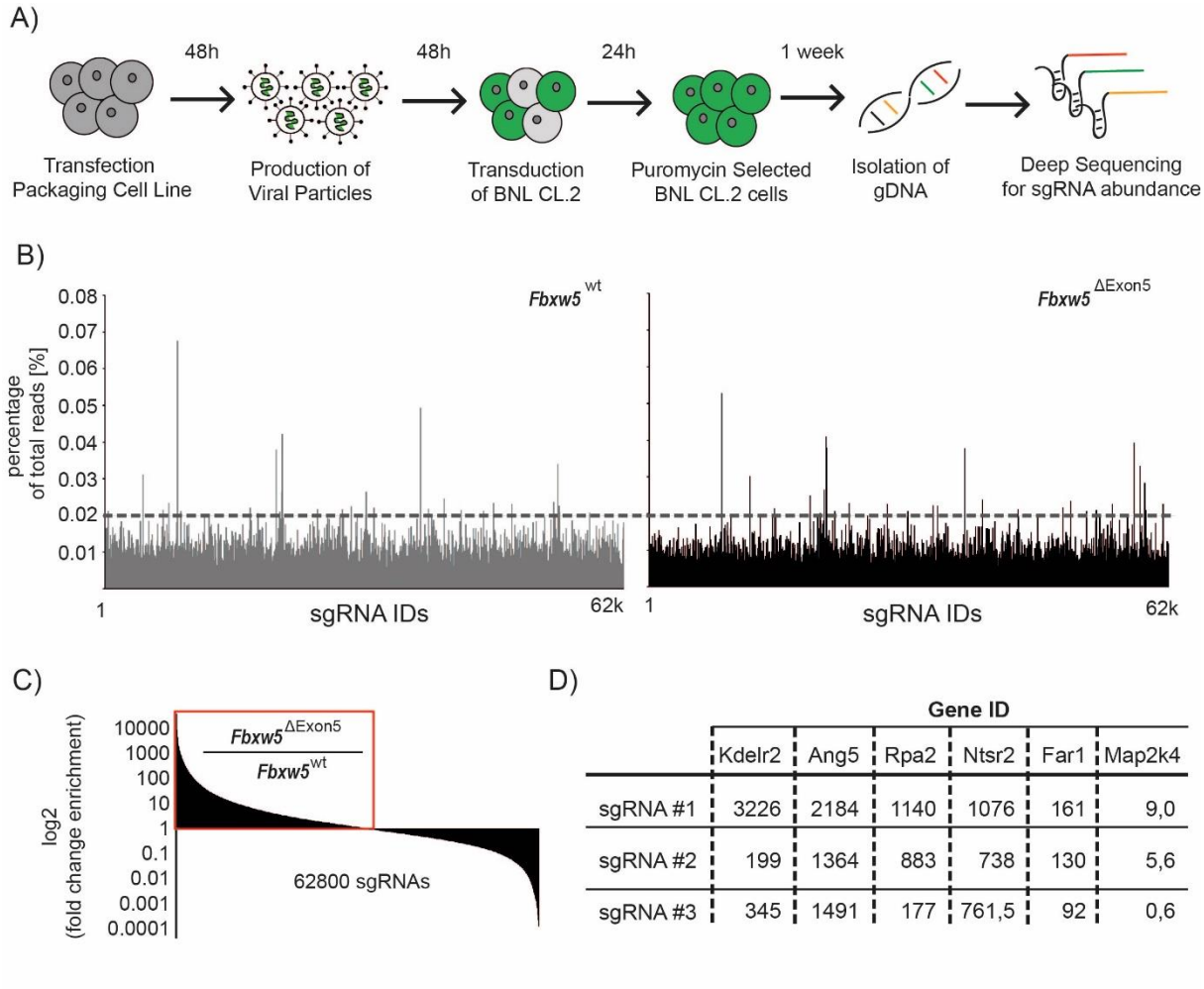

Figure 16 Positive *in vitro* genome wide library screen in FBXW5 depleted cells. (A) Schematic outline of the *in vitro* GeCKO CRISPR/Cas9 genome wide library screen. HEK293T packaging cell line was transfected with the GeCKO CRISPR/Cas9 library, producing infectious lentiviral particles (LPs). Pools of these LPs were used to infect BNL CL.2 cells. 48 hours after infection the cells were selected using puromycin. After selection and recovery of the cells, genomic DNA was isolated and the frequency of all sgRNAs in the population is quantified by deep sequencing. (B) Percentage of total reads of sgRNA abundance after deep sequencing in wildtype (left panel) and *Fbxw5*$^{\Delta Exon5}$ (right panel) cells. (C) Illustration of the enrichment (log_2 scale) of a pool of 62800 different sgRNAs that were encoded by the genome wide library. The representation of each sgRNA in *Fbxw5*$^{\Delta Exon5}$ cells after puromycin selection was compared to BNL CL.2 wildtype cells. (D) Table of targeted genes showing enrichment in all 3 sgRNA sequences in *Fbxw5*$^{\Delta Exon5}$ cells.

A very intriguing finding from this library screen is represented by the identification of replication protein a2 (RPA2) among the 6 candidates. RPA2 is part of the replication protein A complex, which binds and stabilizes single stranded DNA, either during DNA replication, or after DNA damage as part of the DNA damage response (DDR) [104, 105]. Defects in DNA replication or DDR are associated with a prolonged G2 phase [106], genomic instability, and have a high potential to cause oncogenic transformation [107]. Spindle-induced DNA damage [25], perhaps resulting from presumably

deregulated centrosomes in *Fbxw5*$^{\Delta Exon5}$ cells, might call upon this central role of RPA2 in response to DNA damage-induced cellular stress and orchestrate a G_2M delay, just as observed in FBXW5-suppressed cells (Figure 13). Thus, *Fbxw5*$^{\Delta Exon5}$ cells might benefit from loss of RPA2 function. To further investigate consequences of *Rpa2* deficiency on cell fate in presence or absence of functional FBXW5, BNL CL.2 cells were transduced with the same sgRNA triple, which was identified through the genome wide library screen (Figure 16 D). Surprisingly, it was not possible to obtain a viable *Rpa2*-deficient cell line, neither with wildtype nor in the *Fbxw5*$^{\Delta Exon5}$ mutant background (data not shown). Since Illumina deep sequencing analysis only monitors relative abundance of Rpa2 sgRNA loci and cannot assess expression of the protein, it seems possible that the screen enriched for cells carrying only a heterozygous gene disruption. Heterozygosity could lead to a somewhat reduced intracellular RPA2 level, just sufficiently low to be advantageous to *Fbxw5*$^{\Delta Exon5}$, but high enough to maintain viability. In line with this hypothesis, attempts to use RNAi for suppression also failed, strongly suggesting that a complete loss of *Rpa2* is indeed lethal (data not shown). Correspondingly, a fractional reduction of endogenous RPA2 is tolerable as evident from the use of a tet-adjustable miR-E embedded shRNA, which reduces the level of RPA2 to about 50% (Figure 17 A). As expected from the attempts creating the RPA2 null mutant, crystal violet staining as well as the Alamarblue assay revealed that a partial loss of RPA2 led to a very pronounced reduction in cell proliferation, both in wild-type and in *Fbxw5*$^{\Delta Exon5}$ mutant cells (Figure 17 B, C). Surprisingly, this apparent inhibition of proliferation was partially relieved in the *Fbxw5*$^{\Delta Exon5}$ mutant (Figure 17 D), suggesting that FBXW5 deficiency is beneficial to the *Rpa2* mutant, whereas RPA2 reduction negatively affects *Fbxw5*$^{\Delta Exon5}$ cells. Clearly, further analysis has to be conducted to resolve this issue.

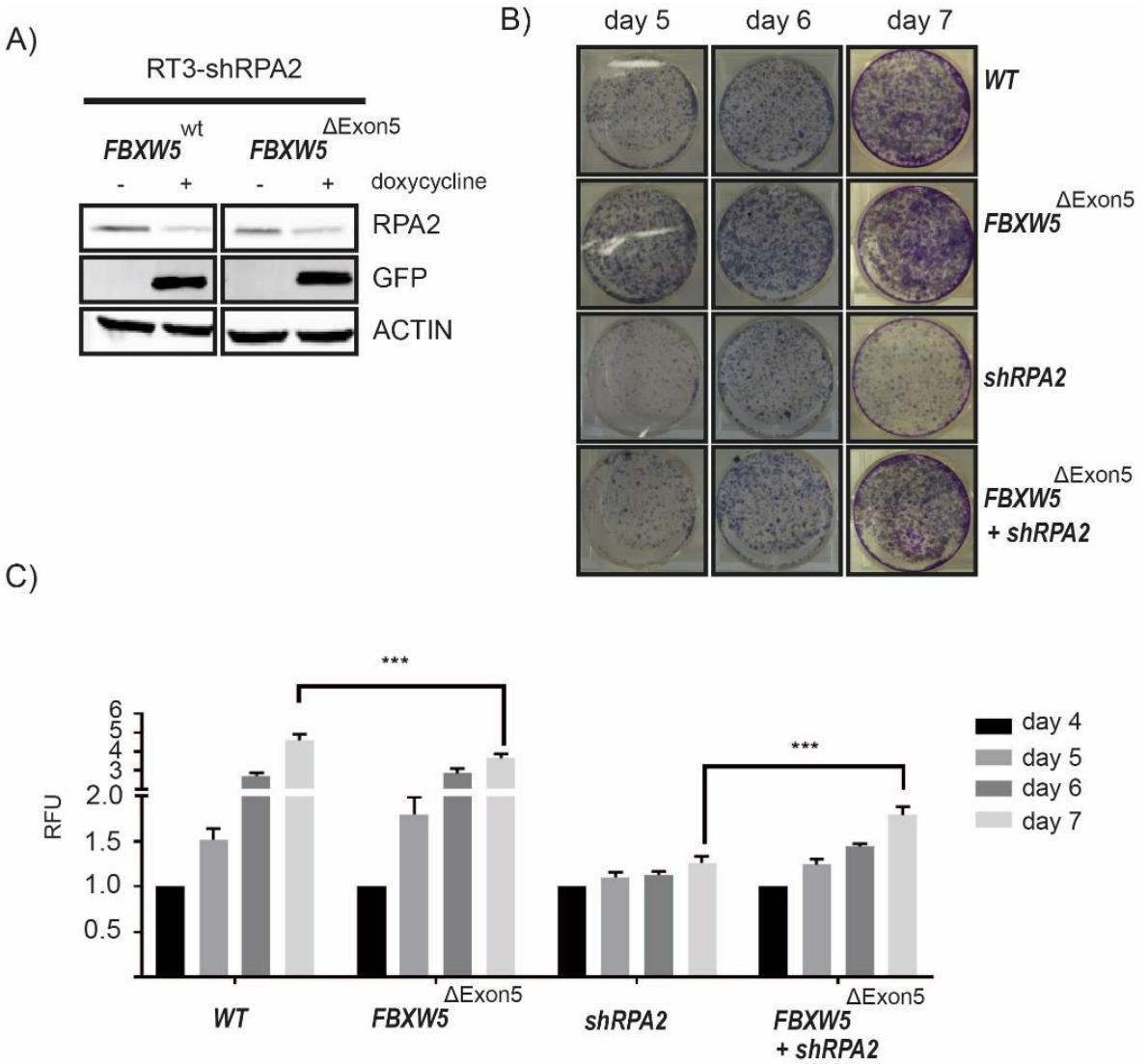

Figure 17 Partial loss of RPA2 is abrogated by *Fbxw5*$^{\Delta Exon5}$ (A) Doxycycline-inducible suppression of RPA2 and GFP induction as determined by western blot using the indicated antibodies (B) Non-quantitative proliferation assay using crystal violet staining. (C) Quantitative cell viability assay using Alamarblue. Error bars represent ±s.d. from at least three experiments (n=3). The significance was calculated by a two-tailed *t*-test and scored as follows: **P<0.005

6.8 Analysis of the pathophysiological influence of FBXW5 suppression in an *in vivo* mosaic mouse model using the SB13 transposase system

The next step was to study the impact of FBXW5 deficiency in adult hepatocytes *in vivo*. Particularly interesting was the question, whether a miR-30-shRNA mediated suppression of FBXW5 and the resulting genomic instability, is sufficient to induce a malignant transformation *in vivo* in wildtype C57BL/6J mice. As a first approach to establish a stable and physiological model allowing induction of FBXW5 suppression and observation of the associated pathophysiological processes in the liver, a transposon mediated delivery of miR-30-shRNA based on the Sleeping Beauty transposon system was applied. It has been reported, that within the first five days after injection, this procedure may yield approximately 38% transfected hepatocytes and 13% stably transfected cells after six days [108]. For that purpose, 25µg of the transposable plasmid pCaggs-miR30-shFbxw5.1730 (shFbxw5) and pCaggs-miR30-shRen.713 (control), together with 5µg of Sleeping Beauty 13 (SB13) transposase were injected into a 4-6-week-old mouse via HDTVi. Isolated livers were then analyzed one week and one month after HDTVi. As expected, the visualization of the native GFP signal showed roughly 10-15% of stably transfected hepatocytes after one week, but no abnormalities in the morphological structure of the liver (Figure 18 A) could be detected. However, if the liver was inspected one month post HDTVi, the GFP signal was no more detectable neither macroscopically nor microscopically (Figure 18 A), indicating that FBXW5-suppressed cells had been eliminated. Consistent with this observation, HE staining did not reveal any significant morphological abnormalities. Similar results were obtained from $p19^{-/-}$, $p21^{-/-}$ and $p53^{albCre}$ mice with genetic backgrounds favoring tumorigenesis (data not shown; summarized in Table 15). To overcome the putative elimination of FBXW5-suppressed hepatocytes, it was decided to use as a second approach: a system for liver repopulation. The fumarylacetoacetate hydrolase (FAH) knockout mouse displays such a powerful repopulation system [90, 109]. Mice harboring an FAH knockout are unable to catabolize tyrosine, which results in the accumulation of 4- fumarylacetoacetic acid, an intermediary hepatotoxin [110]. Treatment of $FAH^{-/-}$ mice with nitisinone (NTBC) prevents this accumulation, and withdrawal of this drug leads to acute liver failure and death.

Instead of treatment with nitisinone, the lethal $FAH^{-/-}$ phenotype can be rescued by the combined injection of a transposon plasmid that expresses FAH together with a transposase expression construct. Here, the transposable element was designed according to Wuestefeld et. al [90]. The resulting FAHIG-shFbxw5.1730 (shFbxw5) and FAHIG-shREN.713 (control) encode a FAH cDNA together with miR-30-shFbxw5, or shRen.713 as a control, respectively. These constructs were co-injected with SB13 transposase into a 6-week-old $FAH^{-/-}$ mice. Immediately after HDTVi, the mice were withdrawn from NTBC to allow liver repopulation with hepatocytes stably expressing FAH-miR-30-shRNA. As expected, non-injected $FAH^{-/-}$ mice suffered from acute liver failure and died within 1 or 2 months after NTBC withdrawal. Two months after delivery of the transposable elements, macroscopic visualization of GFP, as well as FAH-staining showed successful repopulation. However, no significant differences could be observed for FAH-miR-30-shFbxw5 or the control (FAH-miR-30-shRen.713) (Figure 18 B). In addition, HE staining did not reveal morphological abnormalities. Analyzing the liver specimen for FBXW5 expression has shown that it was not possible to detect FBXW5 knockdown, neither with qPCR nor western blot analysis (Figure 18 C). However, it should be kept in mind that the liver specimen does not only consist of the FBXW5 knockdown affected hepatocytes, but also cholangiocytes, Kupffer cells and multiple blood transporting capillaries, considering that the FBXW5 knockdown in the hepatocytes would be masked by the other liver- and blood cells.

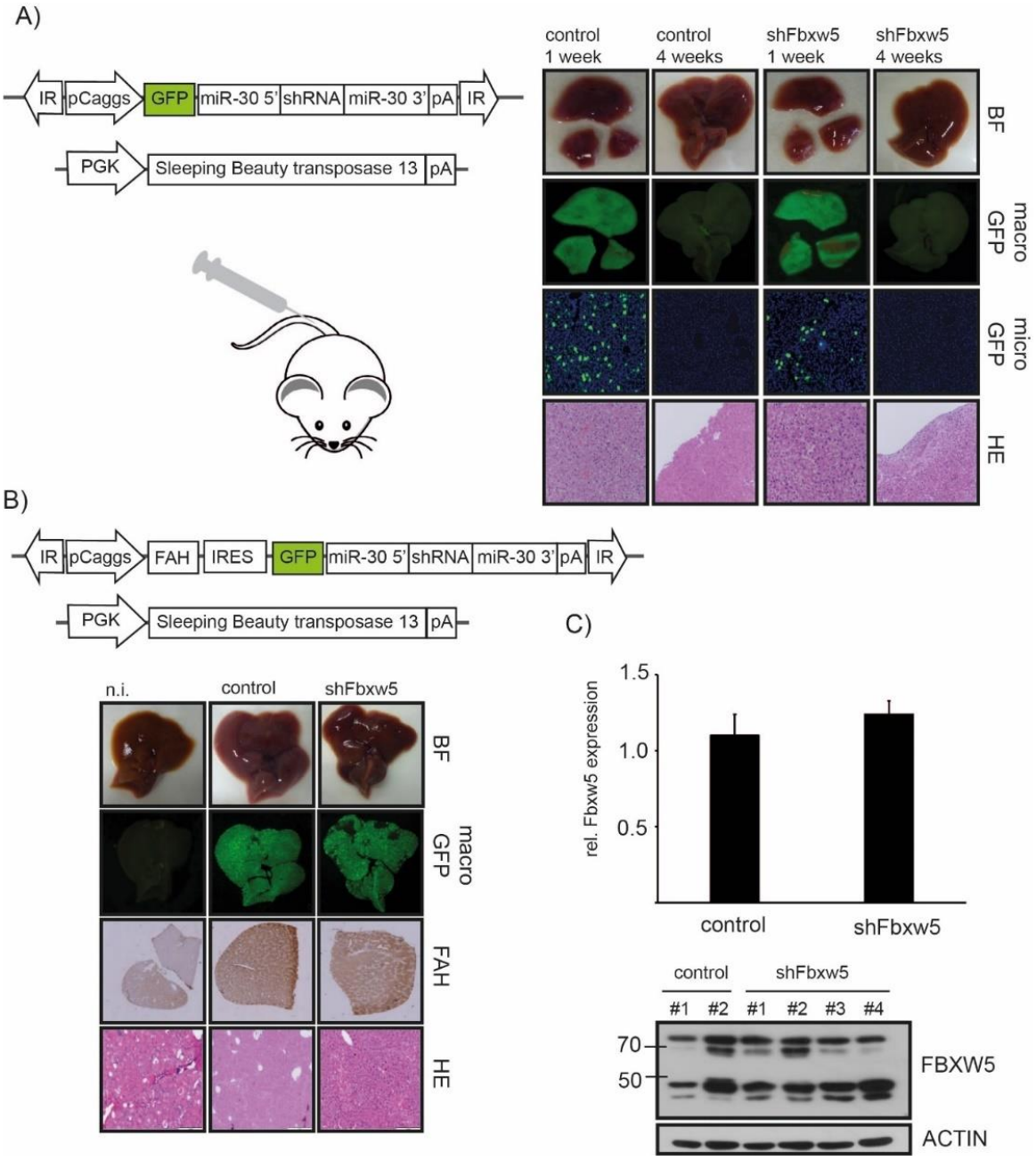

Figure 18 miR-30 shFbxw5 does not lead to malignant transformation *in vivo.* (A) Left panel: Scheme of transposable element and Sleeping Beauty transposase 13, which were injected into the tail vein of a 4-6-week-old mouse within 5-7 seconds. Right panel: wildtype mouse liver samples one and 4 weeks after injection of the transposable elements harboring control- or Fbxw5 shRNA. (B) Upper panel: scheme of transposable FAHIG element. Lower panel: Analysis of repopulated liver harboring control (shRen.713) and shFbxw5. Non-injected (n.i.) specimen represents repopulation control. (C) Upper panel: qPCR analysis of the FAH-miR-shRNA repopulated livers: no significant suppression in FBXW5 is observed. Lower panel: Western blot analysis of FBXW5 suppression in the repopulated specimen. The expected size of FBXW5 is 64kDa. The double band running below 50 kDa resembles a cross-reacting protein (as determined by mass-spectroscopy after excision and elution of the cross-reacting protein, data not shown).

Table 15 List of HDTV injected mice

			macroscopic		microscopic	
Mice strain	**Plasmid DNA**	**Time [weeks]**	**BF**	**GFP**	**HE**	**GFP**
C57BL/6J	pCaggs shRen.713 + SB13	1	normal	+	normal	+
		4	normal	-	normal	-
		12	normal	-	normal	-
	pCaggs shFbxw5.1730 + SB13	1	normal	+	normal	+
		4	normal	-	normal	-
		12	normal	-	normal	-
	pX458 sgFbxw5.2	1	normal	+	normal	+
		4	normal	-	normal	-
		12	normal	-	normal	-
C57BL/6J p19$^{arf-/-}$	pCaggs shRen.713 + SB13	1	normal	+	normal	+
		4	normal	-	normal	-
		12	normal	-	normal	-
	pCaggs shFbxw5.1730 + SB13	1	normal	+	normal	+
		4	normal	-	normal	-
		12	normal	-	normal	-
	pX458 sgFbxw5.2	1	normal	+	normal	+
		4	normal	-	normal	-
		12	normal	-	normal	-
C57BL/6J p21$^{-/-}$	pCaggs shRen.713 + SB13	1	normal	+	normal	+
		4	normal	-	normal	-
		12	normal	-	normal	-
	pCaggs shFbxw5.1730 + SB13	1	normal	+	normal	+
		4	normal	-	normal	-
		12	normal	-	normal	-
	pX458 sgFbxw5.2	1	normal	+	normal	+
		4	normal	-	normal	-
		12	normal	-	normal	-
C57BL/6J (p53^{AlbCre})	pCaggs shRen.713 + SB13	1	normal	+	normal	+
		4	normal	-	normal	-
		12	normal	-	normal	-
	pCaggs shFbxw5.1730 + SB13	1	normal	+	normal	+
		4	normal	-	normal	-
		12	normal	-	normal	-
	pX458 sgFbxw5.2	1	normal	+	normal	+
		4	normal	-	normal	-
		12	normal	-	normal	-

6.9 Creation of a transgenic floxed *Fbxw5* gene for conditional *Fbxw5* knockout models

Since it was not possible to observe any effects in murine liver upon miR-30 shFbxw5 delivery, it was decided to use a third approach, that is, to create a transgenic mouse model, in which the depletion of the *Fbxw5* gene can be achieved in a tissue specific manner. For this purpose, the Cre/loxP recombination system is a very helpful tool [111]. Briefly, this strategy involves flanking the target gene with *loxP* sites which are recognized by Cre recombinase. Tissue-specific expression of Cre recombinase will induce deletion of the target gene. The general scheme of this strategy involves several steps. First, it is necessary to create an *Fbxw5* allele that is flanked by two homologous arms and two *loxP* sites. Next, this construct is transferred into a Cre-expressing mouse. To this end, the floxed *Fbxw5* allele ("floxed = flanked by *loxP* sites) has to be introduced into mouse embryonic stem cells (ES cells), followed by injection of the transformed ES cells into blastocysts, which allows the creation of a chimeric mouse.

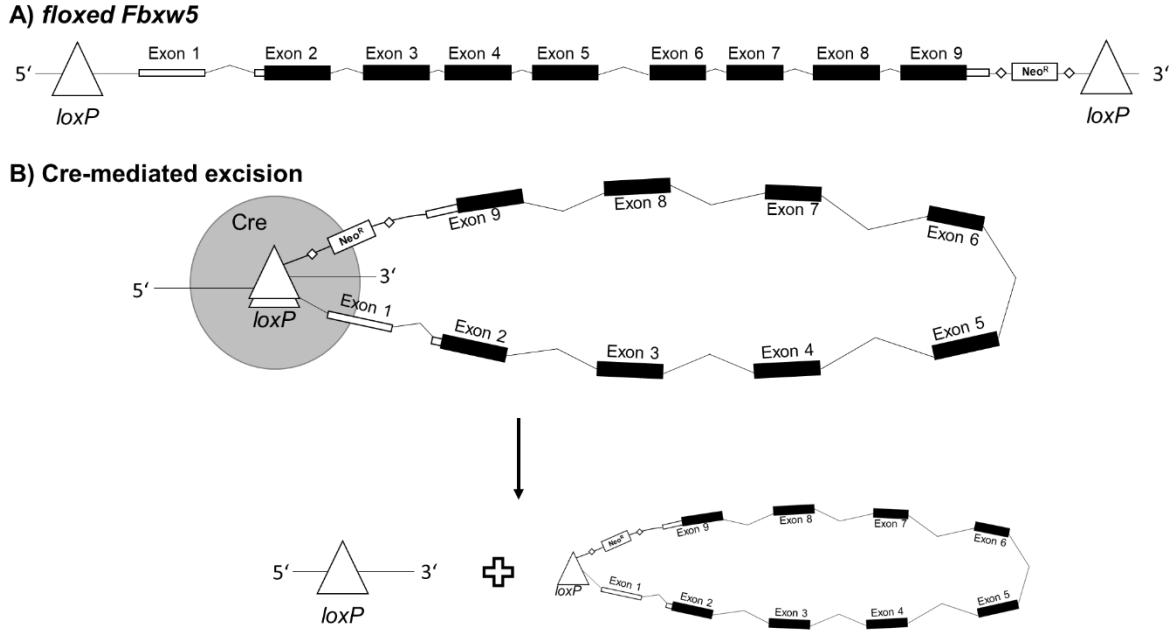

Figure 19 Cre/loxP mediated excision of a *floxed Fbxw5* transgene. (A) Intron-exon structure of the *Fbxw5*-transgene. *LoxP* sites are introduced 5'-upstream, as well as 3' downstream of the *Fbxw5* coding region. (B) The inverted *loxP* consensus sequenced result in a looped structure of *Fbxw5*.Cre recombinase mediates the site-specific deletion of the Fbxw5 sequences between the two *loxP* sites. After Cre mediated site-specific recombination, *Fbxw5* is substituted from the chromosome, resulting in a *Fbxw5* knockout

Such chimeric mice are mated with wildtype mice (backcrossing), whose progenies are screened for the heterozygous transgene. Mice carrying the *floxed Fbxw5* transgene need to be crossed with a Cre-expressing transgenic mouse, where Cre is

expressed from a promoter that is active in hepatocytes. Ultimately, the tissue-specific induction of the loxP-specific recombinase Cre should induce the deletion of the *Fbxw5* gene via site specific recombination (Figure 19).

To create the floxed *Fbxw5* allele, a multistep process using the page lambda (λ) derived Red recombination system was chosen (Figure 20) [84, 112]. The 34 bp loxP sequences (5'-ataacttcgtataatgtatgctatacgaagttat-3') were inserted 5'-upstream as well as 3'-downstream of the Fbxw5 gene (Figure 19 A) in a consecutive manner, according to the method described by Sharan et al. [112]. A bacterial artificial chromosome (BAC) vector partially harboring the mouse DNA sequence of chromosome 2 (BAC$^{e3.6}$; see 5.3.14) [83, 112] was used as a source for *Fbxw5.* The detailed approach for the construction of the knockout mouse and the verification of the individual steps is described below.

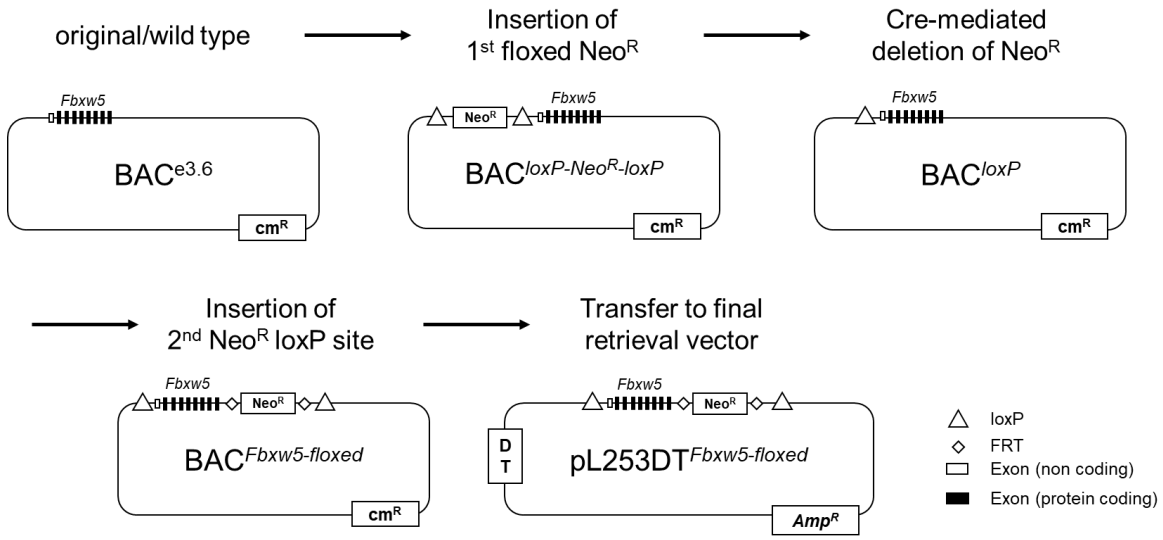

Figure 20 Cloning strategy to design a *Fbxw5$^{loxP/loxP}$* expression vector for the development of a transgenic mouse model. Wildtype mouse *Fbxw5 gene* with its 9 exons and 8 introns is obtained from BAC$^{e3.6}$. The white bars represent non-coding regions of the gene, whereas black bars represent coding regions. Using homologous recombination, a *loxP*-flanked *Neo^R* cassette will be introduced 5' upstream of *Fbxw5* in the 1st recombination step. In the second step the *Neo^R* cassette is excised by a Cre-mediated deletion, leaving one *loxP* site behind. After the introduction of the first *loxP* site in the 5'-UTR of *Fbxw5,* an FRT-flanked *Neo^R* cassette harboring an additional loxP site, is introduced at the 3' end of *Fbxw5*. Shuttling of the floxed *Fbxw5* into a eukaryotic retrieval vector (pL253DT) represents the last step in the generation of the final construct. For the generation of transgenic ES cells, the PGK driven *Neo^R* is used for positive selection, whereas the Diphtheria toxin A fragment represents a negative selection marker to avoid the integration of the plasmid backbone into the eukaryotic genome.

6.10 Insertion of the first *loxP* site at the 5' UTR of *Fbxw5*

The first step for the generation of the *floxed Fbxw5* gene was the insertion of *loxP* sites at the 5' UTR of the first exon of *Fbxw5*, carried on BAC$^{e3.6}$ (see 5.3.14). To this end, a *floxed Neomycin^R (Neo^R)* cassette was introduced upstream of *Fbxw5*, where the EM7 driven neomycin resistance cassette allows for positive selection in *E. coli*. After subsequent excision of *Neo^R*, using an inducible Cre recombinase, a single *loxP* site will remain at the 5´ UTR of *Fbxw5*.

In Detail, the *loxP-Neo^R-loxP*, cassette was amplified from plasmid pL452 (see 5.3.14) which contains a *floxed Neo^R cassette*. 70-80mer primers (lox-Neo-lox fw; lox-Neo-lox rev)) consisting of 20 bp that share homology to the template plasmid (pL452) and additional 50 bp that are homologous to the 5' UTR of *Fbxw5* (Figure 21). Additionally, a *XhoI* recognition site was inserted upstream of the first *loxP* site as well, enabling the possibility to perform in depth southern blot analyses in potential ES-cell clones. The amplified *loxP-Neo^R-loxP* cassette was gel purified, transformed into heat-activated DH10αSW102 carrying BAC$^{e3.6}$, and plated on kanamycin containing LB agar plates to select for the intended recombination.

Single colonies were tested for kanamycin (kan$^+$) and chloramphenicol (cm$^+$) resistance and ampicillin (amp$^+$; negative control) sensitivity on appropriate plates. In addition, genotype analysis was performed by colony-based PCR. To this end, primers were designed to have homology to the *Neo^R* sequence (Neo F1, Neo B1) and the 5' UTR of *Fbxw5* (F2, B2). If the cassette has been inserted correctly, the primer combinations NeoF1/B1 and F1/NeoB1 amplify PCR fragments of approximately 500 bp consisting parts of the 5´UTR of *Fbxw5* and either the upstream or the downstream end of the inserted cassette. In contrast, if the cassette has not been inserted into *Fbxw5*, the primers F2 and B2 amplify a 200 bp fragment consisting of wildtype *FBXW5* As shown in Figure 21 B, two clones (lane 1 and 7) are positive for the 500 bp fragment amplified with both the primer pair NeoF1/B1 and F1/NeoB1 and negative for the 200 bp fragment amplified by using primers F2 and B2. Therefore, these clones are considered to carry the *floxed NeoR* cassette upstream of *Fbxw5*.

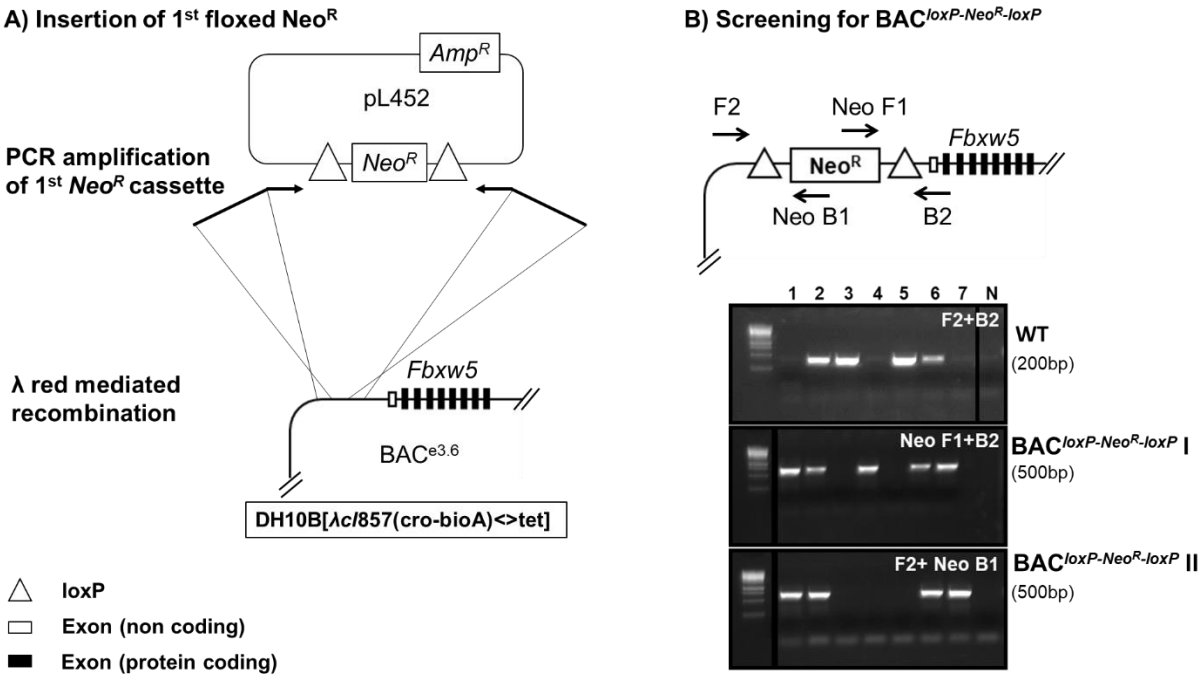

Figure 21 Insertion of *floxed Neo^R* cassette 5‘ upstream of *Fbxw5*. (A) Schematic plot of the first recombination step. The donor plasmid pL452 served as template for the PCR amplification of the *floxed Neo^R* cassette. The 70-80 mer primers for PCR amplification of the cassette consist of 20 bases with homology to the plasmid DNA and 50 bases with homology to 5’ UTR of *Fbxw5*. The PCR-amplified *floxed Neo^R* is used for the homologous recombination with Bac$^{e3.6}$. To this end, both PCR amplicon and *Fbxw5* vector DNA are transformed into heat-activated DH10B[λ*cI*857(cro-bioA)<>tet] (*E.coli* SW102). After homologous recombination, the *floxed Neo^R* cassette is inserted at the 5’UTR of *Fbxw5*. (B) Scheme of primer binding sites for genotyping of Bac$^{loxP\text{-}Neo^R\text{-}loxP}$. Primer pairs F2 and B2 are homologous to the *Fbxw5*, whereas the primer pairs Neo F1 and Neo F2 bind within the *Neo^R* gene. Combination of F2 and B2 results in a wildtype amplicon of 200bp, as observed in clones 2,3,5,6. Combination of the primer pairs Neo F1 with B2, and F2 with Neo B1 verifies the correct integration of the *floxed Neo^R* cassette in the 5’UTR of *Fbxw5*. The clones 1 and 7 were negative for the wildtype band (F2+B2) and positive for the incorporated *Neo^R* cassette and were considered successful.

Next, the newly created “BAC$^{loxP\text{-}Neo^R\text{-}loxP}$“ vector was purified from clone 1 (Figure 21 B) and transformed into *E.coli* SW106 (Figure 22 A), a strain that is able to express Cre-recombinase under the control of the arabinose-inducible pBAD promoter. To induce Cre-recombinase the bacteria were cultured in normal LB containing 0.1% (v/v) arabinose, resulting in the Cre mediated deletion of the *Neo^R* cassette. The bacteria were plated on LB cm$^+$ plates and genotyped for the Neo^R depletion using the primer pair F2/B2, as described before. Successful Cre-mediated, site-directed deletion of the *Neo^R* cassette, results in an PCR amplicon of 300bp (BAC^{loxP}), whereas non-recombined BAC$^{loxP\text{-}Neo^R\text{-}loxP}$ does not show an PCR product. As mentioned previously, wildtype *Fbxw5* (BAC$^{e3.6}$) has a PCR amplicon of 200bp and served as a positive control.

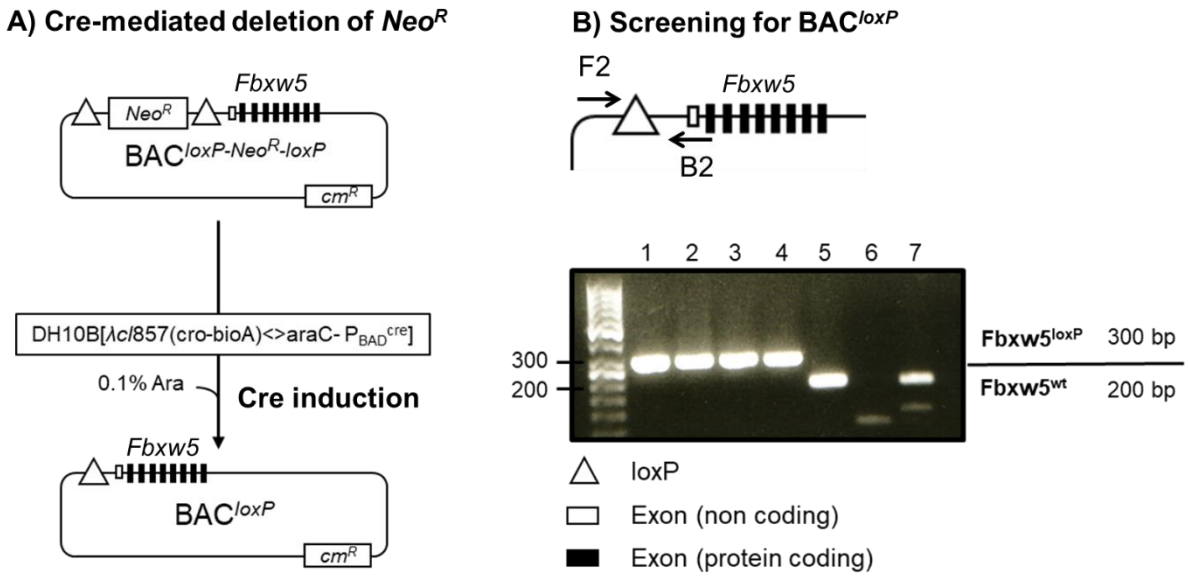

Figure 22 Cre-mediated deletion of *Neo*^{R} and generation of the first single *loxP* site. (A) Bac$^{loxP\text{-}Neo^R\text{-}loxP}$ was transformed into DH10B[λ*cI*857(cro-bioA)<>araC-P_{BAD}^{cre}] (SW106). By adding 0.1% (w/v) L(+) arabinose Cre-recombinase is induced, leading to the deletion of *Neo*^{R}. A single loxP site remains in the 5' UTR of *Fbxw5*. (B) Scheme and representative picture of the genotyping of the first *loxP*-site: clones 1,2,3,4 showing an amplicon of 300bp, representing the first *loxP* site in the 5'UTR of *Fbxw5*. Lane 5 and 7 are wildtype *Fbxw5,* with line 5 representing BACe$^{3.6}$ and line 7 gDNA isolated from NIH/3T3 cells. Line 6 represents H_2O (negative control).

6.11 Insertion of the FRT-Neo^R-FRT-loxP site at the 3' end of *Fbxw5*

For insertion of the second *loxP*-site in the *Fbxw5* gene, the pL451 plasmid (see 5.3.14) was used as a template to PCR-amplify an *FRT-Neo*^{R}*-FRT-loxP* cassette, which is later inserted at the 3' end of *Fbxw5* via homologous recombination. Similar to the first recombination process, 70-80 mer primer pairs were designed and contain 20 base pairs with homology to the *FRT-Neo*^{R} plasmid pL451 and 50 base pairs with homology to the 3'UTR of *Fbxw5,* to ensure correct recombination at the specific foci (Figure 23 A).

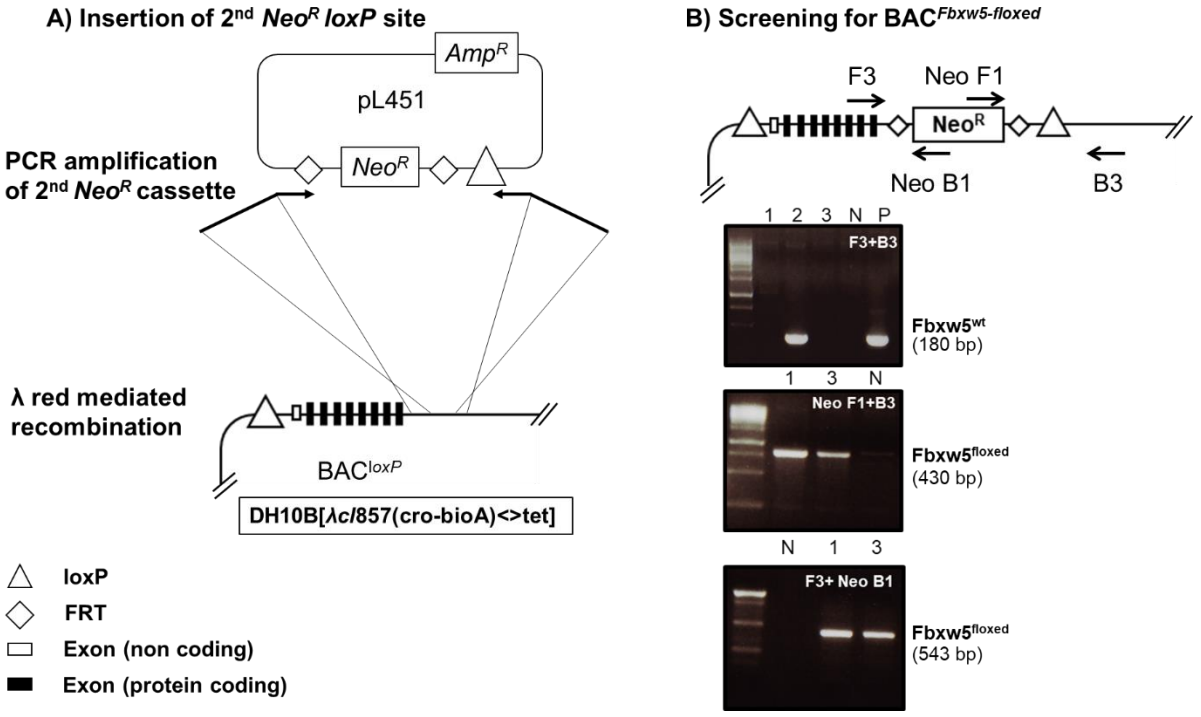

Figure 23 Insertion of 2nd *NeoR loxP* site 3' downstream of *Fbxw5*. (A) Schematic plot for the site-directed recombination of *FRT-NeoR-FRT-loxP* into BAC*loxP*. The plasmid pL451 served as donor for PCR amplification of the *FRT-NeoR-FRT-loxP* cassette. The 70-80mer primers consists of 20 bases with homology to the plasmid pL451 and 50 bases with homology to the 3' UTR of *Fbxw5*. The PCR amplicon (*FRT-NeoR-FRT-loxP*) and BAC^{loxP} are co-transformed into heat-activated DH10B[λ*cI*857(cro-bioA)<>tet] (*E.coli* SW102), resulting in a site directed homologous recombination in the 3' end of *Fbxw5*. (B) Scheme of primer binding sites for genotyping BAC*Fbxw5-floxed*. The primer pair F3 and B3 bind within the *Fbxw5* gene, and a fragment size of 180bp represents wildtype *Fbxw5* (lane 2), whereas no signal is observed when the *FTR-NeoR-FRT-loxP* cassette is incorporated in the 3' UTR of *Fbxw5*. To verify the site directed recombination of *FRT-NeoR-FRT-loxP* the primer pairs Neo F1/B3 (430bp), as well as F3/NeoB1 (543bp) were used. The colonies 1 and 3 are positive for correct insertion of the *FRT-NeoR* cassette.

After the co-transformation of the *FRT-NeoR-FRT-loxP* cassette and the Bac*loxP* template into heat-activated *E. coli* SW102, the appearing single colonies were analyzed regarding the expected recombination event. To this end, single colonies were transferred to kanamycin (kan$^+$) and chloramphenicol (cm$^+$) plates, as well as ampicillin (amp$^+$) plates as a negative control. Only those colonies which showed resistance to kanamycin and chloramphenicol, but sensitivity to ampicillin, were genotyped with respect to the correct insertion of the *FRT-NeoR-FRT-loxP* cassette (Figure 23 B). For genotyping, primers shared homology to the *NeoR* sequence (Neo F1, Neo B1) and the 3' UTR of *Fbxw5* (F3, B3). As shown in Figure 23 B, clone 2 (lane 2) has shown a 180 bp fragment when using primers F3/B3, which corresponds to the expected size for wildtype *Fbxw5.* Therefore, clone 2 is excluded for further experiments. Clones 1 and 3 were positive for the *FRT-NeoR-FRT-loxP* cassette. Here,

a 430 bp fragment is detected using the primer pair NeoF1/B3 and a 540 bp fragment when using F3/NeoB1, which corresponds to the expected sizes for *Fbxw5* carrying the inserted *FRT-Neo*^{R} cassette.

6.12 Shuttling of *floxed Fbxw5* into a eukaryotic expression vector for the generation of transgenic ES-cells

Next, the *floxed Fbxw5* was transferred to the eukaryotic expression vector pL253DT, (see 5.3.14). pL293DT is derived from the vector pL253, described by Liu et al. [84], and has been modified by introducing a diphtheria toxin A (DT) fragment. Besides the DT cassette for negative selection in ES-cells, pL253DT also carries an ampicillin resistance gene for selection and propagation in *E. coli*. Prior to the transfer of the *floxed Fbxw5* gene to pL293DT, it is necessary to insert two homology regions (HRe), located 5' upstream and 3' downstream of *Fbxw5* into pL293DT (Figure 24 A).

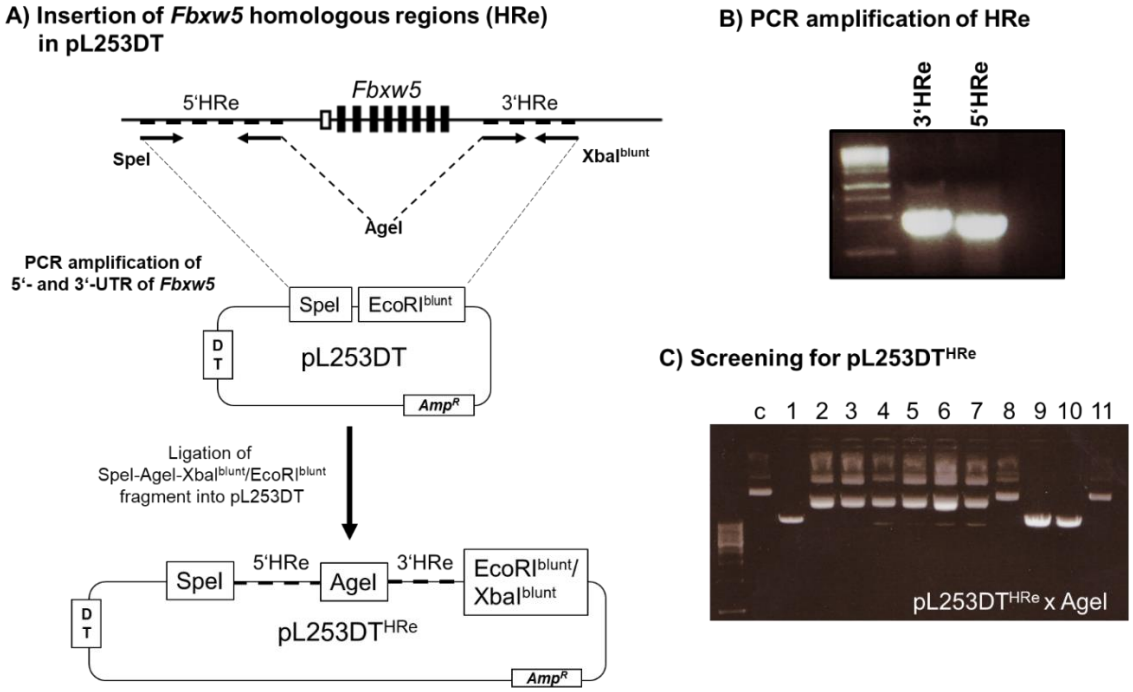

Figure 24 Preparation of *Fbxw5*-retrieval vector pL253DT. (A) Schematic overview of the cloning strategy to prepare the Fbxw5 retrieval vector pL253DT^{HRe}. The forward primer for the 5' homology arm carries an additional SpeI site, and the reverse primer for the 3' homology arm an additional XbaI^{blunt} site. The reverse primer of the 5' homology arm as well as the forward primer of the 3' homology arm carries an AgeI recognition site. The amplified arms were ligated into a SpeI and EcoRI^{blunt} digested pL293DT. (B) Representative picture of the PCR-amplified homologous regions of *Fbxw5.* (C) Representative picture of AgeI digested probes of pL253DT^{HRe} clones. Correct pL253DT^{HRe} will linearize upon AgeI treatment (clones 1, 9, 10), whereas original pL253DT (lane 1, "c") will appear as "uncut" circular DNA (nicked DNA, supercoiled and circular).

To this end, two homology arms were PCR amplified, whereas the 5' homology arm contains the region from bp -6991 to -6581 upstream the transcription start site of *Fbxw5* and an additional Spe restriction site at the 5' end and an AgeI restriction site at the 3' end. The 3' homology arm contains the region from bp +4780 to +5280 downstream of the transcription start site of *Fbxw5* and an additional AgeI restriction site at the 5' end and a blunt ended XbaI (XbaI^{blunt}) restriction site at the 3' end. The two homology arms were fused via AgeI and site ligated into pL293DT using the restriction sites SpeI and blunt ended EcoRI (EcoRI^{blunt}).

This newly generated vector pL253DT^{HRe} was digested with AgeI, which linearizes the plasmid, and co-transformed with BAC$^{Fbxw5\text{-}floxed}$ into heat-activated *E.coli* SW102 (Figure 26 A), which contains the lambda red prophage recombineering system (5.1.1). In case of correct gap repair homologous recombination, the linearized pL253DT^{HRe} becomes circular through the insertion of the *floxed Fbxw5,* resulting in the final vector pl253DT$^{Fbxw\text{-}floxed}$ (Figure 25)

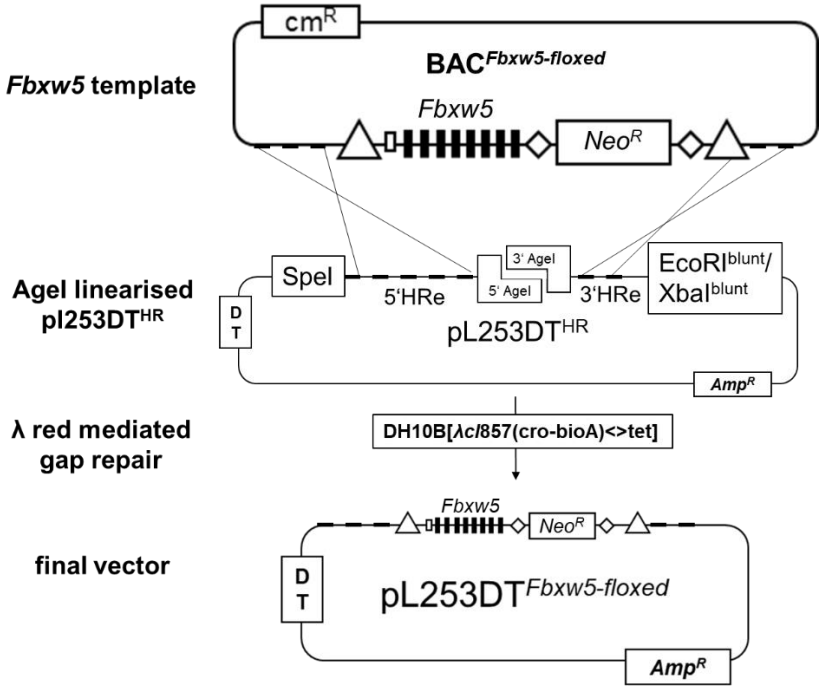

Figure 25 Transfer of floxed *Fbxw5* into final vector construct. BAC$^{Fbxw5\text{-}floxed}$ and linearized pL253DT^{HRe}, containing the *Fbxw5* homology arms, were co-transfected into heat-activated DH10B[λ*cl*857(cro-bioA)<>tet] (*E.coli* SW102). Gap repair results in homologous recombination to yield the final vector pL293DT$^{Fbxw5\text{-}floxed}$.

After co-transformation, single colonies were analyzed regarding their sensitivity against ampicillin, kanamycin and chloramphenicol. Only colonies showing resistance to ampicillin and kanamycin, but not chloramphenicol were chosen for genotyping. The analysis of the final *floxed Fbxw5* vector pL253DT$^{Fbxw5\text{-}floxed}$ was done in comparison

to wildtype genomic NIH/3T3 mouse DNA as well as BAC$^{Fbxw5\text{-}floxed}$ as shown in Figure 26 A - C.

The first PCR, using the primers F1 and B1, gives rise to a 585 bp fragment of the upstream region of wt-*Fbxw5*. As expected, a fragment of this size is only detected for wildtype genomic DNA and BAC$^{Fbxw5\text{-}floxed}$, but not for pL253DT$^{Fbxw5\text{-}floxed}$ since F1 anneals upstream of the 5' homology arm. The second PCR, using the primers F2 and B2, confirmed the presence of the first *loxP* site. Here, in the wildtype scenario a fragment of 200 bp appeared, whereas a shift of 100 bp could be observed for BAC$^{Fbxw5\text{-}floxed}$ (positive control) and pL253DT$^{Fbxw5\text{-}floxed}$, consistent with the expected size of the respective fragments. The third (F3, Neo B1) and fourth (Neo F1, B3) PCR verified the FRT-Neo cassette 3' downstream of *Fbxw5* including the second *loxP* site. The last PCR (NeoF1, B4) verifies the correct genomic foci and is only positive if the *FRT-Neo^R* cassette is located downstream of *Fbxw5* (Figure 26 A-C).In conclusion, the cloned plasmid carried both *Fbxw5*, flanked by the two *loxP* sites, and the *FRT-Neo^R* cassette in the correct orientation and therefore is considered to be the desired gap-repaired plasmid. This final construct, pL253DT$^{Fbxw5\text{-}floxed}$, was linearized using SalI endonuclease and gel purified for the generation of transgenic ES-cell line (data not shown). The transfection of the ES cells was performed by the "Transgenic Facility Tübingen" under the supervision of Dr. Thomas Ott. As shown in Figure 26 A & D, standard PCR was performed to analyze the clones regarding the first *loxP* site (using primers F2 & B2) as well as the correct genomic loci (using primers Neo F1 & B4). However, analyzing over 300 different ES cell clones, it was not possible to find the correct genotype (Figure 26 D). The genotyping analysis revealed either heterogeneous appearance of the first loxP site in an unknown genomic loci (Figure 26 D; clone 1-6), or the correct genomic loci missing the first *loxP* site (Figure 26 D; clone 10). It seems to be necessary to have a recombination arm of at least 2000 base pair. However, the efficiency of the *floxed Fbxw5* vector for the generation of the transgenic ES cell line can still be valuable. With the identification and utilization of the CRISPR/Cas9 system, a new molecular biological tool is available to increase the probability of the correct recombination. A specifically induce DSB 5' and 3' of FBXW5 and usage of the transgenic *Fbxw5*$^{lox/FRT\text{-}Neo\text{-}FRT\text{-}loxP}$ plasmid as a homologous direct repair template, might be sufficient for the generation of a transgenic Fbxw5 cell line.

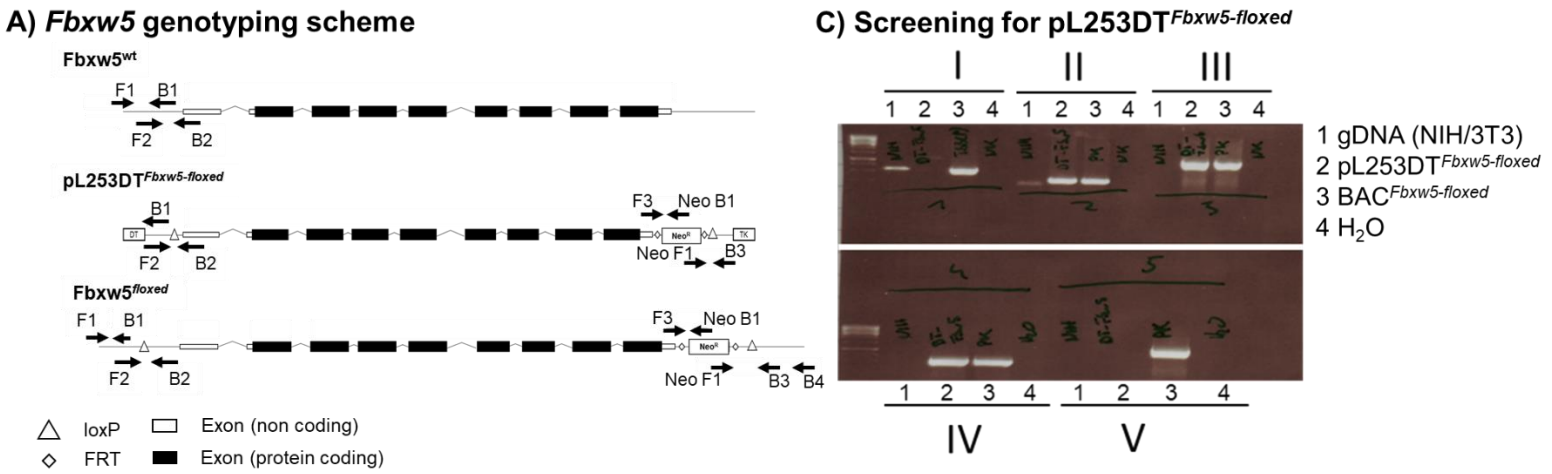

Figure 26 Verification of the final construct pL253DT$^{Fbxw5\text{-}floxed}$ and ES-cell screening: (A) schematic plot of genotyping strategy for the verification of the final vector pL253DT$^{Fbxw5\text{-}floxed}$ and to distinguish wildtype *Fbxw5* from *floxed Fbxw5* (B) Fbxw5 genotyping pattern with respect to the designated genotypes. (C) genotyping of the final construct pL253DT$^{Fbxw5\text{-}floxed}$. 1: gDNA (NIH/3T3; "wt"); 2: pL253DT$^{Fbxw5\text{-}floxed}$; 3: Bac$^{Fbxw5\text{-}floxed}$ (positive control) 4: H_2O (negative control). **(D)** Representative picture of the analyzed ES cells. Most of the cells have revealed heterogeneity for the first loxP site but were negative for the correct genomic loci. Only [10] have shown the correct gene locus, but the first *loxP* site was missing.

7 Discussion

7.1 Loss of the Ubiquitin E3 Ligase FBXW5 impairs cell physiology

Centrosome amplification and polyploidization are well-documented processes in numerous healthy tissues, e.g. the liver parenchyma or the heart [113]. Nevertheless, failure within the control mechanism of the centrosome cycle is hypothesized to also induce genomic instability and cancer [4, 9, 16, 28, 114]. Intriguingly, most solid tumors have an increased centrosome number. This also applies to liver cancer, one of the most lethal diseases in the world which has increased in the last two decades [115, 116]. However, it is quite controversial whether an increased centrosome number is cause or consequence in the tumor formation process.

Many regulatory components that contribute to the maintenance of centrosome homeostasis and the genomic stability of a cell have been described. One such example, PLK4, represents the major kinase mediating the initiation of centrosome duplication. Its excessive expression leads to an increased number of centrosomes [49, 50, 52, 53]. In line with this, Puklowski et al. (2011) described the ubiquitin ligase SCF^{FBXW5} as a direct target of PLK4, and loss of FBXW5, or expression of the phospho-mutant $FBXW5^{S151A}$ leads to a significant increase in centrosome number as well [1]. However, this study was conducted in already diseased cells with genotypes known to promote tumorigenesis: p53 null status (HeLa) or mdm2 overexpression (U2OS). Additionally, it is quite established that centrosome amplification is associated with mutations in p53, especially in HCC [117].

The study presented here, extends these observations on consequences of FBXW5 depletion to uncompromised and “healthy” cells. Although centrosomal staining confirmed the previously identified mechanism from Puklowski et al. (2011) [1], the increase of cells with more than two centrosomes was less pronounced (15-20% vs 50% [1]). As mentioned, this discrepancy might well be attributed to a non-functional p53 in HeLa or U2OS cells, whereas cells used throughout this study (NIH/3T3 and BNL CL.2) had a functional p53. Consequently, this points to a p53-dependent mechanism in cells with an exceeded centrosome number. Intriguingly, the PIDDosome (**p**53-**i**nduced protein with a **d**ead **d**omain), a multicomplex engaged in caspase-2-mediated apoptosis upon genotoxic stress [118], also recognize

centrosome overduplication, leading to MDM2 cleavage, p53 stabilization and a p21-dependent cell cycle arrest [119]. Such a mechanism could restrict the number of FBXW5-depleted cells with too many centrosomes, as observed throughout this study, since both cell lines used have p53 and a presumably intact PIDDosome pathway. Strikingly, the doubling time of FBXW5-depleted cells increased significantly, once a 30%-threshold of centrosome amplified cells is reached. This could point to an activation of the PIDDosome pathway [119], but further studies are required to support this view.

Cell cycle analyses have shown that FBXW5-deficient cells normally progress through the S phase, but fail to enter the next cell cycle synchronously, possibly due to a tetraploidy checkpoint, which is known to arrest the cell cycle of non-transformed cells and thereby ensuring the genomic integrity [120]. According to Ganem et al. (2009) this checkpoint can be overcome by transient p53 suppression, allowing tetraploid and centrosome amplified cells to complete mitosis and enter the next cell cycle [121].

Besides these pathophysiological effects on ploidy and cell cycle, centrosome amplification also affects cell migration. For the FBXW5 depleted BNL CL.2 cells examined in this study, the migratory capability was reduced. A similar migration defect was described in HUVEC, after artificially induced centrosome amplification [122]. Here, the aberrant centrosome number is accompanied with nucleated supernumerary cilia. However, these cilia have a reduced ciliary concentration of Smoothened (SMO) in response to Sonic hedgehog (Shh) stimulation, and obstructions in the Shh signaling pathway usually compromise the migration and proliferation of cells [123].

Altogether, it seems that supernumerary centrosomes are disadvantageous for cell cycle progression and cell migration in non-transformed cells. This stands in sharp contrast to the enhanced invasive and migratory capabilities of tumor cells [96, 124-126].

Besides its role in centrosome number maintenance, FBXW5 also mediates the degradation of the mitotic remodeler EPS8. Upon overexpression, this onco-protein leads to an oncogenic cell transformation *in vitro* and *in vivo* [99, 127]. Based on this, it was hypothesized that FBXW5 depletion triggers tumorigenesis with time, since the expected stabilization of EPS8 should lead to cellular transformation. In addition, those cells should benefit from an increased centrosome number, caused by the FBXW5 depletion. However, the *in vitro* transformation assay in this study does not show

colony formation in a semi-solid soft agar. This observation was also corroborated by the *in vivo* mosaic mouse model. The delivery of the transposable miR-30 shRNA against *Fbxw5* into the wildtype liver of 4 weeks old BL6 mice did not show any abnormalities. More strikingly, the GFP-positive hepatocytes were undetectable one month after injection of the shRNA, possibly due to an elimination mechanism. As mentioned, tumor suppressors like $p19^{arf}$, p21 or p53 might halt the cell cycle progression of cells exhibiting to many centrosomes [128]. However, HDTVi of FBXW5 miR-30 shRNA in p19-, p21-, or p53-deficient mice did not suffer any pathophysiological consequences. Unfortunately, the absence of neoplasia makes it hard to determine the efficiency of the FBXW5 suppression *in vivo,* since only 13% of the hepatocytes take up and express the injected plasmid DNA [108]. To overcome these limitations, a liver repopulation system was applied, using a FAH-knockout mouse model. The ectopic FAH expression together with the *Fbxw5*-shRNA should allow to vastly increase the number of hepatocytes carrying a FBXW5 deficiency. But even when over 90% of the liver becomes repopulated with the Fbxw5 shRNA, no morphological abnormalities were detected. Surprisingly, and although strong re-expression of FAH could be verified, no significant suppression in FBXW5 was identified, neither via qPCR nor via western blot. Yet, it should be considered that the *in vitro* experiments - in which the FBXW5 suppression was verified -were performed with a pure culture of cells, whereas the extracted liver tissue was composed of hepatocytes, cholangiocytes and remaining blood cells, resulting in a higher background interference. Given that the knockdown efficiency in the *in vitro* study was only about 50% as determined by qPCR, it is plausible that the knockdown cannot be detected in a tissue sample - at least not when applying western blot or qPCR.

However, the putative failure in the centrosome duplication did not lead to malignant changes, neither in the *in vitro* nor the *in vivo* studies. It may be possible that a dysregulated centrosome cycle only displays consequences after longer periods of time. The studies from Levine et al. [34] and Vitre et al. [33] provide notable examples for this assumption. Whereas, strong PLK4 overexpression did not cause spontaneous tumorigenesis, Levine and colleagues found that modest PLK4 overexpression promotes the tumor formation in the intestine 9 months after the induction of supernumerary centrosomes [34]. Moreover, the intestine is composed of a hierarchal origin structure. Lgr5-positive stem cells continuously regenerate the intestine, and

malignant degeneration of such stem cells is thought to be the origin of tumor formation within the intestine [129]. Thus, it can be easily imagined that continuously dividing cells are more susceptible towards centrosome amplification and genomic instability. In sharp contrast to this, the undamaged liver is classified as a quiescent organ. Even after substantial surgical removal, 1-2 cell divisions of the hepatocytes are sufficient to regenerate an entire liver [130, 131]. In the study by Levine et al. (2017), it took approximately 9 months for a continuously regenerative organ like the colon to display neoplasms [34]. It may be worthwhile to analyze a FBXW5 deficient liver for its continued regenerative capacity, using a pulse-driven approach. Interestingly, a recent study by Bai et al. (2019) revealed that hepatocyte-specific deletion of *Fbxw5* significantly prevents ASK1 activation during non-alcoholic steatohepatitis (NASH) development, suggesting SCF^{Fbxw5} as promising target to treat NASH [132]. However, and because of the missing verification of the FBXW5 suppression *in vivo* in this study, it is still not fully understood what kind of long-term consequences a FBXW5 suppression might cause. The generation of a transgenic *Fbxw5* knockout model might fill this gap. Additionally, creating an inducible *in vivo* knockout model displays several advantages, compared to the mosaic mouse which relies on oncogenic transformation within a short period of time. The analysis of the effect of the *Fbxw5* knockout in different tissues using a tissue-specific driven Cre-recombinase, would be easier. Furthermore, in hindsight of the data from the genome wide library screen (Figure 16), it might be more convenient to perform *in vivo* double knockout studies.

7.2 A genome wide CRISPR/Cas9 library screen identifies several genes promoting a transient cell cycle arrest in response to cellular stress

As mentioned before, the loss of FBXW5 led to an increase in centrosome number and cell doubling time. It is hypothesized that the observed delay in cell cycle progression at G_2M is due to the spindle assembly checkpoint (SAC), which prevents the separation of the duplicated chromosomes until a bipolar arrangement of the spindles is manifested [133, 134]. The SAC plays an extraordinary role in centrosome clustering, a time-critical process initiated once the spindles are rendered from a multipolar to a bipolar state. Defects in the spindle assembling checkpoint can lead to a multipolar cell division, predominantly causing mitotic catastrophe and subsequent cell death [135].

In some cases, chromosomal instability resulting from such a multipolar division can also promote cellular transformation, due to gain or loss of chromosomal DNA, or due to chromosomal rearrangements in the daughter cells, a process known as chromothripsis [11, 21, 22]. In such a scenario, centrosome amplification due to loss of FBXW5 might cause a malignant preposition, but at least one further mutation, for example within in the SAC, a would be necessary to push the FBXW5 negative cells towards carcinogenesis.

An interesting finding in the genome-wide library screen is the identification of the replication protein a2 (RPA2). As mentioned in the results,[136] a complete loss of *Rpa2* appears to be lethal and the candidates retrieved in the screen display some residual RPA2. Partial gene knockdown occurs quite frequently using shRNA technology, but is rarely observed with CRISPR/Cas9. However, CRISPR/Cas9 study by Morgens et al. (2016), also described the phenomenon of heterozygous gene depletion, possibly occurring through in-frame InDels mutations, thereby creating wildtype and heterozygous subpopulations [137]. In normal cells, the RPA2 subunit of the RPA complex becomes hyperphosphorylated through cyclin B-Cdc2, and it was shown that during mitosis this hyperphosphorylation of RPA2 occurs in response to mitotic DNA damage [105, 138]. As mentioned, the investigations of the cell cycle progression upon FBXW5 loss did not show a S-Phase delay, but a prolonged G_2M phase. This prolonged G_2M phase might be associated with physical DNA damage, originating from incorrect merotelic attachment and physical chromosomal breakages during mitosis [25]. This in turn would activate a DNA damage checkpoint, as well as the SAC during mitosis, rather than a replication checkpoint during the S/G2 phase. Anantha et al. (2008) hypothesized that phosphorylated RPA2 communicates with the SAC complex and transmits a signal for DNA reparation [138, 139]. However, a reduced level of RPA2 might be insufficient to report to the SAC that DNA repair is necessary. Consequently, instead of a mitotic delay for DSB repair, the cell cycle progresses normally into G_1, while cells still harbor multiple damages within their DNA. Nevertheless, it seems that the FBXW5 depletion is more advantageous to cells with a partial loss of RPA2. In addition to its role in regulating onco-proteins and tumor-suppressors, FBXW5 can also “inactivate” proteins [140]. C-myb for example is a protein that *trans*-activates the expression of proto-oncogenes like *c-myc*, *Bcl-2* and *Gbx*, which are regulating the cell cycle control, apoptosis, cell growth and

differentiation [141-143]. Kanei-Ishii and colleagues (2012) could show that FBXW5, together with the DDB-Cul4-Rbx1 complex, binds to the WD domain of c-myb leading to its sumolyation, which results in an inhibition of the expression of c-myc [140]. Perhaps the loss of FBXW5 triggers trans-activating genes such as c-myc, which are responsible for an increased proliferation of RPA2-suppressed cells. Further analysis must be conducted to resolve this issue.

In the genome-wide library screen, the gene *ang5* was also identified to be advantageous for the *Fbxw5*$^{\Delta Exon5}$ mutant. This gene encodes angiogenin, a protein that facilitates the cleavage of mature tRNA into tiRNAs under various stress conditions, like DNA damage or oxidative stress [144, 145]. Such tiRNAs can promote a phospho-eIF2 α-independent translational repression in stressed cells, allowing for a modest reprogramming of protein synthesis, which plays an important role in the cellular stress response program [145-148]. Furthermore, angiogenin is a secretory protein taken up by surrounding cells. Once environmental stress occurs, angiogenin "warns" the neighboring cells, leading to a stress-induced translational arrest [148]. Interestingly, such an extracellularly induced stress might also activate the stress-responsive MAPK pathway. A study by Nakamura and colleagues has shown that PLK4, which also targets FBXW5, becomes hyperactivated by multiple stress-associated protein kinases (SAPK), like MTK1, TAK1 or MEKK1-C. Phosphorylation of PLK4, at its active-site T170, protects stressed cells from apoptosis by inhibiting stress induced AKT1 [1, 149]. One might speculate, that the loss of FBXW5 causes cellular stress, which leads to an angiogenin mediated G_2M arrest via p53 activation [149, 150]. The increase in cellular stress also activates the SAPK pathway to phosphorylate PLK4, which antagonizes the angiogenin induced cell cycle arrest (Figure 27). The outcome from those two opposing pathways might be the reason for the temporary cell cycle delay in the G_2M phase. The identification of the *map2k4* gene in the CRISPR/Cas9 library screen here seems to strengthen this hypothesis. In the same study by Nakamura et al. (2013), MKK4 was identified as a potential tumor suppressor in centrosome amplified cells, and mutational inactivation of MKK4 is also known to promote carcinogenesis [151].

Altogether, it can be concluded that the loss of FBXW5 alone is unlikely to induce a cellular transformation towards tumorigenesis. On the contrary, there is evidence that FBXW5 loss is more likely associated with reduced cell growth and cell motility,

possibly due to checkpoint mechanisms at the G_2M transition. Further exploration of the genome-wide CRISPR/Cas9 library screen applied here might yield new insights into the regulatory role of FBXW5 in the DNA damage response, as well as in the cellular stress response.

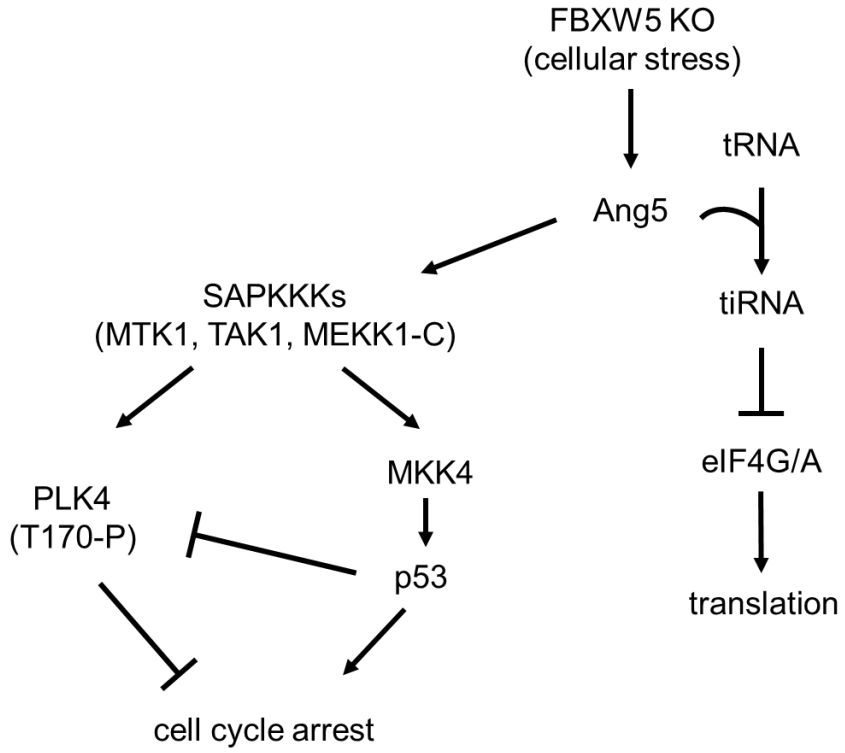

Figure 27 Loss of FBXW5 induces cellular stress and promotes a transient cell cycle arrest. With respect to the findings in the CRISPR/Cas9 genome wide library screen, it is hypothesized that the loss of FBXW5 leads to an induction of Ang5. Ang5 promotes the cleavage of tRNA into tiRNA, resulting in an inhibition of protein synthesis and modest cellular stress response. Additionally, Ang5 also "warns" other cells, ultimately inducing stress-associated protein kinase kinase kinases (SAPKKKs) like MTK, TAK1 or MEKK1-C. Those SAPKKKs phosphorylate PLK4 at its active site T170 and promote the cell cycle. However, in parallel to that, SAPKKKs also activate MKK4, leading to an induction of p53, which antagonizes the effect of PLK4. It is hypothesized that loss of Fbxw5 induces a transient delay of the cell cycle, which is mediated by Ang5 and/or MKK4. Loss of one of these proteins would rescue such a delay in proliferation of Fbxw5 deficient cells.

8 References

1. Puklowski, A., et al., *The SCF-FBXW5 E3-ubiquitin ligase is regulated by PLK4 and targets HsSAS-6 to control centrosome duplication.* Nat Cell Biol, 2011. **13**(8): p. 1004-1009.
2. Boveri, T., *Concerning the origin of malignant tumours by Theodor Boveri. Translated and annotated by Henry Harris.* J Cell Sci, 2008. **121 Suppl 1**: p. 1-84.
3. Luders, J. and T. Stearns, *Microtubule-organizing centres: a re-evaluation.* Nat Rev Mol Cell Biol, 2007. **8**(2): p. 161-167.
4. Nigg, E.A. and T. Stearns, *The centrosome cycle: Centriole biogenesis, duplication and inherent asymmetries.* Nature cell biology, 2011. **13**(10): p. 1154-1160.
5. Schatten, H., *The mammalian centrosome and its functional significance.* Histochemistry and cell biology, 2008. **129**(6): p. 667-686.
6. Winey, M., *Cell cycle: driving the centrosome cycle.* Curr Biol, 1999. **9**(12): p. R449-52.
7. Fujita, H., Y. Yoshino, and N. Chiba, *Regulation of the centrosome cycle.* Molecular & Cellular Oncology, 2016. **3**(2): p. e1075643.
8. Hardy, P.A. and H. Zacharias, *Reappraisal of the Hansemann—Boveri hypothesis on the origin of tumors.* Cell Biology International, 2005. **29**(12): p. 983-992.
9. Chan, J.Y., *A clinical overview of centrosome amplification in human cancers.* International journal of biological sciences, 2011. **7**(8): p. 1122-1144.
10. Nakayama, K.I. and K. Nakayama, *Ubiquitin ligases: cell-cycle control and cancer.* Nat Rev Cancer, 2006. **6**(5): p. 369-381.
11. Pihan, G., *Centrosome Dysfunction Contributes to Chromosome Instability, Chromoanagenesis, and Genome Reprograming in Cancer.* Frontiers in Oncology, 2013. **3**: p. 277.
12. Brinkley, B.R., *Managing the centrosome numbers game: from chaos to stability in cancer cell division.* Trends in Cell Biology, 2001. **11**(1): p. 18-21.
13. Prosser, S.L., K.R. Straatman, and A.M. Fry, *Molecular Dissection of the Centrosome Overduplication Pathway in S-Phase-Arrested Cells.* Molecular and Cellular Biology, 2009. **29**(7): p. 1760-1773.
14. Loncarek, J. and A. Khodjakov, *Ab ovo or de novo? Mechanisms of centriole duplication.* Molecules and cells, 2009. **27**(2): p. 135-142.
15. La Terra, S., et al., *The de novo centriole assembly pathway in HeLa cells.* The Journal of Cell Biology, 2005. **168**(5): p. 713.
16. Kramer, A., A.D. Neben K Fau - Ho, and A.D. Ho, *Centrosome replication, genomic instability and cancer.* Leukemia, 2002. **16**(0887-6924 (Print)): p. pages 767–775.
17. Tarapore, P. and K. Fukasawa, *Loss of p53 and centrosome hyperamplification.* Oncogene, 2002. **21**(0950-9232 (Print)): p. 6234-6240.
18. D'Angiolella, V., et al., *SCF(Cyclin F) controls centrosome homeostasis and mitotic fidelity via CP110 degradation.* Nature, 2010. **466**(7302): p. 138-142.
19. Silkworth, W.T., et al., *Multipolar Spindle Pole Coalescence Is a Major Source of Kinetochore Mis-Attachment and Chromosome Mis-Segregation in Cancer Cells.* PLOS ONE, 2009. **4**(8): p. e6564.
20. Bayani, J., et al., *Genomic mechanisms and measurement of structural and numerical instability in cancer cells.* Seminars in Cancer Biology, 2007. **17**(1): p. 5-18.
21. Stephens, P.J., et al., *Massive Genomic Rearrangement Acquired in a Single Catastrophic Event during Cancer Development.* Cell, 2011. **144**(1): p. 27-40.
22. Kloosterman, W.P., et al., *Chromothripsis is a common mechanism driving genomic rearrangements in primary and metastatic colorectal cancer.* Genome Biology, 2011. **12**(10): p. R103.
23. Tubio, J.M.C. and X. Estivill, *Cancer: When catastrophe strikes a cell.* Nature, 2011. **470**(7335): p. 476-477.
24. Cimini, D., et al., *Merotelic Kinetochore Orientation Is a Major Mechanism of Aneuploidy in Mitotic Mammalian Tissue Cells.* The Journal of Cell Biology, 2001. **153**(3): p. 517.
25. Guerrero, A.A., C. Martínez-A, and K.H.M. van Wely, *Merotelic attachments and non-homologous end joining are the basis of chromosomal instability.* Cell Division, 2010. **5**(1): p. 13.
26. Wilkens, L., et al., *Induction of aneuploidy by increasing chromosomal instability during dedifferentiation of hepatocellular carcinoma.* Proceedings of the National Academy of Sciences of the United States of America, 2004. **101**(5): p. 1309-1314.
27. Hanahan, D. and Robert A. Weinberg, *Hallmarks of Cancer: The Next Generation.* Cell, 2011. **144**(5): p. 646-674.
28. Basto, R., et al., *Centrosome Amplification Can Initiate Tumorigenesis in Flies.* Cell, 2008. **133**(6): p. 1032-1042.
29. Sabino, D., et al., *Moesin Is a Major Regulator of Centrosome Behavior in Epithelial Cells with Extra Centrosomes.* Current Biology, 2015. **25**(7): p. 879-889.
30. Li, Z., et al., *Expression of Polo-Like Kinase 4(PLK4) in Breast Cancer and Its Response to Taxane-Based Neoadjuvant Chemotherapy.* Journal of Cancer, 2016. **7**(9): p. 1125-1132.
31. Marthiens, V., et al., *Centrosome amplification causes microcephaly.* Nature Cell Biology, 2013. **15**: p. 731.

32. Dzafic, E., et al., *Centriole Amplification in Zebrafish Affects Proliferation and Survival but Not Differentiation of Neural Progenitor Cells.* Cell Reports, 2015. **13**(1): p. 168-182.
33. Vitre, B., et al., *Chronic centrosome amplification without tumorigenesis.* Proceedings of the National Academy of Sciences of the United States of America, 2015. **112**(46): p. E6321-E6330.
34. Levine, M.S., et al., *Centrosome Amplification Is Sufficient to Promote Spontaneous Tumorigenesis in Mammals.* Developmental Cell, 2017. **40**(3): p. 313-322.e5.
35. Fan, G., et al., *Loss of KLF14 triggers centrosome amplification and tumorigenesis.* Nature Communications, 2015. **6**: p. 8450.
36. Nam, H.-J., R.M. Naylor, and J.M. van Deursen, *Centrosome dynamics as a source of chromosomal instability.* Trends in cell biology, 2015. **25**(2): p. 65-73.
37. Tsou, M.-F.B. and T. Stearns, *Mechanism limiting centrosome duplication to once per cell cycle.* Nature, 2006. **442**(7105): p. 947-951.
38. Prosser, S.L., et al., *Oscillation of APC/C activity during cell cycle arrest promotes centrosome amplification.* Journal of cell science, 2012. **125**(0 22): p. 5353-5368.
39. Peters, J.-M., *The Anaphase-Promoting Complex: Proteolysis in Mitosis and Beyond.* Molecular Cell, 2002. **9**(5): p. 931-943.
40. Gönczy, P., *Centrosomes and cancer: revisiting a long-standing relationship.* Nature Reviews Cancer, 2015. **15**(11): p. 639-652.
41. Nakamura, A., H. Arai, and N. Fujita, *Centrosomal Aki1 and cohesin function in separase-regulated centriole disengagement.* The Journal of Cell Biology, 2009. **187**(5): p. 607-614.
42. Thein, K.H., et al., *Astrin is required for the maintenance of sister chromatid cohesion and centrosome integrity.* The Journal of Cell Biology, 2007. **178**(3): p. 345-354.
43. Mardin, B.R. and E. Schiebel, *Breaking the ties that bind: New advances in centrosome biology.* The Journal of Cell Biology, 2012. **197**(1): p. 11-18.
44. Peel, N., et al., *The C. elegans F-box proteins LIN-23 and SEL-10 antagonize centrosome duplication by regulating ZYG-1 levels.* Journal of cell science, 2012. **125**(Pt 15): p. 3535-3544.
45. Bashir, T., et al., *Control of the SCF(Skp2-Cks1) ubiquitin ligase by the APC/C(Cdh1) ubiquitin ligase.* Nature, 2004. **428**(6979): p. 190-3.
46. Tang, C.-J.C., et al., *CPAP is a cell-cycle regulated protein that controls centriole length.* Nat Cell Biol, 2009. **11**(7): p. 825-831.
47. Strnad, P., et al., *Regulated HsSAS-6 Levels Ensure Formation of a Single Procentriole per Centriole during the Centrosome Duplication Cycle.* Developmental cell, 2007. **13**(2): p. 203-213.
48. Harbour, J.W. and D.C. Dean, *Rb function in cell-cycle regulation and apoptosis.* Nat Cell Biol, 2000. **2**(4): p. E65-7.
49. Ohta, M., et al., *Direct interaction of Plk4 with STIL ensures formation of a single procentriole per parental centriole.* Nature Communications, 2014. **5**: p. 5267.
50. Habedanck, R., et al., *The Polo kinase Plk4 functions in centriole duplication.* Nat Cell Biol, 2005. **7**(11): p. 1140-1146.
51. Gudi, R., et al., *Centrobin-centrosomal protein 4.1-associated protein (CPAP) interaction promotes CPAP localization to the centrioles during centriole duplication.* The Journal of biological chemistry, 2014. **289**(22): p. 15166-15178.
52. Sonnen, K.F., et al., *Human Cep192 and Cep152 cooperate in Plk4 recruitment and centriole duplication.* Journal of Cell Science, 2013. **126**(14): p. 3223.
53. Arquint, C., et al., *Cell-cycle-regulated expression of STIL controls centriole number in human cells.* Journal of Cell Science, 2012. **125**(5): p. 1342.
54. Arquint, C. and Erich A. Nigg, *STIL Microcephaly Mutations Interfere with APC/C-Mediated Degradation and Cause Centriole Amplification.* Current Biology, 2014. **24**(4): p. 351-360.
55. Pfaffl, M.W., *A new mathematical model for relative quantification in real-time RT–PCR.* Nucleic Acids Research, 2001. **29**(9): p. e45-e45.
56. Kohlmaier, G., et al., *Overly Long Centrioles and Defective Cell Division upon Excess of the SAS-4-Related Protein CPAP.* Current Biology, 2009. **19**(12): p. 1012-1018.
57. Bustin, S.A., *Absolute quantification of mRNA using real-time reverse transcription polymerase chain reaction assays.* J. Mol Endocrinol, 2000(0952-5041 (Print)).
58. Janke, C. and J. Chloë Bulinski, *Post-translational regulation of the microtubule cytoskeleton: mechanisms and functions.* Nat Rev Mol Cell Biol, 2011. **12**(12): p. 773-786.
59. Chang, C.-W., et al., *CEP295 interacts with microtubules and is required for centriole elongation.* Journal of Cell Science, 2016. **129**(13): p. 2501-2513.
60. Sharma, A., et al., *Centriolar CPAP/SAS-4 Imparts Slow Processive Microtubule Growth.* Developmental Cell, 2016. **37**(4): p. 362-376.
61. Wang, Y., *The role of Sas-4 in ciliogenesis and centriole biogenesis in Drosophila.* 2016.
62. Mardin, B.R., et al., *Components of the Hippo pathway cooperate with Nek2 kinase to regulate centrosome disjunction.* Nature cell biology, 2010. **12**(12): p. 1166-1176.
63. Mardin, Balca R., et al., *Plk1 Controls the Nek2A-PP1γ Antagonism in Centrosome Disjunction.* Current Biology, 2011. **21**(13): p. 1145-1151.
64. Faragher, A.J. and A.M. Fry, *Nek2A kinase stimulates centrosome disjunction and is required for formation of bipolar mitotic spindles.* Molecular Biology of the Cell, 2003. **14**(7): p. 2876-2889.

65. Bertran, M.T., et al., *Nek9 is a Plk1-activated kinase that controls early centrosome separation through Nek6/7 and Eg5.* The EMBO Journal, 2011. **30**(13): p. 2634-2647.
66. Rapley, J., et al., *The NIMA-family kinase Nek6 phosphorylates the kinesin Eg5 at a novel site necessary for mitotic spindle formation.* Journal of Cell Science, 2008. **121**(23): p. 3912.
67. Wang, G., Q. Jiang, and C. Zhang, *The role of mitotic kinases in coupling the centrosome cycle with the assembly of the mitotic spindle.* Journal of Cell Science, 2014. **127**(19): p. 4111.
68. Glickman, M.H. and A. Ciechanover, *The Ubiquitin-Proteasome Proteolytic Pathway: Destruction for the Sake of Construction.* Physiological Reviews, 2002. **82**(2): p. 373-428.
69. Hershko, A. and A. Ciechanover, *The Ubiquitin System.* Annual Review of Biochemistry, 1998. **67**(1): p. 425-479.
70. Pickart, C.M. and M.J. Eddins, *Ubiquitin: structures, functions, mechanisms.* Biochimica et Biophysica Acta (BBA) - Molecular Cell Research, 2004. **1695**(1): p. 55-72.
71. Bellare, P., et al., *A role for ubiquitin in the spliceosome assembly pathway.* Nature Structural & Molecular Biology, 2008. **15**(5): p. 444-451.
72. Schulman, B.A. and J.W. Harper, *Ubiquitin-like protein activation by E1 enzymes: the apex for downstream signalling pathways.* Nature reviews. Molecular cell biology, 2009. **10**(5): p. 319-331.
73. Ye, Y. and M. Rape, *Building ubiquitin chains: E2 enzymes at work.* Nature reviews. Molecular cell biology, 2009. **10**(11): p. 755-764.
74. Pickart, C.M., *Back to the Future with Ubiquitin.* Cell, 2004. **116**(2): p. 181-190.
75. Komander, D. and M. Rape, *The Ubiquitin Code.* Annual Review of Biochemistry, 2012. **81**(1): p. 203-229.
76. Wickliffe, K.E., et al., *The mechanism of linkage-specific ubiquitin chain elongation by a single-subunit E2.* Cell, 2011. **144**(5): p. 769-781.
77. Zachariae, W., *Destruction with a Box: Substrate Recognition by the Anaphase-Promoting Complex.* Molecular Cell, 2004. **13**(1): p. 2-3.
78. Bettencourt-Dias, M. and D.M. Glover, *Centrosome biogenesis and function: centrosomics brings new understanding.* Nat Rev Mol Cell Biol, 2007. **8**(6): p. 451-463.
79. Scheffner, M., et al., *The state of the p53 and retinoblastoma genes in human cervical carcinoma cell lines.* Proceedings of the National Academy of Sciences of the United States of America, 1991. **88**(13): p. 5523-5527.
80. Landers, J.E., S.L. Cassel, and D.L. George, *Translational Enhancement of mdm2 Oncogene Expression in Human Tumor Cells Containing a Stabilized Wild-Type p53 Protein.* Cancer Research, 1997. **57**(16): p. 3562.
81. Serrano, M., et al., *Oncogenic ras Provokes Premature Cell Senescence Associated with Accumulation of p53 and p16INK4a.* Cell, 1997. **88**(5): p. 593-602.
82. Chen, C. and H. Okayama, *High-efficiency transformation of mammalian cells by plasmid DNA.* Molecular and Cellular Biology, 1987. **7**(8): p. 2745-2752.
83. Frengen, E., et al., *A modular, positive selection bacterial artificial chromosome vector with multiple cloning sites.* Genomics, 1999(0888-7543 (Print)).
84. Liu, P., N.A. Jenkins, and N.G. Copeland, *A highly efficient recombineering-based method for generating conditional knockout mutations.* Genome research, 2003. **13**(3): p. 476-484.
85. Buchholz, F., P.-O. Angrand, and A.F. Stewart, *Improved properties of FLP recombinase evolved by cycling mutagenesis.* Nature Biotechnology, 1998. **16**(7): p. 657-662.
86. Fellmann, C., et al., *An Optimized microRNA Backbone for Effective Single-Copy RNAi.* Cell Reports, 2013. **5**(6): p. 1704-1713.
87. Sanjana, N.E., O. Shalem, and F. Zhang, *Improved vectors and genome-wide libraries for CRISPR screening.* Nat Meth, 2014. **11**(8): p. 783-784.
88. Shen, C.-H., *Chapter 8 - Quantification and Analysis of Proteins*, in *Diagnostic Molecular Biology*, C.-H. Shen, Editor. 2019, Academic Press. p. 187-214.
89. Laemmli, U.K., *Cleavage of Structural Proteins during the Assembly of the Head of Bacteriophage T4.* Nature, 1970. **227**(5259): p. 680-685.
90. Wuestefeld, T., et al., *A Direct In Vivo RNAi Screen Identifies MKK4 as a Key Regulator of Liver Regeneration.* Cell, 2013. **153**(2): p. 389-401.
91. Hinterberger, M., et al., *Autonomous role of medullary thymic epithelial cells in central CD4+ T cell tolerance.* Nat Immunol, 2010. **11**(6): p. 512-519.
92. Lee, Y., et al., *MicroRNA genes are transcribed by RNA polymerase II.* The EMBO Journal, 2004. **23**(20): p. 4051-4060.
93. Cheung, H.T. and D.S. Terry, *Effects of nocodazole, a new synthetic microtubule inhibitor, on movement and spreading of mouse peritoneal macrophages.* Cell Biology International Reports, 1980. **4**(12): p. 1125-1129.
94. Ma, H.T. and R.Y.C. Poon, *Synchronization of HeLa Cells*, in *Cell Cycle Synchronization: Methods and Protocols*, G. Banfalvi, Editor. 2011, Humana Press: Totowa, NJ. p. 151-161.
95. Bjursell, G. and P. Reichard, *Effects of Thymidine on Deoxyribonucleoside Triphosphate Pools and Deoxyribonucleic Acid Synthesis in Chinese Hamster Ovary Cells.* Journal of Biological Chemistry, 1973. **248**(11): p. 3904-3909.
96. Godinho, S.A., et al., *Oncogene-like induction of cellular invasion from centrosome amplification.* Nature, 2014. **510**: p. 167.

97. Liang, C.-C., A.Y. Park, and J.-L. Guan, *In vitro scratch assay: a convenient and inexpensive method for analysis of cell migration in vitro.* Nature Protocols, 2007. **2**: p. 329.
98. Borowicz, S., et al., *The Soft Agar Colony Formation Assay.* Journal of Visualized Experiments : JoVE, 2014(92): p. 51998.
99. Werner, A., et al., *SCF(Fbxw5) mediates transient degradation of actin remodeler Eps8 to allow proper mitotic progression.* Nature cell biology, 2013. **15**(2): p. 179-188.
100. Kim, T.Y., et al., *CRL4A-FBXW5–mediated degradation of DLC1 Rho GTPase-activating protein tumor suppressor promotes non-small cell lung cancer cell growth.* Proceedings of the National Academy of Sciences of the United States of America, 2013. **110**(42): p. 16868-16873.
101. Hu, J., et al., *WD40 protein FBW5 promotes ubiquitination of tumor suppressor TSC2 by DDB1–CUL4–ROC1 ligase.* Genes & Development, 2008. **22**(7): p. 866-871.
102. Knudson, A.G., *Two genetic hits (more or less) to cancer.* Nature Reviews Cancer, 2001. **1**: p. 157.
103. Vogelstein, B. and K.W. Kinzler, *The multistep nature of cancer.* Trends in Genetics, 1993. **9**(4): p. 138-141.
104. Zou, Y., et al., *Functions of Human Replication Protein A (RPA): From DNA Replication to DNA Damage and Stress Responses.* Journal of cellular physiology, 2006. **208**(2): p. 267-273.
105. Vassin, V.M., et al., *Human RPA phosphorylation by ATR stimulates DNA synthesis and prevents ssDNA accumulation during DNA-replication stress.* Journal of cell science, 2009. **122**(Pt 22): p. 4070-4080.
106. Smits, V.A.J., et al., *Polo-like kinase-1 is a target of the DNA damage checkpoint.* Nature Cell Biology, 2000. **2**: p. 672.
107. Karanika, S., et al., *DNA damage response and prostate cancer: defects, regulation and therapeutic implications.* Oncogene, 2015. **34**(22): p. 2815-2822.
108. Kang, T.-W., et al., *Senescence surveillance of pre-malignant hepatocytes limits liver cancer development.* Nature, 2011. **479**(7374): p. 547-551.
109. Overturf, K., et al., *Hepatocytes corrected by gene therapy are selected in vivo in a murine model of hereditary tyrosinaemia type I.* Nat Genet, 1996. **12**(3): p. 266-273.
110. Grompe, M., et al., *Pharmacological correction of neonatal lethal hepatic dysfunction in a murine model of hereditary tyrosinaemia type I.* Nat Genet, 1995. **10**(4): p. 453-460.
111. Kim, H., et al., *Mouse Cre-LoxP system: general principles to determine tissue-specific roles of target genes.* Laboratory animal research, 2018. **34**(4): p. 147-159.
112. Sharan, S.K., et al., *Recombineering: A Homologous Recombination-Based Method of Genetic Engineering.* Nature protocols, 2009. **4**(2): p. 206-223.
113. Gentric, G., C. Desdouets, and S. Celton-Morizur, *Hepatocytes Polyploidization and Cell Cycle Control in Liver Physiopathology.* International Journal of Hepatology, 2012. **2012**: p. 282430.
114. Lingle, W.L., et al., *Centrosome amplification drives chromosomal instability in breast tumor development.* Proceedings of the National Academy of Sciences of the United States of America, 2002. **99**(4): p. 1978-1983.
115. Golabi, P., et al., *Mortality assessment of patients with hepatocellular carcinoma according to underlying disease and treatment modalities.* Medicine, 2017. **96**(9): p. e5904.
116. El-Serag, H.B., *Hepatocellular Carcinoma.* New England Journal of Medicine, 2011. **365**(12): p. 1118-1127.
117. Nakajima, T., et al., *Centrosome aberration accompanied with p53 mutation can induce genetic instability in hepatocellular carcinoma.* Modern Pathology, 2004. **17**: p. 722.
118. Tinel, A. and J. Tschopp, *The PIDDosome, a Protein Complex Implicated in Activation of Caspase-2 in Response to Genotoxic Stress.* Science, 2004. **304**(5672): p. 843.
119. Fava, L.L., et al., *The PIDDosome activates p53 in response to supernumerary centrosomes.* Genes & Development, 2017. **31**(1): p. 34-45.
120. Andreassen, P.R., et al., *Tetraploid state induces p53-dependent arrest of nontransformed mammalian cells in G1.* Molecular biology of the cell, 2001. **12**(5): p. 1315-1328.
121. Ganem, N.J., S.A. Godinho, and D. Pellman, *A mechanism linking extra centrosomes to chromosomal instability.* Nature, 2009. **460**(7252): p. 278-282.
122. Kushner, E.J., et al., *Excess centrosomes disrupt endothelial cell migration via centrosome scattering.* The Journal of cell biology, 2014. **206**(2): p. 257-272.
123. Mahjoub, M.R. and T. Stearns, *Supernumerary centrosomes nucleate extra cilia and compromise primary cilium signaling.* Current biology : CB, 2012. **22**(17): p. 1628-1634.
124. Mittal, K., et al., *Amplified centrosomes may underlie aggressive disease course in pancreatic ductal adenocarcinoma.* Cell cycle (Georgetown, Tex.), 2015. **14**(17): p. 2798-2809.
125. Arnandis, T., et al., *Oxidative Stress in Cells with Extra Centrosomes Drives Non-Cell-Autonomous Invasion.* Developmental Cell, 2018. **47**(4): p. 409-424.e9.
126. Godinho, S.A. and D. Pellman, *Causes and consequences of centrosome abnormalities in cancer.* Philosophical transactions of the Royal Society of London. Series B, Biological sciences, 2014. **369**(1650): p. 20130467.
127. Maa, M.-C., C.-Y. Hsieh, and T.-H. Leu, *Overexpression of p97Eps8 leads to cellular transformation: implication of pleckstrin homology domain in p97Eps8-mediated ERK activation.* Oncogene, 2001. **20**: p. 106.
128. Mikule, K., et al., *Loss of centrosome integrity induces p38—p53—p21-dependent G1—S arrest.* Nature Cell Biology, 2006. **9**: p. 160.

129. Puglisi, M.A., et al., *Colon cancer stem cells: Controversies and perspectives.* World Journal of Gastroenterology : WJG, 2013. **19**(20): p. 2997-3006.
130. Furchtgott, L.A., C.C. Chow, and V. Periwal, *A model of liver regeneration.* Biophysical journal, 2009. **96**(10): p. 3926-3935.
131. Gagner, M., T. Rogula, and D. Selzer, *Laparoscopic liver resection: benefits and controversies.* Surgical Clinics of North America, 2004. **84**(2): p. 451-462.
132. Bai, L., et al., *FBXW5 mediates the ubiquitination of ASK1 and exacerbates nonalcoholic steatohepatitis.* Hepatology, 2019. **0**(ja).
133. Kwon, M., et al., *Mechanisms to suppress multipolar divisions in cancer cells with extra centrosomes.* Genes & development, 2008. **22**(16): p. 2189-2203.
134. Lens, S.M.A. and R.H. Medema, *Cytokinesis defects and cancer.* Nature Reviews Cancer, 2019. **19**(1): p. 32-45.
135. Krämer, A., B. Maier, and J. Bartek, *Centrosome clustering and chromosomal (in)stability: a matter of life and death.* Molecular oncology, 2011. **5**(4): p. 324-335.
136. Binz, S.K., et al., *Functional assays for replication protein A (RPA).* Methods Enzymol, 2006. **409**: p. 11-38.
137. Morgens, D.W., et al., *Systematic comparison of CRISPR/Cas9 and RNAi screens for essential genes.* Nature biotechnology, 2016. **34**(6): p. 634-636.
138. Anantha, R.W., E. Sokolova, and J.A. Borowiec, *RPA phosphorylation facilitates mitotic exit in response to mitotic DNA damage.* Proceedings of the National Academy of Sciences of the United States of America, 2008. **105**(35): p. 12903-12908.
139. Anantha, R.W. and J.A. Borowiec, *Mitotic crisis: The unmasking of a novel role for RPA.* Cell Cycle, 2009. **8**(3): p. 357-361.
140. Kanei-Ishii, C., et al., *Fbxw5 suppresses nuclear c-Myb activity via DDB1-Cul4-Rbx1 ligase-mediated sumoylation.* Biochemical and Biophysical Research Communications, 2012. **426**(1): p. 59-64.
141. Nakagoshi, H., et al., *Transcriptional activation of the c-myc gene by the c-myb and B-myb gene products.* Oncogene, 1992. **7**(6): p. 1233-40.
142. Frampton, J., T. Ramqvist, and T. Graf, *v-Myb of E26 leukemia virus up-regulates bcl-2 and suppresses apoptosis in myeloid cells.* Genes Dev, 1996. **10**(21): p. 2720-31.
143. Taylor, D., P. Badiani, and K. Weston, *A dominant interfering Myb mutant causes apoptosis in T cells.* Genes Dev, 1996. **10**(21): p. 2732-44.
144. Fu, H., et al., *Stress induces tRNA cleavage by angiogenin in mammalian cells.* FEBS Letters, 2009. **583**(2): p. 437-442.
145. Emara, M.M., et al., *Angiogenin-induced tRNA-derived stress-induced RNAs promote stress-induced stress granule assembly.* The Journal of biological chemistry, 2010. **285**(14): p. 10959-10968.
146. Gebetsberger, J., et al., *tRNA-Derived Fragments Target the Ribosome and Function as Regulatory Non-Coding RNA in Haloferax volcanii.* Archaea, 2012. **2012**: p. 260909.
147. Ivanov, P., et al., *Angiogenin-Induced tRNA Fragments Inhibit Translation Initiation.* Molecular Cell, 2011. **43**(4): p. 613-623.
148. Yamasaki, S., et al., *Angiogenin cleaves tRNA and promotes stress-induced translational repression.* The Journal of cell biology, 2009. **185**(1): p. 35-42.
149. Nakamura, T., H. Saito, and M. Takekawa, *SAPK pathways and p53 cooperatively regulate PLK4 activity and centrosome integrity under stress.* Nature Communications, 2013. **4**: p. 1775.
150. Taylor, W.R. and G.R. Stark, *Regulation of the G2/M transition by p53.* Oncogene, 2001. **20**: p. 1803.
151. Wagner, E.F. and Á.R. Nebreda, *Signal integration by JNK and p38 MAPK pathways in cancer development.* Nature Reviews Cancer, 2009. **9**: p. 537.

9 List of Figures

10 List of tables

11 Declaration of Authorship

Hereby, I declare that I have composed the presented paper independently on my own and without any other resources than the ones indicated. All thoughts taken directly or indirectly from external sources are properly denoted as such.

_____ (Place, Date)

_____ (Signature)

12 Acknowledgements

I would like to thank my supervisor Professor Nisar Malek for the opportunity to work in his laboratory, for the possibility to join many interesting topic and for the support during my whole thesis. Furthermore, I especially thank the members of the Malek lab for their entire help during my doctoral thesis in terms of animal experiments, practical help and supporting me beyond research.